

EFFECTS OF STRONTIUM LOADED CALCIUM PHOSPHATE CEMENT ON OSTEOPOROTIC FRACTURE DEFECT HEALING

Inaugural Dissertation
submitted to the
Faculty of Medicine
in partial fulfillment of the requirements
for the PhD-Degree
of the Faculties of Veterinary Medicine and Medicine
of the Justus Liebig University Giessen

by

SEEMUN, RAY
Born 16th July 1986, INDIA

S. Ray
Labor for Experimentalle Unfallchirurgie
35392, Giessen 2014

*“This thesis is dedicated to my beloved parents
and
my loving husband Siddharth”*

From Experimental Trauma Surgery, Faculty of Medicine

Director/chairman **Univ. Prof. Dr. Christian Heiß**

of the Faculty of Medicine of the Justus Liebig University Giessen

Supervisor

Prof. Dr. med. Dr. biol. hom Volker Alt

Committee Members

Gutachter: **Prof. Dr. Peter Augat**

Prüfungsvorsitzender: **Prof. Dr. Norbert Weißmann**

Beisitzer: **Prof. Dr. med. vet. Sabine Wenisch**

Date of Doctoral Defense

4th December 2014

TABLE OF CONTENTS

I. Table of contents	<i>Page</i>
I. Table of contents	I
II. Lists of figures	IV
III. Lists of tables	VI
IV. Abbreviations	VII
1. Introduction	1
1.1. Bone remodeling	2
1.2. Bone healing	6
1.2.1. Reactive phase	7
1.2.2. Reparative phase	7
1.2.2.1. Intramembranous ossification	8
1.2.2.2. Endochondral ossification	8
1.2.3. Remodeling phase	8
1.3. Delayed and non-union healing	8
1.4. Properties and characteristics of osteoporotic bones	9
1.5. Preclinical models for bone healing in osteoporotic bone	11
1.6. Anti-osteoporosis therapy	14
1.6.1. Effect of anti-catabolic drugs on osteoporosis	14
1.6.2. Effect of anabolic drugs on osteoporosis	14
1.6.3. Effect of strontium ranelate in osteoporosis	14
1.7. Effects of osteoporosis medication on fracture healing	15
1.7.1. Effect of bisphosphonates on fracture healing	15
1.7.2. Effect of PTH (1-34) on fracture healing	15
1.7.3. Effects of estrogen/ raloxifene/vitamin D on fracture healing	15
1.7.4. Effect of strontium ranelate on fracture healing	16
1.8. Strontium	16
1.9. Pharmacokinetics of strontium	16
1.10. Effect on bone tissue	18
1.11. Mechanism of action at molecular and cellular level	18
1.12. Detection of elements by TOFSIMS	19
2. Objectives of this study	21
3. Materials and Methods	22

3.1. Experimental design	22
3.2. Cement preparation	23
3.3. Surgical instrumentation	24
3.4. Animal model	25
3.5. Animal maintenance and surgical procedures	25
3.5.1. Osteoporosis induction	25
3.5.2. Surgical procedure of osteotomy	26
3.6. Bone density measurement using DXA	28
3.7. Euthanasia and specimen collection	28
3.8. Preparation of tissues for histological analysis	28
3.8.1. Protocol for Technovit 9100 embedding	28
3.8.2. Sectioning of Technovit 9100 blocks	32
3.9. Histology	33
3.9.1. Standard staining	33
3.9.2. Immunohistochemical staining	37
3.10. Histomorphometry	44
3.11. mRNA preparation and expression analysis	46
3.12. TOFSIMs	48
3.13. Statistical analysis	49
4. Results	51
4.1. Induction of osteoporosis	51
4.2. Clinical observations	52
4.3. Descriptive histology	52
4.3.1. New bone formation	52
4.3.2. Osteoid formation	53
4.3.3. Cartilage formation	54
4.4. Immunohistochemical analysis	57
4.4.1. Macrophage activity	57
4.4.2. BMP2 expression	57
4.4.3. OPG /RANKL expression	58
4.4.4. OCN expression	61
4.4.5. Vascularization	62
4.4.6. α -SMA expression	62

4.5. Histomorphometry	63
4.5.1. Bone formation	63
4.5.2. Unmineralised tissue	63
4.5.3. Macrophage count	64
4.6. Molecular biology	65
4.6.1. Genes involved in bone formation	65
4.7. TOF-SIMs	65
4.7.1. Strontium release in SrCPC	65
4.7.2. Strontium concentration gradient from implant into bone	67
5. Discussion	69
6. Conclusion and future prospects	76
7. References	78
8. Summary/ Zusammenfassung	95
9. Thesis declaration	97
10. Acknowledgement	98
11. Curriculum vitae	100

III. List of figures	<i>Page</i>
Figure 1: Bone remodeling	2
Figure 2: Signaling pathway for normal osteoclastogenesis	5
Figure 3: Course of bone healing in a standard closed fracture model in rat	6
Figure 4: Comparison between normal healthy bone and osteoporotic bone	10
Figure 5: Potential mechanism of action of strontium on bone cells	17
Figure 6: Dual mechanism of action of strontium on bone cells through CaSR	17
Figure 7: Schematic diagram for TOF-SIMS analysis	19
Figure 8: Schematic overview of metaphyseal osteotomy	22
Figure 9: Instrumentation used for surgical procedure	24
Figure 10: Surgical procedure for creation of metaphyseal osteotomy	26
Figure 11: Surgical procedure for filling of the biomaterial	27
Figure 12: Sectioning procedure using Kawamoto's film	32
Figure 13: Histomorphometric analysis using adobe photoshop CS6	43
Figure 14: Schematic diagrams depicting the two ROI's	45
Figure 15: Qualitative PCR	48
Figure 16: DXA results	51
Figure 17: Movat pentachrome overviews	53
Figure 18: Von-Kossa / Van-Gieson overviews	54
Figure 19: Toluidine blue overviews	55
Figure 20: Movat pentachrome magnified images at biomaterial interface	56
Figure 21: Movat pentachrome depicting shifts in cortical bone	56
Figure 22: Movat pentachrome depicting tissue type in the defect gap	56
Figure 23: ED1 staining	57
Figure 24: BMP2 immunohistochemistry	58
Figure 25: OPG immunohistochemistry	59

Figure 26: RANKL immunohistochemistry	60
Figure 27: OCN immunohistochemistry	61
Figure 28: CD31 immunohistochemistry	62
Figure 29: ASMA immunohistochemistry	62
Figure 30: Histomorphometrical analysis of new bone formation	63
Figure 31: Histomorphometrical analysis of unmineralized tissue	64
Figure 32: Macrophage count based on ED1 immunohistochemistry	64
Figure 33: Relative gene expression analysis between CPC and SrCPC	65
Figure 34: TOF-SIMS analysis overview	66
Figure 35: TOF-SIMS analysis at biomaterial interface	67

III. List of tables	<i>Page</i>
Table 1: Preclinical models addressing bone healing in osteoporotic bones	12
Table 2: Experimental design	23
Table 3: Technovit 9100-embedding	29
Table 4: Preparation of ingredients for movat pentachrome staining	33
Table 5: Preparation of ingredients for toluidine blue staining	35
Table 6: Preparation of ingredients for Von-Kossa / Van-Gieson staining	36
Table 7: Preparation of ingredients for immunohistochemistry	41
Table 8: Primer sequences used	47

IV. LIST OF ABBREVIATIONS

Sr ²⁺	Strontium
Ca ²⁺	Calcium
SrCPC	Strontium modified calcium phosphate cement
CPC	Calcium phosphate cement
OVX	Ovariectomized
DXA	Dual-energy X-ray absorptiometry
BMD	Bone mineral density
BMP 2	Bone morphogenetic protein 2
OPG	Osteoprotegerin
RANKL	Receptor activator of nuclear factor kappa-B ligand
ASMA	Alpha smooth muscle actin
PECAM-1	Platelet endothelial cell adhesion molecule-1
ED1	Anti-CD68
OCN	Osteocalcin
ALPL	Alkaline phosphatase
Runx2	Runt-related transcription factor 2
Colla1	Collagen, type I, alpha 1
Col10a1	Collagen, type X, alpha 1
Car2	Carbonic anhydrase 2
BV/TV	Bone volume over tissue volume
Tb. Ar	Trabecular area
ROI's	Regions of interest
TOF-SIMS	Time-of-Flight Secondary Ion Mass Spectrometry
PTH	Parathyroid hormone
IGFs	Insulin like growth factors

TGF- β	Tumor growth factor beta
BMU	Basic multicellular unit
TNF	Tumor necrosis factor
ODF	Osteoclast differentiation factor
PDGF	Platelet derived growth factor
TRAF	TNF receptor associated factor
NFAT	Nuclear factor of activated T-cells
NF- κ B	Nuclear factor kappa-light-chain-enhancer of activated B cells
FOS	FBJ murine osteosarcoma viral oncogene homolog
IL	Interlukin
CaSR	Calcium sensing receptors
PGE	Prostaglandins
PI	Primary ions
SI	Secondary ions
α -TCP	Alpha tricalcium phosphate
CaHPO ₄	Calcium hydrogen phosphate
Ca ₁₀ (PO ₄) ₆ (OH) ₂	Calcium hydroxyl apatite
CaCO ₃	Calcium carbonate
Na ₂ HPO ₄	Disodium phosphate
AgNO ₃	Silver nitrate
PMMA	Poly methyl methacrylate

1. INTRODUCTION

Osteoporosis is one of the most debilitating diseases in the elderly population which results in decreased bone quality and delays the healing process, the underlying mechanism being an imbalance in the bone remodeling process. Recent epidemiological studies have shown an increase in the incidence of fractures with age thereby leading to morbidity and mortality in elderly people [1]. While anti-osteoporotic therapies significantly lower the risk of a fracture, osteoporotic fractures represent one of the most common causes of disability and affect the health and economic budget of many countries in the world. It is thus a matter of serious clinical concern. Manipulating the local fracture environment in terms of filling the defect gap with a bone graft or natural or synthetic material that aids new bone formation has been considered as the most current treatment option. Hence an ideal biomaterial, with excellent bio-compatibility and osteo-integration characteristics and potential to aid bone healing in osteoporotic fractures is preferable.

Injectable calcium phosphate cements have been shown to have excellent osteoconductive properties thereby stimulating new bone formation [2]. Strontium (II) (Sr^{2+}) has been also shown to optimize bone formation and resorption. It effectively stimulates bone formation and inhibits osteoclastic activity and has therefore been introduced into all day clinical practice as oral strontium ranelate medication against osteoporosis [3, 4]. Pharmacological studies in animals have also shown strontium ranelate decreases bone resorption and increases bone formation, resulting in increased bone mass. However, local administration of strontium mainly from functionalized titanium implant surfaces [5-10] or from strontium-substituted hydroxyapatite coatings [11, 12] have gained interest due to the positive effects of strontium on new bone formation.

In this study, effort was made to use a composite material which combines the osteoconductive calcium phosphate cement and strontium in bone defects in order to leverage the osteo-anabolic and anti-osteoclastic activity of strontium in a local environment.

For *in vivo* evaluation of the effects of strontium and the above mentioned biomaterial implants in new bone formation in osteoporotic bone, a clinically relevant animal model that mimics an osteoporotic fracture defect condition was used [13]. This model shows important reduction in the bone mineral density of the spine and femur (which are the

major anatomical sites affected during osteoporosis) after ovariectomy and special calcium, phosphorus- and vitamin D3-, soy- and phytoestrogen-free diet. The osteotomy was created in the metaphyseal region of the distal femur respecting the fact that metaphyseal fractures are the most common in osteoporotic patients and uses the clinically relevant technique of plate fixation in such a fracture defect. This was then filled with SrCPC, CPC cements or left empty.

Thus the current study focuses on

1. Histological, histomorphometric, immunologic, molecular biology analyses of the above mentioned implants that have been substituted in a critical size metaphyseal defect model in osteoporotic rats.
2. Integrating TOF-SIMS technology together with biomaterials to visualize material behavior in vital tissue.

1.1 BONE REMODELING

The skeleton is a metabolically active organ that undergoes continuous remodeling throughout life. Bone remodeling involves the removal of mineralized bone by osteoclasts followed by formation of new bone matrix through the osteoblasts that subsequently becomes mineralized (Fig. 1). The remodeling cycle thus consists of three

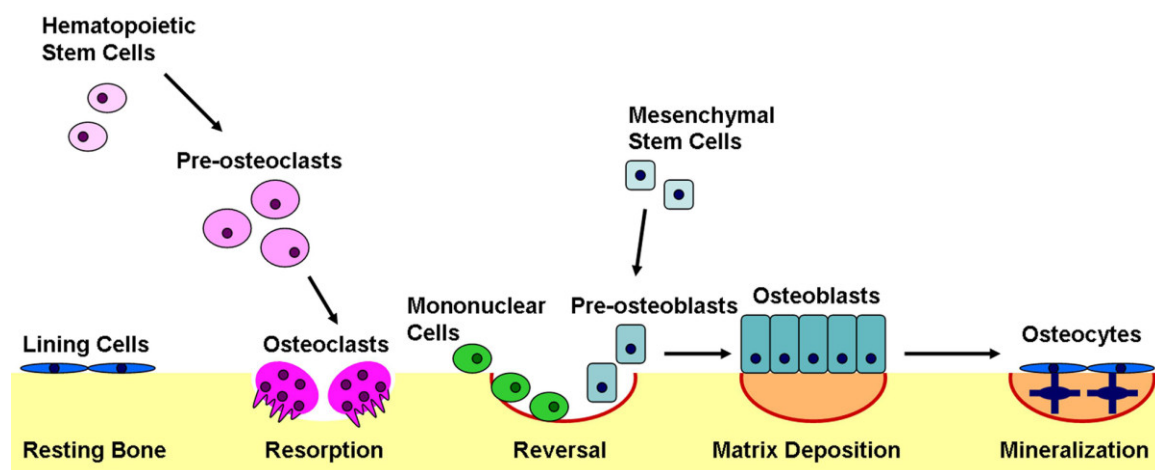


Fig. 1: Bone remodeling. It begins when the osteoclasts resorb bone mineral and matrix. Mononuclear cells prepare the resorbed surface for osteoblasts, which generate newly synthesized matrix as they differentiate. Matrix mineralization and the differentiation of some osteoblasts into osteocytes completes the remodeling cycle. (Kapinas K, Delany AM - *Arthritis Res. Ther.* (2011), *MicroRNA biogenesis and regulation of bone remodeling*)

consecutive phases: resorption, during which osteoclasts digest old bone; reversal, when mononuclear cells appear on the bone surface; and formation, when osteoblasts lay down new bone until the resorbed bone is completely replaced. These processes control the reshaping or replacement of bone following injuries e.g. fracture. In the first year of life, almost 100% of the skeleton is replaced. In adults, remodeling proceeds at about 10% per year. An imbalance in either of the two processes i.e. bone resorption and bone formation, results in many metabolic bone diseases, such as osteoporosis.

Bone remodeling serves to adjust bone architecture to meet changing mechanical needs and it helps to repair micro-damages in bone matrix preventing the accumulation of old bone. It also plays an important role in maintaining plasma calcium homeostasis. The regulation of bone remodeling is both systemic and local. The major systemic regulators include parathyroid hormone (PTH), calcitriol, and other hormones such as growth hormone, glucocorticoids, thyroid hormones, and sex hormones. Factors such as insulin-like growth factors (IGFs), prostaglandins, tumor growth factor-beta (TGF-beta), bone morphogenetic proteins (BMPs), and cytokines are involved as well. As far as local regulation of bone remodeling is concerned, a large number of cytokines and growth factors that affect bone cell functions have been recently identified. Furthermore, through the RANK / receptor activator of NF-kappa B ligand (RANKL) / osteoprotegerin (OPG) system the processes of bone resorption and formation are tightly coupled allowing a wave of bone formation to follow each cycle of bone resorption, thus maintaining skeletal integrity.

The bone remodeling comprises a series of highly regulated steps that depend on the interactions of two cell lineages, the mesenchymal osteoblastic lineage and the hematopoietic osteoclastic lineage. The initial “activation” stage involves the interaction of osteoclast and osteoblast precursor cells (Fig. 1) which leads to the differentiation, migration, and fusion of the large multinucleated osteoclasts. These cells attach to the mineralized bone surface and initiate resorption by the secretion of hydrogen ions and lysosomal enzymes, particularly cathepsin K, which can degrade all the components of bone matrix, including collagen, at low pH. The attachment of osteoclasts to bone may require specific changes in the so-called “lining cells” on the bone surface, which can contract and release proteolytic enzymes to uncover a mineralized surface. Osteoclastic resorption produces irregular scalloped cavities on the trabecular bone surface, called Howship lacunae, or cylindrical Haversian canals in cortical bone [14].

Once the osteoclasts have completed their work of bone removal, there is a reversal phase during which mononuclear cells, which may be of the macrophage lineage, are seen on the bone surface. The events during this stage are not well understood, but they may involve further degradation of collagen, deposition of proteoglycans to form the so-called cement line, and release of growth factors to initiate the formation phase. During the final “formation” phase of the remodeling cycle, the cavity created by resorption can be completely filled in by successive layers of osteoblasts, which differentiate from their mesenchymal precursors and deposit a mineralizable matrix which helps in its mineralization process [15]. Thus, bone formation takes place as mesenchymal cells proliferate into osteoblast precursors and ultimately differentiate into mature osteoblasts. Osteoblasts in turn synthesize a matrix of osteoid composed mainly of type 1 collagen [16]. At a later stage, mature osteoblasts mineralize the osteoid matrix. Osteoblast proliferation and differentiation are governed by many soluble factors such as Runt-related Transcription Factor 2 (Runx2) [17] and a Zinc Finger-containing Transcription Factor (Osterix) [18].

Together, the cells that are responsible for bone remodeling are known as the basic multicellular unit (BMU), and the temporal duration (i.e. lifespan) of the BMU is referred to as the bone remodeling period. BMU is thus composed of various cells responsible for dissolving and refilling an area of bone surface. Osteoclast-mediated bone resorption (dissolving) takes place in 3 weeks; while osteoblast-mediated bone formation requires 3 - 4 months. Further, bone type is also relevant, trabecular bone remodeling takes place faster than cortical bone remodeling. The initiation of the process takes place when exposed to mechanical stress, cytokine signaling or tissue destruction [19, 20]. In this context, osteoblasts can initiate BMU through the expression of RANKL (Receptor Activator of Nuclear factor kappa B Ligand) [20]. Termination of BMU function, on the other hand, depends on inhibiting osteoclast activity. An *in vitro* study previously suggested that osteoclasts are inhibited upon engulfing osteocytes during bone resorption [21]. However, it has been established that the presence of either TGF-(Transforming Growth Factor - beta) or estrogens induce apoptosis in osteoclasts [22, 23].

In addition, other cell types such as macrophages (i.e. mononuclear cells) prepare the bone lacuna for osteoblasts right after the resorption is terminated. Macrophages synthesize a thin collagen layer and release osteopontin, which facilitates the attachment of osteoblast [24].

The OPG / RANKL / RANK system is the main system regulating osteoblast and osteoclast interaction. Receptor activator of nuclear factor kappa-B ligand (RANKL), also known as tumor necrosis factor ligand super-family member 11 (TNFSF11), TNF-related activation-induced cytokine (TRANCE), osteoprotegerin ligand (OPGL), and osteoclast differentiation factor (ODF). Critical for adequate bone metabolism, this surface-bound molecule is found on osteoblast's helps in osteoclast's activation. Osteoclastic activity is triggered via the osteoblast's surface-bound RANKL activating the osteoclast's surface-

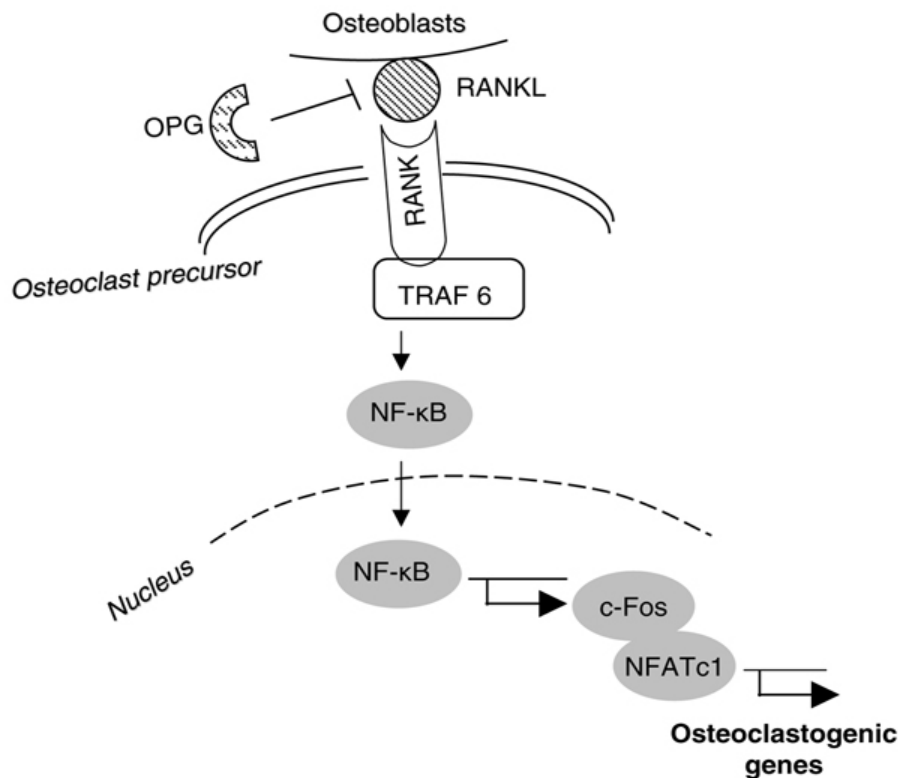


Fig. 2: The essential signaling pathway for normal osteoclastogenesis. Under physiologic conditions, RANKL produced by osteoblasts binds to RANK on the surface of osteoclast precursors and recruits the adaptor protein TRAF6, leading to NF-κB activation and translocation to the nucleus. NF-κB increases c-Fos expression and c-Fos interacts with NFATc1 to trigger the transcription of osteoclastogenic genes. OPG inhibits the initiation of the process by binding to RANKL. NFAT, nuclear factor of activated T cells; NF-κB, nuclear factor-κB; OPG, osteoprotegerin; RANKL, receptor activator of nuclear factor-κB ligand; TRAF, tumor necrosis factor receptor associated factor. (Figure modified from Boyce and Xing *Arthritis Research & Therapy* 2007 9(Suppl 1):S1 doi:10.1186/ar2165)

bound receptor activator of nuclear factor kappa-B RANK. RANK is a member of the Tumor Necrosis Factor (TNF)-receptor family; its activation results in translocation of Nuclear Factor Kappa-light-chain-enhancer of activated B cells (NF-κB) to the nucleus, which causes an increase in the transcription of genes involved in osteoclastogenesis (Fig.

2) [25]. This interaction and activation could be inhibited solely by the decoy receptor osteoprotegerin (OPG), which eventually terminates resorption. Support for the role of RANK / RANKL in osteoclastogenesis also comes from the *in vitro* studies which show the prevention of osteoclastogenesis when RANK is blocked.

The decisive role played by these factors in regulating bone metabolism was demonstrated by the findings of extremes of skeletal phenotypes (osteoporosis vs. osteopetrosis) in mice with altered expression of these molecules [26].

1.2 BONE HEALING

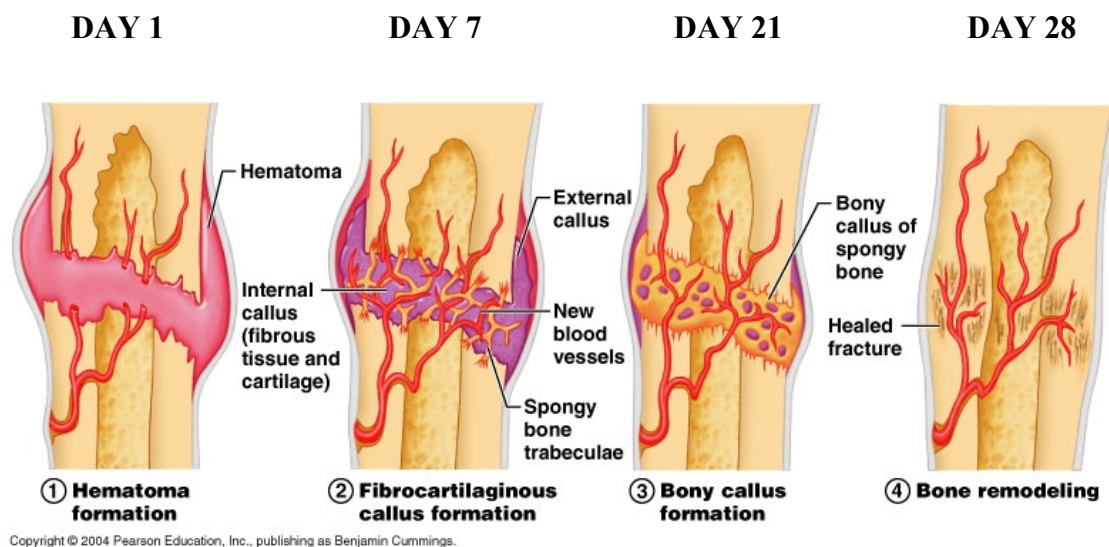


Fig. 3: Course of bone healing in a standard closed fracture model in rat. Day 1) Bone matrix and blood vessels are disrupted, thereby leading to hematoma formation. Day 7) Chondrogenesis and bone formation from the periosteum. By the Day 14, beginning of cartilage calcification and start of the remodeling phase. Day 21) Callus is composed mainly of calcified cartilage. The cortical bone is almost partially bridged. Day 28) Newly formed woven bone and late stage of remodeling. (Figure modified from Bone Fracture, Chapter 6, 2004, Pearson Education Inc.)

Fracture healing is an extremely important biological process that is necessary for the survival of the animal. It is a unique biological event that takes a considerably long period of time to complete. A short phase of endochondral external callus formation is followed by a prolonged remodeling phase. There is always a danger of non-union and possible fracture occurring during the endochondral phase [27, 28]. The healing process is primarily mediated by the periosteum, which is the source of precursor cells that develop into chondroblasts and osteoblasts. The bone marrow, endosteum, small blood vessels, and fibroblasts are other sources of precursor cells. Thus the key players involved in bone

healing apart from the above mentioned cells include growth factors, inflammatory cytokines, antioxidants, hormones, nutrients and amino acid. Upon bone fracture blood supply is disrupted, connective tissue is damaged and there is a loss of the mechanical stability. Bone healing takes place which includes the initial stage of hematoma formation and inflammation. Subsequently there is angiogenesis and cartilage formation followed by cartilage calcification, cartilage removal, bone formation and finally bone remodeling (Fig. 3) [29]. Thus the fracture healing process can be divided into three different, two of which can be further sub-divided to make a total of five phases are as follows:

1. Reactive phase

- I. Fracture and inflammatory phase
- II. Granulation tissue formation

2. Reparative phase

- III. Cartilage callus formation
- IV. Lamellar bone deposition

3. Remodeling phase

- V. Remodeling to original bone contour

1.2.1 Reactive phase

The first stage in the repair of a bone fracture induces the formation of a fracture hematoma where the localized inflamed swelling is filled with blood clot as a result of disruption in the blood vessel [29]. Hematoma is followed and accompanied by inflammation [30]. The hematoma in turn initiates a cascade of cellular events, critical for fracture healing [31]. Cytokines and growth factors including TNF- α , PDGF, GDF and BMP are released from the site [29, 32]. IL-1 and IL-6 secreted by the inflammatory cells, are both known to recruit mesenchymal cells [33]. These MSCs in turn are stimulated by TGF- β and PDGF released by degranulating platelets in the clot to differentiate into chondrocytes and osteoblasts [31].

1.2.2 Reparative phase

In this phase, the cells of the periosteum replicate and transform. During the first 7-10 days the periosteum undergoes an intramembranous response and forms a procallus material that usually extends beyond the volume previously occupied by the uninjured bone. By the middle of the second week, abundant cartilage tissue overlies the fracture

site and this chondroid tissue initiates the calcification process [29]. In general at this stage, proteins produced by the osteoblasts and the osteoclasts begin to consolidate into what is known as soft callus which eventually hardens and forms the hard callus. Thus calcification of the callus takes place by two types of ossification.

1.2.2.1 Intramembranous ossification

It takes place in the hard callus. Hypertrophic chondrocytes are the dominant cell types which in turn form the vesicularized bodies also called as matrix vesicles. These in turn migrate to extracellular matrix to participate in the calcification process. These vesicles help by transporting calcium [34] and possess the proteolytic enzymes for matrix degradation, a vital step for preparation of the callus for calcification [35].

1.2.2.2 Endochondral ossification

The soft callus undergoes endochondral ossification. At this stage the woven bone is substituted by the lamellar bone formation. The lamellar bone begins forming soon after the collagen matrix of either tissue becomes mineralized. At this point, the mineralized matrix is penetrated by vessels and numerous osteoblasts. The osteoblasts form new lamellar bone upon the recently exposed surface of the mineralized matrix. This new lamellar bone is in the form of trabecular bone. Eventually, all of the woven bone and cartilage of the original fracture callus is replaced by trabecular bone, restoring most of the bone's original strength [29].

1.2.3 Remodeling phase

The remodeling process substitutes the newly formed woven bone to lamellar bone. The bone is first resorbed by osteoclasts, creating a shallow resorption pit known as a "Howship's lacuna". Then osteoblasts deposit compact bone within the resorption pit. Eventually, the fracture callus is remodeled into a new shape which closely duplicates the bone's original shape and strength. The remodeling phase takes 3 to 5 years depending on factors such as age or general condition and there is a danger of non-union [34].

1.3 DELAYED AND NON-UNION HEALING

Non-union is a serious complication of a fracture and may occur when there is permanent failure in fracture repair. The normal process of bone healing is interrupted or stalled, e.g.

pseudo-joint (pseudarthrosis) develops between the two fragments with cartilage formation and a joint cavity or a scar tissue found between the un-united fragments.

Since the process of bone healing is quite variable, a nonunion may go on to heal without intervention in a very few cases. The differentiation between delayed union and non-union is sometimes difficult. Non-union is defined as the cessation of all reparative processes of healing without bony union. Since all of the factors discussed under delayed union usually occur to a more severe degree in non-union, the differentiation between delayed and nonunion is often based on radiographic criteria and time. In humans, failure to show any progressive change in the radiographic appearance for at least 3 months after the period of time during which normal fracture union would be thought to have occurred, is evidence of non-union [36].

Statistical analysis shows in the United States 5-10 % of the over 6 million fractures occurring annually develop into delayed or non-unions [29]. Although advanced methods in trauma surgery are conducted, delayed and non-union are a matter of serious clinical concern [37]. In general, bone fractures have also a socio-economical impact. Large annual budgets cover not only primary treatment, and follow-up operations due to delayed or non-unions but also the cost of lost employment resulting from such procedures. Furthermore, it has been predicted that 40% of all postmenopausal women will suffer a new fracture in their lifetime with a high associated risk of non-union [38, 39]. Hence, understanding prevention and treatment of such complications is desirable. The relationship between fracture healing and osteoporosis is complex. The underlying etiology and the therapies involved may all together affect the healing process.

1.4 PROPERTIES AND CHARACTERISTICS OF OSTEOPOROTIC BONE

Osteoporotic fractures represent the major cause for disability and account for the major health economic budget in the world, affecting almost 200 million people [40]. Estimations show that by 2020 approximately 41 million women will be osteoporotic or osteopenic [41]. In Europe it has been shown that the incidence of fracture will increase by 20% to 25% in 2025 [42]. Fragility fractures are especially meta-epiphyseal with slow healing process and morbidity [43].

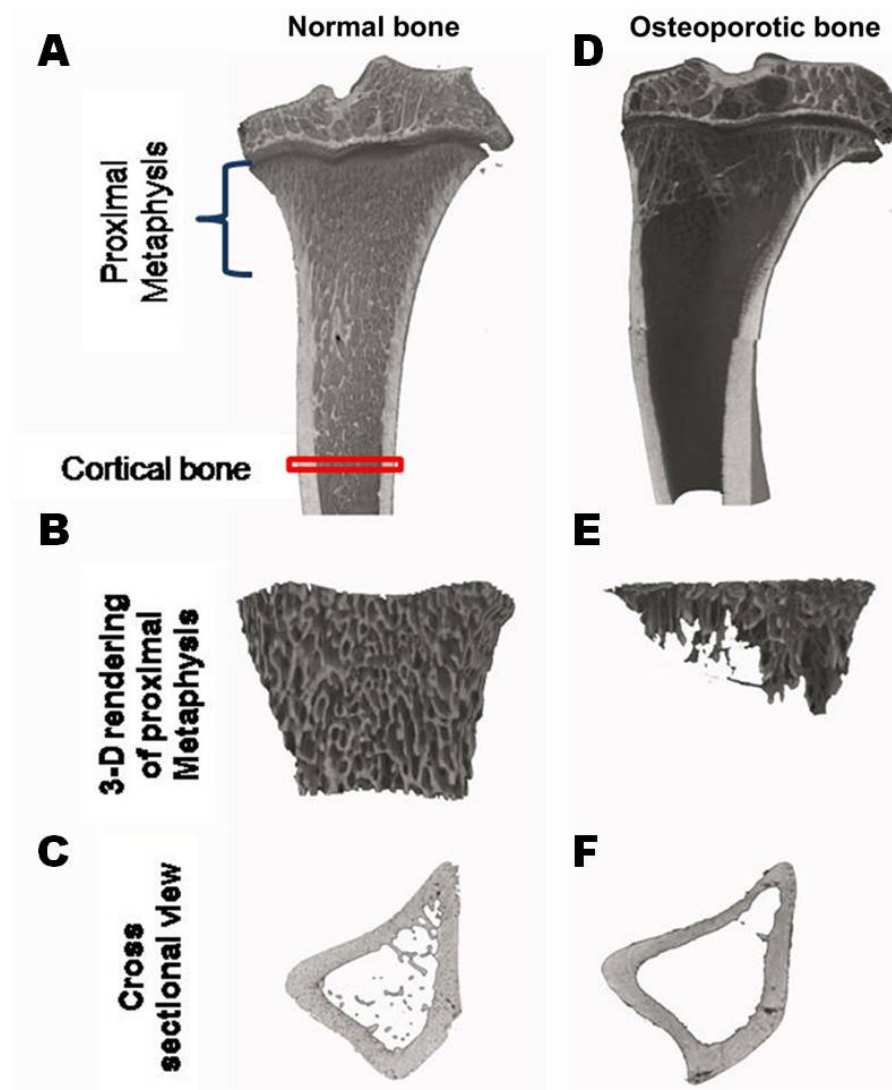


Fig. 4: Normal healthy bone (A, B, C) compared to an osteoporotic bone (D, E, F). The later shows a decrease in the trabecular bone in the metaphysis along with increased porosity (E) and thinning in the cortical bone (F) (Modified from Khassawna et. al 2013, PLOS ONE).

Bone mass and the mechanical performance of the bone is affected in osteoporosis due to changes in hormone levels especially estrogen levels in women. There is a loss not only in the cortical bone but also trabecular bone thereby leading to thinning and reduced connectivity. The loss of cancellous bone also adversely affects the fixation of osteoporotic fractures [44, 45]. In addition there is also a decrease in the bone mineral content of the osteoporotic tissues [46]. The decreased thickness and increased porosity of the cortical bone affects the fixation strengths of the implant as well as the postoperative complications and the recovery times [47]. The loss of density is seen both in the cortical and cancellous bone which increases in the elderly [48]. The figure showing a

comparison between the normal and the osteoporotic bone is given in Fig. 4 and the effect of osteoporosis on fracture healing is tabulated in Table 1.

1.5 PRECLINICAL MODELS FOR BONE HEALING IN OSTEOPOROTIC BONES

The relationship between fracture healing and osteoporosis is complex, the underlying etiology may include aging, hormonal imbalances and therapies commonly used for osteoporosis which may in turn affect fracture healing. Due to these complexities, animal osteoporotic models are considered more appropriate to study the effects of osteoporosis and to test drugs and biomaterials on the fracture repair process. Preclinical testing of those biomaterials requires clinical relevant models that allow for stimulation of the clinical relevant situation [49].

Experimental fracture healing studies in the past have mostly concentrated on diaphyseal femur or tibia with intermedullary pin fixation of the fracture (Table 1) based on the model from Bonnarens and Einhorn (1984) [50]. However, osteoporosis mainly affects the metaphyseal trabecular bone and not at the diaphyseal part of long bones [51-54]. Thus, the models do not mimic the actual clinical relevant situation in osteoporotic patients. Furthermore there are differences in bone healing between the metaphysis and diaphysis [53, 55]. Thus studies on osteoporotic fracture healing should primarily focus on metaphysis than in diaphysis. There are two published model on metaphyseal fracture healing in rat tibiae in which just an osteotomy or a 0.5mm defect gap size was created [51, 56] and the effect of systemic anti-osteoporotic treatment such as estrogen, alendronate and raloxifene was tested. However, a defect of 0.5mm is too small to test locally applied biomaterials. Thus the preclinical studies on bone healing in osteoporotic bones do not represent the clinical relevant situation. The following table presents the different preclinical models for bone healing in osteoporotic bones.

Table 1: Different preclinical models addressing bone healing in osteoporotic bones

STUDY	INDUCTION OF OSTEOPOROSIS	ANATOMIC REGION	RESULTS
Kubo et al. 1999 [57]	Test group: OVX-low calcium diet- Osteoporosis Control group (7 month old female Wistar rats)	Femoral shaft fracture 3 months post ovariectomy	12 weeks post fracture a decrease in the BMD at the fracture site in the osteoporosis group.
Meyer et al. 2000 [58]	Test group : OVX Control group: SHAM surgery (6 month old female Sprague-Dawley rats)	Drilled hole in the intercondylar notch	Lower bone rigidity and breaking load in the ovariectomized rats.
Namkung et al. 2001 [59]	Test group: OVX-low calcium diet- Osteoporosis Control group: SHAM surgery (2 month old female Sprague-Dawley rats used)	Right femoral mid-shaft fracture created and stabilized by intramedullary pins	Reduction in fracture callus and BMD in the healing femur of the OVX rats.
Lill et al. 2003 [60]	Test group: Osteoporotic Control group: Healthy animals (Swiss female mountain sheep used)	3mm mid-shaft tibial osteotomy stabilized by external fixator	Delay in the bending stiffness of the callus in the osteoporotic animals.
Xu et al. 2004 [61]	Test group: OVX- Osteoporotic Control group: SHAM surgery (Female wistar rats used)	Femoral shaft fracture 3 months after OVX.	Decrease in the callus and BMD along with a decrease in the osteoblast count in the bone trabecula in OVX rats
Islam et al. 2005 [62]	Test group: OVX-low calcium diet- Osteoporosis Control group: SHAM surgery (3 month old female Wistar rats used)	Fracture in right side of mandibular ramus 3 months after OVX	Prolonged endochondral ossification with an increased osteoclast no. in the osteoporotic group.

Wang et al. 2005 [63]	Test group: OVX-Osteoporosis Control group: SHAM surgery (4 months old Sprague Dawley rats used)	Mid shaft tibia model 10 weeks after OVX.	Decrease in the callus BMD, failure loss in the osteoporotic group along with a delay in the endochondral bone formation.
Qiao et al. 2005 [64]	Test group: OVX-Osteoporosis Control group: SHAM surgery (6 month old Sprague Dawley rats used)	Femoral shaft fracture 2 months after OVX	Decreased callus density and osteoclasts number in the OVX group.
Kolios et al. 2009 [56]	Test group: 36 OVX . Divided into 3 groups of 12 animals each and fed with phytoestrogen free food, estradiol supplement and alendronate supplement. Control group: 12 SHAM operated rats (12 weeks old female Sprague-Dawley rats used)	Metaphyseal tibia osteotomy and standardized plate fixation 10 weeks after ovariectomy.	Qualitative and quantitative increase of metaphyseal fracture healing by estrogen whereas no visible effects of alendronate seen.
Stuermer et al. 2010 [55]	Test group : OVX Control group: SHAM surgery (3 month old female Sprague-Dawley rats used)	0.5mm metaphyseal osteotomy at the same time of ovariectomy	Improved fracture healing in osteoporotic bone treated with estrogen and raloxifene.
Alt et al. 2013 [13]	Test group: OVX-Osteoporosis-multi deficient diet devoid of Calcium. Phosphorus, Vit D3. Control group: SHAM surgery (10 week old female Sprague Dawley rats used)	3mm and 5mm osteotomy in the metaphyseal region of femur, 6 weeks after OVX	1) Successful induction of osteoporosis using a combined approach of ovariectomy and multi-deficient diet. 2) Complete bridging in the 3mm defect when compared to the 5mm defect.

1.6 ANTI-OSTEOPOROSIS THERAPY AND FRACTURE HEALING

Osteoporosis treatments are now classified into three groups: anti-catabolic (bisphosphonates, antibody to RANKL), anabolic (PTH) and dual action (catabolic + anabolic) mainly represented by the strontium ranelate categories.

1.6.1 Effect of anti-catabolic drugs on osteoporosis

Bisphosphonates is a widely used medication for osteoporotic patients [27]. They are anti-resorptive in nature which slows or stops the natural process that dissolves bone tissue, resulting in maintained or increased bone density and strength. This may prevent the development of osteoporosis. If osteoporosis already has developed, it exerts its effect by slowing the bone resorption through the inhibition of osteoclastic activity [65]. This however, raises the concern that its interference with bone remodeling may impair fracture healing. A human monoclonal body to RANKL has been recently developed for the treatment of osteoporosis [66, 67]. It is anti-catabolic in nature and exerts its action through prevention of the differentiation of osteoclast precursors into mature osteoclasts.

1.6.2 Effect of anabolic drugs on osteoporosis

Although anti-resorptive or anti-catabolic therapies are the medical options for the treatment of osteoporosis, at present a lot of focus has been paid on anabolic or potentially anabolic compounds that can increase bone density and restore the micro architecture. Parathyroid hormone being one of them marked the first anabolic agent for the treatment of osteoporosis. Its effect on bone metabolism depends on its duration of exposure. It is shown to increase bone resorption if administered continuously [68]. However, if administered intermittently, leads to an increase in bone formation by activation of the osteoblasts [69]. Although the exact mechanism of action of PTH has not been fully understood, an increased recruitment and differentiation of chondrocytes have been shown [70].

1.6.3 Effect of strontium ranelate in osteoporosis

Strontium ranelate has been recently approved as an anti-osteoporotic medication in many countries. It exerts a dual mode of action, both anabolic and catabolic [3]. It produces an anabolic effect by increasing the differentiation rate of pre-osteoblasts to osteoblasts and through osteoblast modulation [71, 72]. On the other hand, it produces a catabolic effect by inhibiting the osteoclast formation [72].

1.7 EFFECTS OF OSTEOPOROSIS MEDICATION ON FRACTURE HEALING

Fracture healing is an extremely important biological process which is severely compromised in osteoporotic patients. As fractures are more common in people with osteoporosis who may be already undergoing anti-osteoporotic medication, it is of great clinical importance to know whether these drugs exert a positive or negative effect on the biological process of fracture repair.

1.7.1 Effect of bisphosphonates on fracture healing

Bisphosphonates have a pronounced inhibitory effect on the bone resorption process, especially in cases of high bone turnover [27]. Larger callus with increased bone mineral content was found in a sheep fracture model treated with pamidronate, with no effect on the mechanical properties [73]. Incadronate treatment given to growing rats with a femoral shaft fracture resulted in larger callus, increased stiffness and load of the same [74]. A similar effect was also found after administration of ibandronate in ovariectomized rats [75].

1.7.2 Effect of PTH (1-34) on fracture healing

It is known to improve the biomechanical properties of fracture callus and accelerates callus formation, endochondral ossification and bone remodeling [76, 77]. It is also a potent agent for enhancing fracture healing in patients with osteoporosis [77]. Animal studies show an enhancement in the fracture repair by systemic administration of PTH [76, 78].

1.7.3 Effects of estrogen, raloxifene and vitamin D on fracture healing

Estrogens and raloxifene improve fracture healing histologically and mechanically in closed tibial fractured ovariectomized rat model [55]. Similarly, vitamin D3 has been shown to improve both fracture healing and mechanical strength in the callus [79]. Thus vitamin D3 is implicated to increase the BMD and also promotes the cartilaginous phase of fracture healing [80].

1.7.4 Effect of strontium ranelate on fracture healing

Strontium ranelate is implicated to stimulate bone formation and inhibit bone resorption [3]. This dual action thus enables it to be used as a possible therapeutic agent for enhancing fracture healing and increasing its mechanical properties. Local application of strontium salts in implants used in fracture fixation has been suggested for fracture repair promotion [81]. Strontium ranelate is also known to increase the callus volume in a closed femoral fracture experimental rat model, while the torsional strength is improved by strontium alone [75].

1.8 STRONTIUM

Strontium, a chemical element (Sr) with atomic number 38 is not freely available in nature due its property of oxidation. Interestingly, the human body absorbs strontium like calcium. Due to the chemical similarity of the elements, the stable forms of strontium are not harmful for human health [82].

Recent studies using strontium on osteoblasts in vivo showed marked improvement on bone-building osteoblasts [83]. The drug strontium ranelate, made by combining strontium with ranelic acid, also aids bone growth, increase bone density, and reduces vertebral, peripheral, and hip fractures [84, 85]. Women receiving the drug showed a 12.7% increase in bone density compared to women receiving a placebo who had a 1.6% decrease. Half the increase in bone density (measured by X-ray densitometry) is attributed to the higher atomic weight of Sr compared with calcium, whereas the other half a true increase in bone mass [83].

1.9 PHARMACOKINETICS OF STRONTIUM

The gastrointestinal tract is the main route of entrance for strontium into the human body [82]. The absorption efficiency of strontium is almost the same as that of calcium. Almost all the absorbed strontium (99.1%) is deposited in bone, the prime site being the newly formed bone [86]. The blood being the second most important site for strontium in the body. In OVX rats, the administration of 0.3-1.2 nmol Sr/kg/day in the form of strontium ranelate prevented the trabecular bone loss [87]. Similarly administration of strontium after 3 months of OVX increased the bone turnover rate and the bone mineral content lost due to ovariectomy [88].

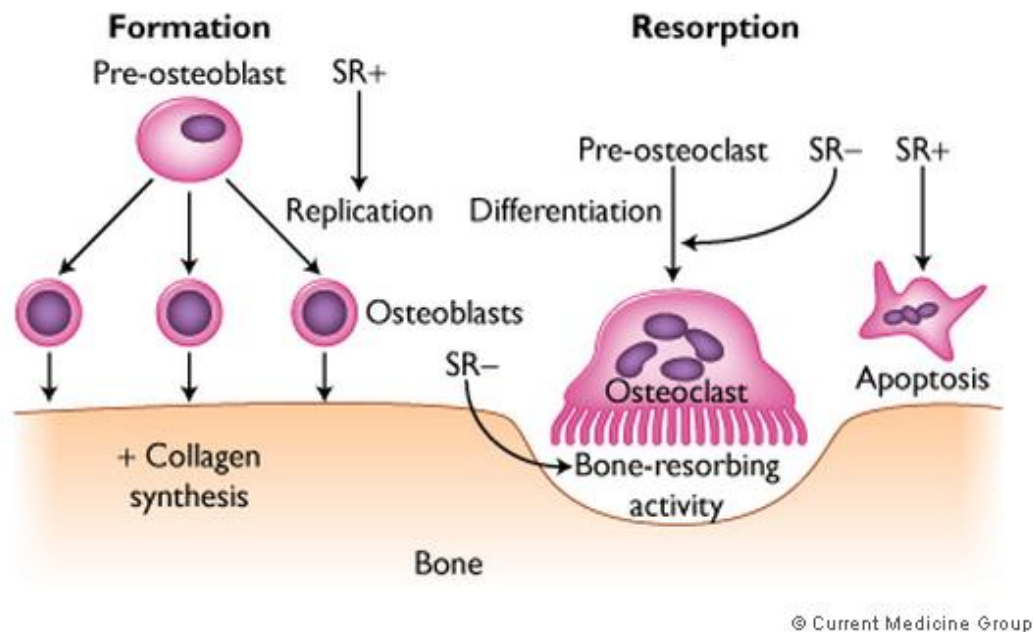


Fig 5: Potential mechanisms of action of strontium on bone cells. Strontium stimulates pre-osteoblast replication, leading to an increase of matrix synthesis. On the contrary, strontium appears to inhibit osteoclast differentiation and activity. +: stimulatory effect; -: inhibitory effect (From Marie PJ. Bone. 2006; 38 (Suppl 1): S10-S14)

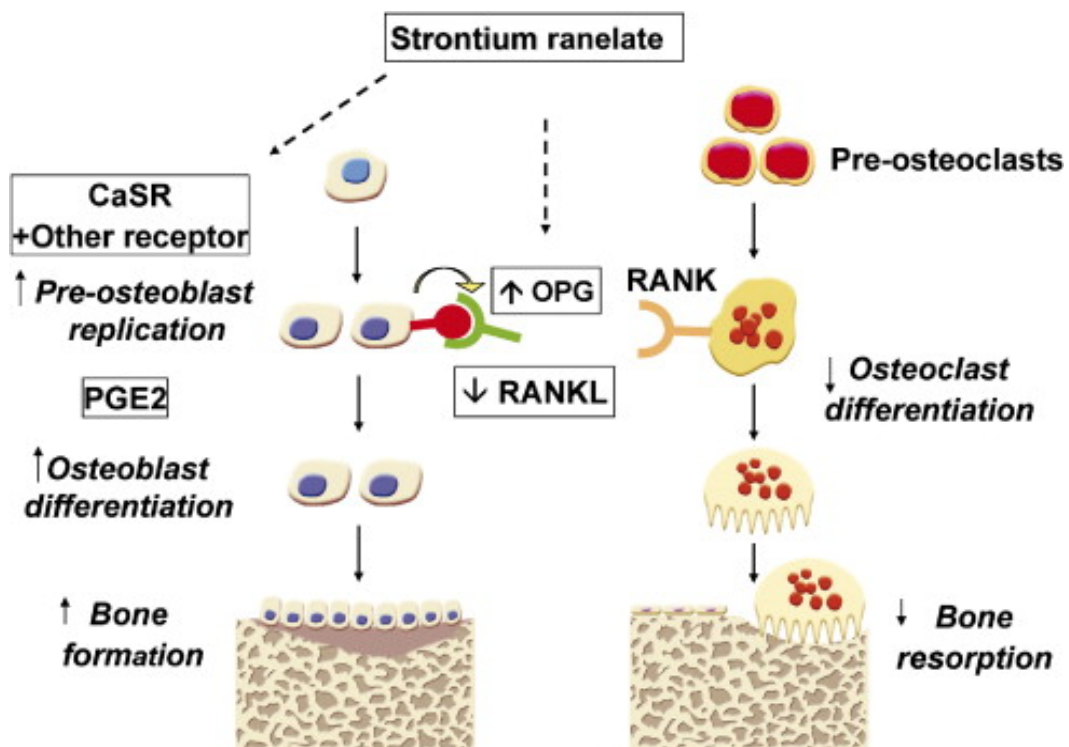


Fig.6: Dual mechanism of action of strontium on bone cells through calcium-sensing receptors (CaSR). Strontium stimulates pre-osteoblast replication, leading to osteoblast differentiation and eventually new bone formation. It also increases the osteoprotegerin level which decreases the RANKL expression and prevents the cross talk with RANK on osteoclasts. This leads to inhibition of osteoclast differentiation, resulting in bone resorption. (PJ Marie Bone 2006 40: S5-S8)

The single most important excretion route is by the kidneys, and a secondary excretion route is by the intestines [82, 89]. The majority of animal studies of strontium are made on rodents which have a high bone formation rate and do not reach a steady-state of remodeling. Therefore care should be taken while interpreting the studies of bone formation and bone resorption performed in rodents and must be considered preliminary [90]. In a study by Raffalt et al. the content of strontium in bone was increased to 9 mg/g bone, when 3000 mg/kg/day strontium malonate was administered orally [91]. The calcium content remained constant in spite of strontium administration. Boivin et al. found the average Sr/Ca ratio in bone can be as high as 1:10 after oral strontium ranelate administration for 13 weeks in monkeys [86]. He also showed a quick clearance of strontium after the bone treatment. However in this study, the strontium was applied locally.

1.10 EFFECT ON BONE TISSUE

When administered orally as strontium ranelate, the strontium gets incorporated into hydroxyapatite instead of calcium at Sr/Ca ratio of 1:10 [86, 92]. Grynepas et al. has shown in rats fed on a normal calcium-containing diet, an increase in the bone formation by a relative low strontium dosage [93]. Several studies on humans, monkeys, and dogs show an increase in parameters of bone formation, such as osteoblast surface, mineral apposition rate, and S-alkaline phosphatase [94]. Ammann et al. also showed the positive effect of strontium on the mechanical properties of bone in rats where strontium increased the mechanical property by increase in the bone volume and improved micro-architecture [95]. Clinically, in the treatment of osteoporosis, strontium ranelate has not only been shown to reduce the risk of especially non-vertebral fracture but also vertebral fractures [96]. Similar studies on strontium containing bone graft substitutes in rats are also promising [97-99].

1.11 MECHANISM OF ACTION AT THE MOLECULAR AND CELLULAR LEVELS

Strontium is known to have dual mechanism of action (Fig. 5). Studies have shown that strontium stimulate the calcium-sensing receptor, CaSR, situated in the membrane of osteoblasts and osteoclasts [100-102] (Fig. 6). Stimulation of these receptors present in the surface of the osteoblast cell line triggers mitogenic signals leading to proliferation, differentiation, and activation of the osteoblasts [71, 72]. Similarly, when the CaSR

situated in the osteoclast cell line is stimulated, the cells retract and bone resorption is inhibited [72]. It is through the increased OPG production, strontium can also suppress the interaction of RANKL on osteoblasts with the RANK present on the surface of the osteoclasts, thereby leading to diminished proliferation, differentiation, and survival of the osteoclasts [71, 103]. Thus the effects of strontium on the cellular level are to increase the pool of active osteoblasts and decrease the number of less active osteoclasts.

1.12 DETECTION OF ELEMENTS BY TOF-SIMS

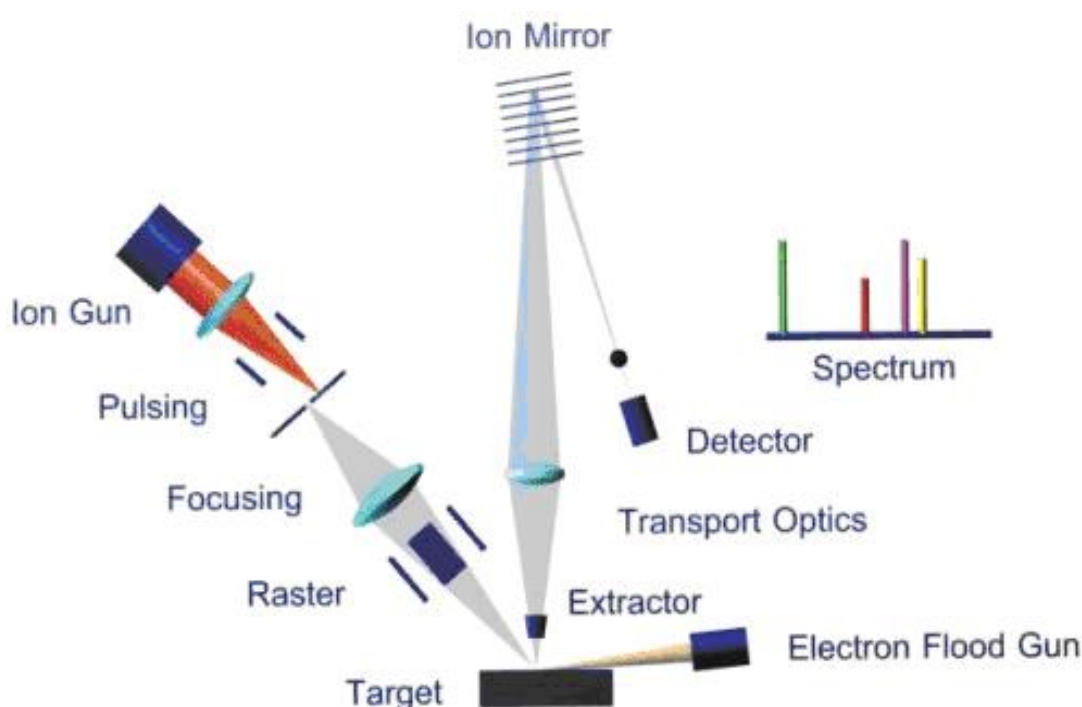


Fig. 7: Schematic diagram for TOF-SIMS analysis (ION-TOF GmbH)

Time of flight secondary ion mass spectrometry (TOF-SIMS) originates from the material science with increasing applications in life science due to its ability to assess chemical composition of solid surfaces down to 100nm lateral resolution [104, 105]. In this technique, a high energetic primary ion beam from the machine is focussed to a solid sample. These primary ions (PI) hit the sample surface and results in the release of atomic and molecular fragments as well as electrons from the top surface layer.

These charged atoms and molecules are called secondary ions (SI) which are collected via an electrical field and analysed in a mass analyser by their time of flight (Fig. 7). In this method the primary ion beam is scanning the surface and enables us to perform a mass

mapping of the sample surface. Moreover, a 3D mass distribution can also be achieved by using an additional more intensive ion beam onto the surface which in turn can be removed layer by layer. Although this technique results in a high fragmentation rate of organic molecules, it could be overcome by the use of modern cluster ion beams [106-108].

TOF-SIMS has found numerous applications in life sciences. As shown by Borner et al. the possibility to image the distribution of cholesterol in frozen sections of rat cerebellum [109]. Hagenhoff et al. also showed the uptake and the localisation of nano-particles in the cytoplasm of mammalian cells [110]. Moreover TOF-SIMS was also used for the chemical analysis of bone-implant interfaces as shown by Palmquist et al. [111] and for the assessment of bone quality by Henss et al. [112].

The investigation of bone by mass spectrometry is very promising. Bone tissue being primarily composed of calcium hydroxyapatite crystals and collagen-type I fibrils makes it interesting for imaging mass spectrometry. Calcium and several calcium phosphate ions as well as numerous organic fragments derived from collagen can be detected precisely with TOF-SIMS.

2. OBJECTIVES OF THIS STUDY

The study primarily focuses on the bone formation capabilities of strontium if any, when substituted into CPC and implanted in critical size metaphyseal defects in osteoporotic rats and its comparison with CPC and empty defect group. Thus the objectives of this study are to investigate:

1. The effects of strontium modified calcium phosphate (SrCPC) on new bone formation in comparison with the pure calcium phosphate cement (CPC), devoid of any strontium and empty defect group in a metaphyseal bone defect model in osteoporotic rats.
2. To assess the possibility to detect strontium release from SrCPC along with the estimation of calcium and collagen mass distribution in the defect area of metaphyseal bone using TOF-SIMS technology.

Thus the hypothesis are:

1. Strontium substitution into calcium phosphate cements optimizes bone formation and resorption *in vitro*, and improves bone mass *in vivo* compared to CPC and empty defect group.
2. TOF-SIMS is able to detect the local release of strontium from SrCPC which in turn results in enhanced bone formation.

3. MATERIALS AND METHODS

3.1. EXPERIMENTAL DESIGN

45 female Sprague-Dawley rats were randomly assigned to three different groups: (1) strontium modified calcium phosphate cement (SrCPC), (2) calcium phosphate cement (CPC) and (3) empty defect control group. The animals underwent induction of osteopenic bone status by bilateral ovariectomy combined with a multi-deficient diet as described later (3.5.1). A critical size defect of 4mm was then created in the metaphysis of these rats which were subsequently filled with SrCPC, CPC implant material in the metaphyseal region of the osteoporotic rat femur (Fig. 8), was used to study the effects of strontium loaded implants on bone remodeling. A control group with a critical size metaphyseal defect, without biomaterial implant was compared with test groups consisting of CPC and SrCPC respectively. Resulting bone formation was investigated using histomorphometry, immunohistochemistry, molecular biology and TOF-SIMS analysis. The TOF-SIMS analysis was carried out as a collaboration work with the Institute for Physical Chemistry, Justus-Liebig-University of Giessen. All interventions were performed in full compliance with the institutional and German protection laws and approved by the local animal welfare committee (Reference number: V 54 – 19 c 20-15 (1) GI 20/28 Nr. 108/2011).

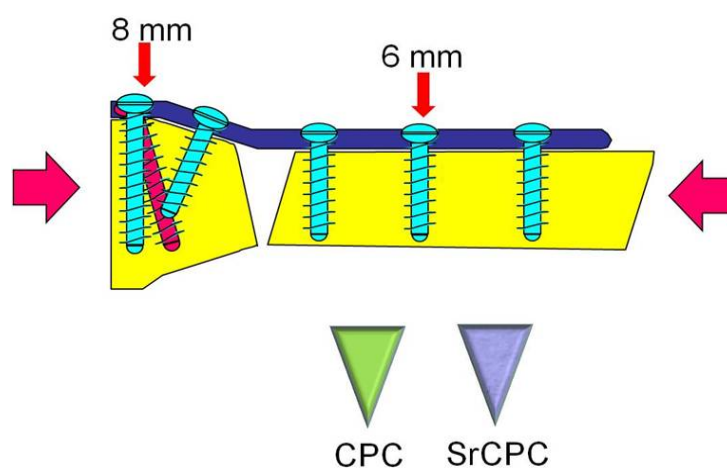


Fig. 8: Schematic overview of metaphyseal osteotomy in the left femur depicting the wedge shaped defect and the plate fixation. The defect was then filled with CPC or SrCPC cements.

PROCEDURE	EMPTY GROUP (CONTROL)	CPC GROUP	SrCPC GROUP
Osteoporosis induction	15	15	15
Defect creation and biomaterial implantation	15	15	15
Sacrifice and harvest	11	13	15
DXA	11	13	15
Undecalcified histology*	6	7	8
Histomorphometry*	6	7	8
Immunohistochemistry*	6	7	8
Molecular biology	5	6	7
TOF-SIMS*	6	7	8

Table 2: Experimental design showing animal groups and planned experiments. Star () indicates the consecutive sections from the same animal. Discrepancies in the total count are due to the animal deaths.*

3.2 CEMENT PREPARATION

Calcium phosphate cement was used as a starting material. A hydroxyapatite-forming α -tricalcium phosphate (α -TCP) based bone cement and strontium-containing modifications, as previously described by Schumacher M. et al., 2013, were used in this study. In brief, calcium phosphate cement (CPC) comprised of 58 wt.% α -TCP (α -Ca₃(PO₄)₂), 25 wt.% calcium hydrogen phosphate (CaHPO₄) along with small amounts of hydroxyapatite (Ca₁₀(PO₄)₆(OH)₂) of almost 8.5 wt.% and calcium carbonate (CaCO₃) of the same quantity which was supplied by InnoTERE GmbH, (Radebeul, Germany). In case of strontium-containing SrCPC, CaCO₃ was replaced completely with strontium carbonate (SrCO₃, 99.994%, Alfa Aesar, Karlsruhe, Germany), resulting in the formation of a Sr²⁺-substituted apatite cement matrix with a Sr/Ca ratio of 0.123.

Cement precursor powders were supplied by InnoTERE GmbH (Radebeul, Germany) and were sterilized by γ -radiation at 25 kGy. Prior to implantation, cement powder was manually mixed with 4 wt. % aqueous Na₂HPO₄ to form a moldable paste. The liquid-to-powder (l/p) ratio was varied to obtain comparable mould ability for the different cements

being used. Hence, a ratio of 0.40 and 0.35 ml/g for CPC and SrCPC was used respectively.

3.3 SURGICAL INSTRUMENTATION

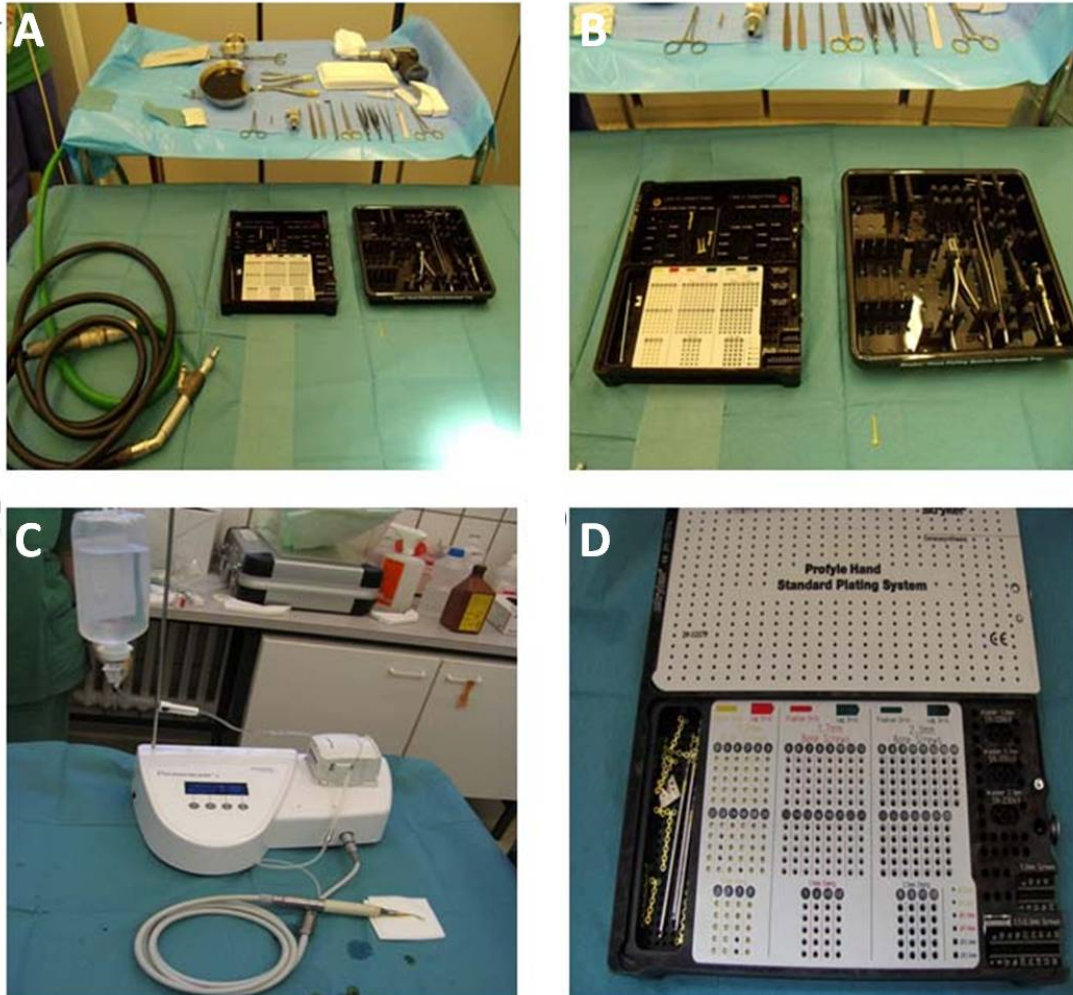


Fig. 9: Instrumentation overview used for the surgical procedure (A, B) comprising of the Piezosurgery[®] Insert OTS7-3 (C) and the Leibinger[®] XS-miniplate (D).

The wedge shaped osteotomy was performed on the distal end of the left femur (with a lateral length of 4 mm and a medial gap of 0.35 mm using Piezosurgery[®] Insert OTS7-3, (Fig. 9C) Mectron, Köln, Germany. It is a highly effective saw-like insert suitable for microsurgical applications. The cutting portion of the insert is 0.35 mm thick and 11 mm long. The presence of convenient laser-etched markings at 7 mm, 8.5 mm, and 10 mm indicate the osteotomy depth while performing the surgery. The insert is thinner and more suitable for microsurgical, minimally invasive procedures. In addition it also has a smaller cutting surface and is preferable when working in limited space/volume.

The Leibinger[®] XS-miniplate from Stryker (Schönkirchen, Germany) includes the T-shaped mini-plate, screws (ranging from 4 mm to 20 mm in length and are 2.0 and 2.3 mm in diameter) and drill-free screws. (Fig. 9D).

3.4 ANIMAL MODEL

Female Sprague-Dawley rats (Charles River, Sulzfeld, Germany) were used for the study group. The experimental procedures and protocols performed were approved by the local animal welfare committee and were in accordance with the institutional and German animal protection laws of district government of Giessen (Reference number: V 54 – 19 c 20-15 (1) GI 20/28 Nr. 108/2011).

3.5 ANIMAL MAINTENANCE AND SURGICAL PROCEDURE

Forty-five, ten week old female Sprague-Dawley rats (Charles River, Sulzfeld, Germany) were maintained in a pathogen-free standard animal facility. The animals were kept in filter-topped plastic cages (2 - 4 rats/cage) and had free access to food and water until three months of age. The rooms were maintained at 22°C and 40 – 60% humidity. The study includes two operative procedures. The first procedure aimed at induction of osteoporosis by using the procedure of bilateral ovariectomy. The second procedure involved creating a femoral wedge-shaped osteotomy (which was left empty in control group) of 4 mm lateral gap and 0.35 mm medial fracture gap and subsequent biomaterial substitution in the test groups. After either of the operative procedure rats were kept single for one week to allow recovery.

3.5.1 Osteoporosis induction

The present animal model in this study is based on major risk factors accepted in general for osteoporosis: menopause and calcium restricted diet. Bilateral ovariectomy was performed on all the female Sprague Dawley rats by means of a low median laparotomy under general anesthesia. The animals received an intraperitoneal injection of ketamine (62.5 mg/kg bodyweight, Hostaket[®], Hoechst) and xylazine (7.5 mg/kg bodyweight, Rompun[®], Bayer). Care was taken to ligate the ovarian vessels twice. Post-operative pain medication was given as necessary.

The ovariectomized group (OVX) received a calcium-phosphorous and vitamin D3, soy and phytoestrogen-free diet (10 mm pellets, Altromin-C1034, Altromin Spezialfutter GmbH, Lage, Germany). Whereas the SHAM group (placebo surgery) received normal

diet. SHAM group used for comparison in this study was taken from another project only to ensure a successful osteoporosis induction.

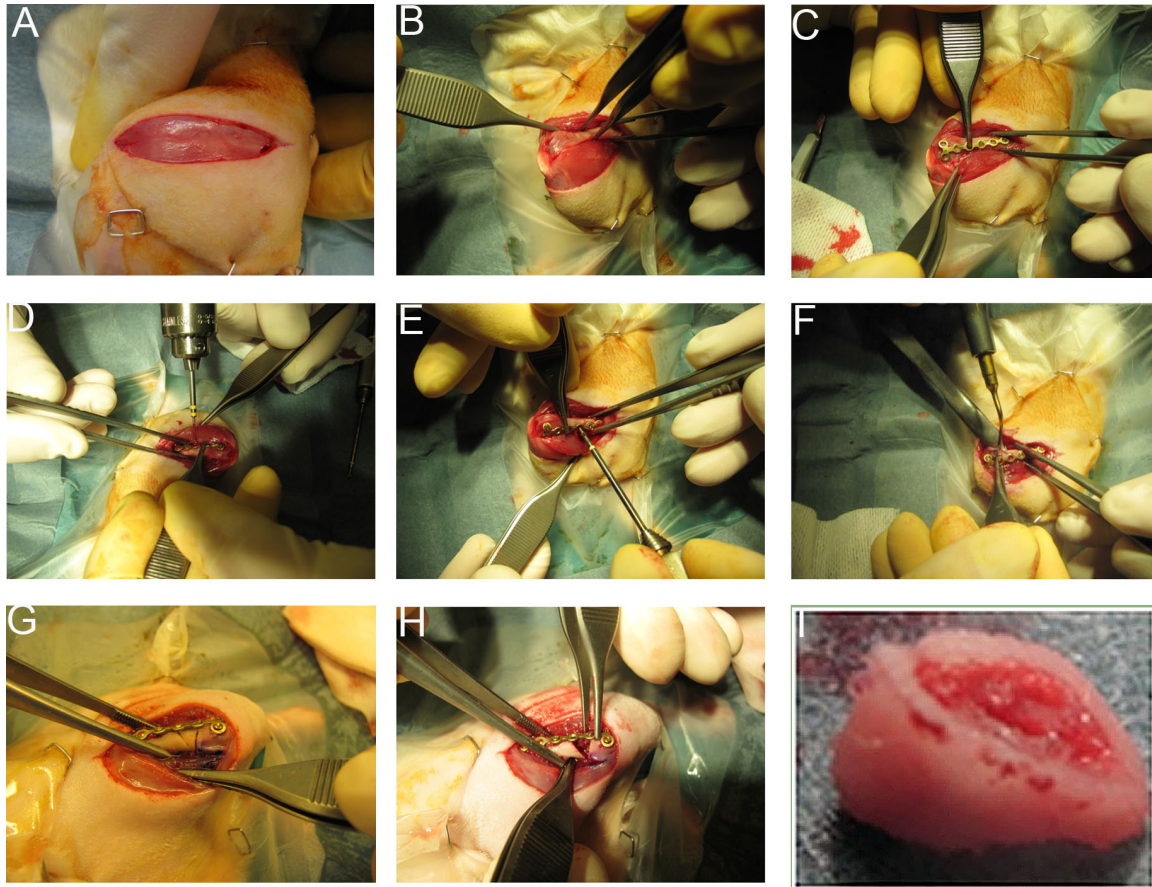


Fig. 10: *Surgical procedure for creation of metaphyseal osteotomy in the left femur. Under anesthesia, a medial incision was made to expose the left femur (A-D). T-shaped plate was first fixed (E) with the screws followed by measurement and determination for the wedge shaped defect (F) 4 mm in length and 0.35 mm medial gap. Defect was then created using an oscillating saw (G) and the osteotomized wedge was removed (H, I).*

3.5.2 Surgical procedure of the osteotomy

Prior to the operation, all animals were weighed and the left hind portion, including the entire leg, was shaved and disinfected with povidone iodine (Braunol[®], Braun, Melsungen, Germany). The animals were laid on their right side on a heating plate (37°C) covered with a sterile drape leaving the left hind exposed. A 4 cm skin incision was made over the lateral aspect of the left thigh and the lateral femur was exposed from the lateral condyle area to the midshaft area between the lateral vastus muscle and the lateral head of the femoral biceps muscle (Fig. 10). A 7-hole T-shaped miniplate (Leibinger[®] XS-miniplate, Stryker[®], Schönkirchen, Germany) was slightly bended and fixed with 1.7 mm screws on the lateral femur (Fig. 10). There were two 8 mm long

screws in the distal fragment running perpendicular to the knee articular surface and one 8 mm oblique screw from more proximal through the femoral condyles. The proximal part of the plate was fixed with four 6 mm screws at the midshaft area.

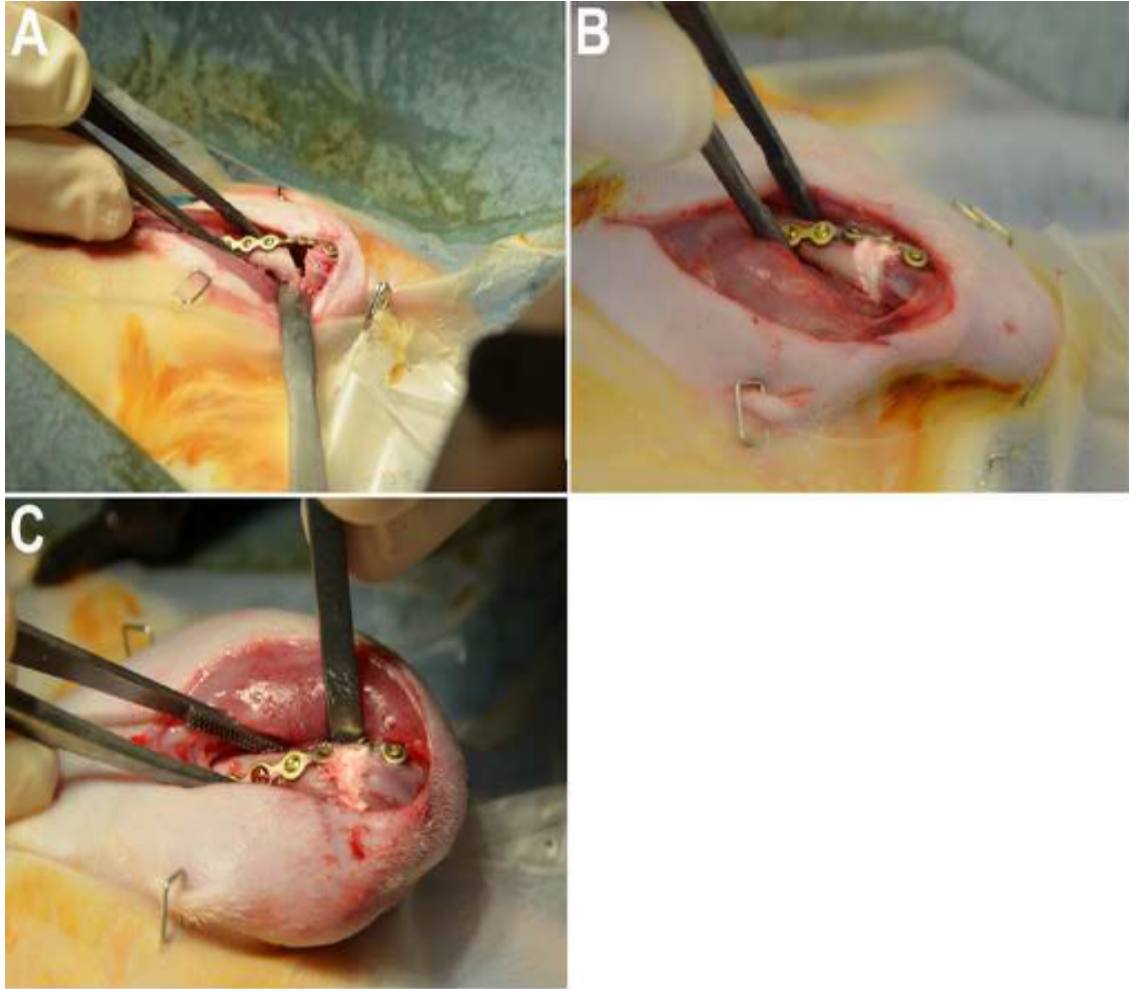


Fig. 11: Surgical procedure for filling of the biomaterial in the osteotomized gap. The gap was left empty to serve as control (A), filled with CPC (B) and SrCPC (C).

A wedge shaped defect with a lateral gap of 4 mm and medial gap of 0.35 mm was then created using an ultrasound bone saw Piezosurgery 3[®], saw blade OT7S-3, Mectron Köln, Germany (Fig. 10). The bone segment was removed and filled with different materials (CPC and SrCPC) or left empty to serve as control (Fig. 11). The fascia of the muscle was sutured with absorbable sutures, the skin then closed with absorbable sutures and stapled with vickostat skin stapler, which were removed after 1 week during the wound care routine. The animals were closely monitored after the surgery. Necessary post-operative pain medication was also given. Afterwards the animals were observed daily, the wound was monitored, and weight was controlled weekly.

3.6 BONE DENSITY MEASUREMENTS USING DUAL ENERGY X-RAY ABSORPTIOMETRY (DXA)

Bone mineral density (BMD in g/cm^2) was measured by DXA (Lunar prodigy, GE Healthcare, Germany) before induction of osteoporosis (0 month) and three months after the described induction of osteoporosis (3 months), at the point the fracture defect was created in order to ensure onset of osteoporosis. BMD of the left femur at the site of defect region, right femur and spine were analyzed as these are the major anatomical sites affected during osteoporosis. Analysis was carried out using the small-animal mode of the enCORE software (GE Healthcare, v. 13.40).

T score was calculated according the formula $T \text{ score} = (\text{BMD} - \text{YN}) / \text{SD}$, where BMD is the mean bone mineral density of the experimental group (OVX + diet), YN is the “young normal mean” of the control group (SHAM) and SD is the standard deviation. The DXA measurements were done with compliance to the quality control and calibration as described by the manufacturer’s protocol.

3.7 EUTHANASIA AND SPECIMEN COLLECTION

6 weeks post fracture creation in the metaphysis of the left femur in the osteoporotic animals and biomaterial implantation, animals were euthanized with CO_2 after general anesthesia. Soft tissue surrounding cortical bone surface of the femora was completely removed without disrupting the newly formed tissue. Specimens were assessed for stability before any further assessment. Bone was considered stable when both proximal and distal fragment did not dislocate after plate removal.

3.8 PREPARATION OF TISSUES FOR HISTOLOGICAL ANALYSIS

3.8.1 Protocol for Technovit 9100 - Embedding

The time for fixing is usually between 12 and 48 h. The following method of fixation can be used when detecting antigens or enzymes. After the fixation with 4 % neutral buffered paraformaldehyde and 6 times washing with 0.1 M phosphate buffer pH 7.2 – 7.4, the dehydration and infiltration process is carried out as tabulated below (ingredients listed in table 3). The time of dehydration and infiltration depends on the size of the sample.

Table 3: Technovit® 9100 – embedding: Time plan for dehydration and infiltration of rat femur

Solution	Temperature	Time; Shaking
70 % Ethanol	room temperature	2 days
80 % Ethanol	room temperature	3 days
96 % Ethanol	room temperature	2 days
100 % (1) Ethanol	room temperature	3 days
100 % (2) Ethanol	room temperature	3 days
100 % (3) Ethanol	room temperature	2 days
100 % (4) Ethanol	room temperature	3 days
100 % p.A. Ethanol	room temperature	3 days
Xylene (1)	room temperature	12 hours
Xylene (2)	room temperature	12 hours
Preinfiltration 1	room temperature	3 days
Preinfiltration 2	room temperature	3 days
Preinfiltration 3	4°C	3 days
Infiltration	4°C	6 days
Polymerisation	- 4°C	2 days
	4°C	1 day

Components

1. Destabilising the basic solution

Fill a chromatography column with 25-30 g aluminium oxide and allow the Technovit® 9100 NEW basis solution (Component No. 1) to flow through it. A column prepared as above is sufficient to destabilise 3 – 4 litres of basic solution. Store the destabilised basis solution in portions in corked brown glass bottles. The storage

should be done either at 4°C for shorter time periods or at -15°C to -20°C for longer time period.

2. Preparation of ready-to-use solutions

Preinfiltration 1: Basic solution, stabilised: Xylene 1 : 1

300 ml + 300 ml in a 1000 ml plastic sample tube.

Store in dark at 4°C.

Preinfiltration 2: Basic solution, stabilised + hardener 1

500 ml + 2.5 g hardener powder 1 in a 1000 ml plastic sample tube.

Store in dark at 4°C.

Preinfiltration 3: Basic solution, destabilised + hardener 1

500 ml + 2.5 g hardener powder 1 in a 1000 ml plastic sample tube.

Store in dark at 4°C.

Infiltration: Basis solution, destabilised + PMMA (Granulate 2) + hardener 1

500 ml + 40 g PMMA + 2 g hardener

Use a magnetic stirrer to stir the mixture:

Put 400 ml Basis solution, destabilised in a 1000 ml plastic sample tube; add PMMA portion by portion, stir for 30 minutes, add the hardener 1 and stir until the solution is clear.

Fill to an end volume of 500 ml with Basic solution destabilised.

Store in dark at 4°C.

Polymerisation

Stock solution A: 500 ml Basis solution, destabilised

80 g PMMA

3 g hardener 1

Use a magnetic stirrer to stir the mixture:

Put 400 ml Basic solution, destabilised in a beaker; add PMM portion by portion, stir for 30 minutes, add the hardener 1 and stir until the solution is clear (approximate time is 2 hrs).

Fill to an end volume of 500 ml with basic solution destabilised.

Put in a 500 ml plastic bottle. Seal the bottle with parafilm, cover with aluminium foil and store in dark at -20°C.

Stock solution B: 44 ml Basic solution, destabilised

4 ml hardener 2

2 ml regulator

Put in a 100 ml plastic bottle. Seal the bottle with parafilm, cover with aluminium foil and store in dark at -20°C.

Polymerisation mixture: 9 parts Stock solution A + 1 part Stock solution B

3.8.2 Sectioning of Technovit® 9100 blocks

After embedding, technovit blocks were sectioned into 5 μm thickness with the aid of Kawamoto's film in order to keep the biomaterials intact (Fig. 12). This was done using a counting microtome (Leica RM2155, Germany). The sections were then covered with a butter paper and pressed in a French Press at RT overnight before the staining procedure was applied.

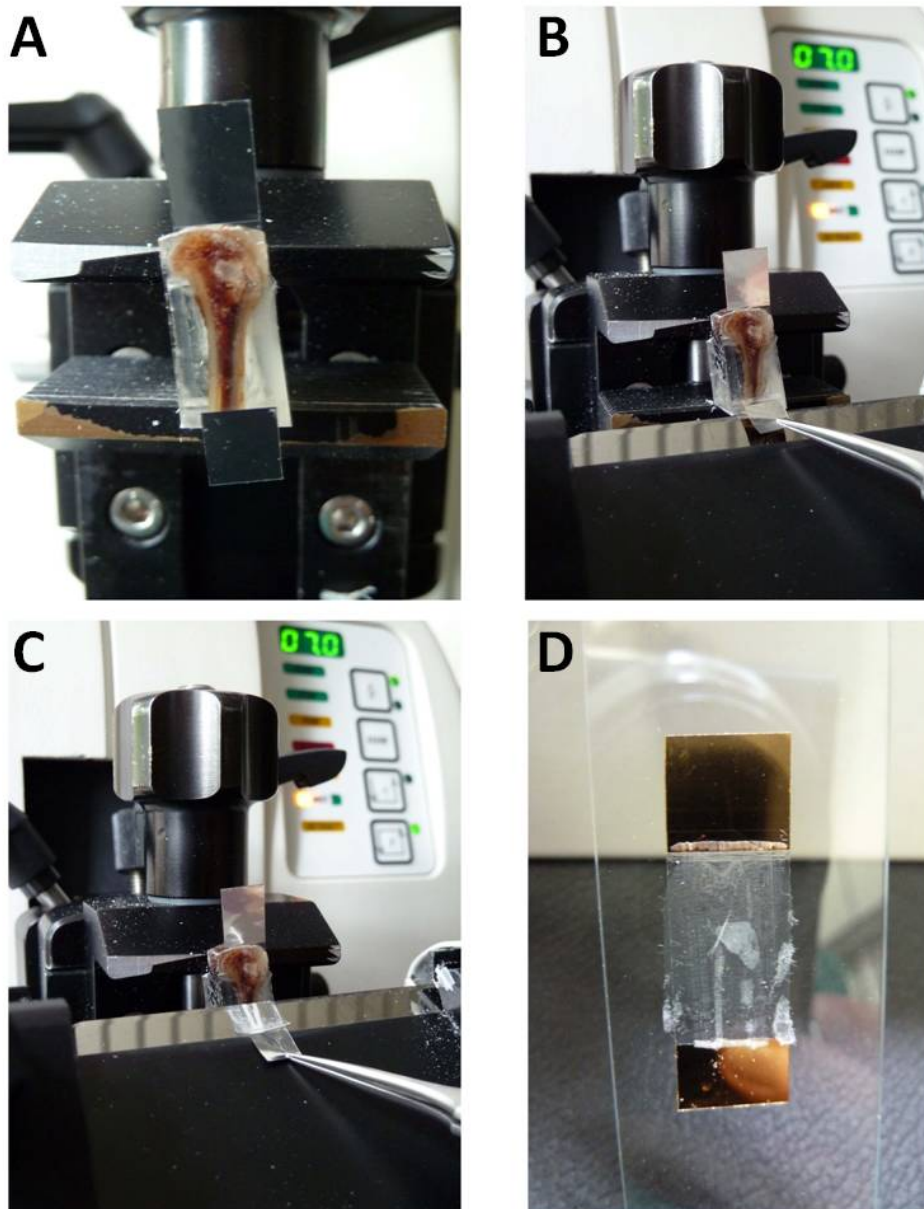


Fig. 12: Sectioning procedure using Kawamoto's film. A: Place the film on the surface of the block, B. C: lower the block slowly over the edge of the knife and grab with pliers during the cutting and D: place the cut on a glass slide adhered to double sided tapes.

3.9 HISTOLOGY

3.9.1 STANDARD STAINING

3.9.1.1 Movat Pentachrome Staining

Movat Pentachrome staining (ingredients listed in table 4) on undecalcified bone sections yield excellent contrast between mineralized and unmineralized compartments of the bone and also reflects the various stages of chondrocyte hypertrophy. It also allows easy distinction of different cell types. It stains the nuclei - black to bluish grey; cytoplasm - red; collagen fibers - yellow; calcified cartilage - green; osteoid - red and the mineralized bone - yellow. This stain is thus useful for the study of the bone healing as it facilitates image analysis for histology and histomorphometrical measurements.

Table 4: Preparation of the ingredients for movat pentachrome staining

MATERIAL	
Alcian Blue	Dissolve 1 g 8GS, (Chroma, 1A288) in 99 ml ddH ₂ O and add 1 ml glacial acetic acid, filtrate before use
Weigert's Iron Hematoxylin	<p>Solution A: (Roth, X906.1) 500 ml</p> <p>Solution B: (Roth, X907.1) 500 ml</p> <p>Working solution: mix A and B 1:1, filtrate before use → Can be stored for 7 days, 4°C.</p>
Brilliant Crocein-Fuchsin	<p>Solution A: 0.1 g Brilliant Crocein R (Chroma 1B109) in 99.5 ml dd. water → add 0.5 ml glacial acetic acid</p> <p>Solution B: 0.1 g acid fuchsin (Merck 7629) in 99.5 ml dd. water → add 0.5 ml glacial acetic acid</p> <p>Working solution: mix A and B 5:1, filtrate before use</p>

PWS	5 % PWS (Merck, 1.00583.0250, 250 g) in ddH ₂ O
Saffron du Gâtinais	Dissolve 6 g (Chroma 5A394) in 100 ml of 100% EtOH and incubate at 50°C for 48 hours. Filtrate before use
Alkaline ethanol	10 ml Ammonium hydroxide 90 ml Ethanol 95%
0.5 % acetic acid	In distilled water: glacial acetic acid (Merck, 1.00063.1000)
Ethanol	Ethanol 522 (with 1 % Petroläther, Stockmeier Chemie1001043227002)
Xylene	(Roth, 9713.3)
Eukitt	(Fluka, 03989)
MEA (2-methoxyethyl)-acetate:	(Merck, 8.06061.100)

Protocol

1. Deplastify sections via MEA 3 x 5 minutes and dehydrate using a descending percentage of ethanol 100%, 96%, 80%, 70% for 5 minutes each.
2. Rehydrate in distilled water for 2 x 5 minutes
3. Stain in Alcian blue for 30 minutes
4. Wash in running tap water for 5 minutes
5. Stain in alkaline ethanol for 1 hour
6. Wash in running tap water for 5 minutes
7. Rinse in distilled water
8. Place in the Weigert's iron hematoxylin stain for 14 minutes (stains connective tissues)
9. Rinse in distilled water
10. Wash in running tap water for 6 minutes
11. Place in Brilliant Crocein-Fuchsin solution for 6 minutes
12. Place in 0.5% aqueous acetic acid for 1 minute

13. Place in 5% PWS (phosphor/ Tungsten mix solution). Until collagen is clear and ground substance is blue
14. Place in 0.5% aqueous acetic acid for 2 minutes with shaking
15. Place in three changes of absolute ethanol for 2 minutes each
16. Place in the Saffron du Gâtinais dye to stain collagen and connective tissue for 10 minutes
17. Dehydrate quickly in absolute ethanol, 3 changes. Then place it in absolute ethanol for 2 minutes
18. Clear in xylene, two changes for 5 minutes each
19. Cover slip slides using Eukitt

3.9.1.2 Toluidine blue staining

The toluidine blue staining (ingredients listed in table 5) is one of the standard staining for microscopic examination of the bone. It stains nucleic acids blue. Due its property of metachromasia it stains the polysaccharides purple and also increases the sharpness of histological slides due to high contrast. It stains the nuclei - blue, mineralized bone - light purple, osteoid - colorless or pale blue and chondrocytes - purple. The staining was used for histological analysis.

Table 5: Preparation of ingredients for toluidine blue staining

MATERIAL	
Solution A	Dissolve 8 g Natrium Tetraborate, (Merck, 1.06306.0250) in 8 g toluidine blue O (Chroma, 1B 481) 800 ml ddH ₂ O for 15 minutes using a magnetic stirrer
Solution B	2 g Pyronin G (Merck, 7518) in 200 ml ddH ₂ O for 15 minutes using a magnetic stirrer
Working solution	mix A and B 1:1 and filter twice

Protocol

1. Deplastify sections via MEA 3 x 5 minutes and dehydrate using a descending percentage of ethanol 100%, 96%, 80%, 70% for 5 minutes each

2. Rehydrate in distilled water for 2 x 5 minutes
3. Stain with undiluted filtered toluidine blue for 10 seconds.
4. Dehydrate gradually along an increasing gradient of alcohol 70%, 80%, 96%, 100% quickly
5. Clear in xylene, two changes for 5 minutes each
6. Cover slip slides using Eukitt

3.9.1.3 Von Kossa-Van Gieson staining

Osteoid is the unmineralized and immature, organic portion of the bone matrix. It is secreted by the osteoblasts which eventually become mineralized to form the new bone tissue. A lack of proper nutrient minerals or osteoblast dysfunction hampers the mineralization process of the osteoblasts which in turn accumulates. To detect osteoid in the technovit sections, a double staining of Von Kossa-Van Gieson (ingredients listed in table 6) was thus used. The stain principle of Von Kossa is a precipitation reaction in which the silver ions react with phosphate (not calcium) in the presence of acidic material. Photochemical degradation of silver phosphate to silver then occurs under light illumination. The Van Gieson on the other hand is a mixture of picric acid and acid fuchsin. It is the simplest method of differential staining of collagen and other connective tissue. Thus such a dual staining stains the osteoid red and mineralized tissue black.

Table 6: Preparation of the ingredients for Von Kossa-Van Gieson staining

MATERIAL	
Silver nitrate solution	Dissolve 3 g silver nitrate (Merck, 1512) in 100 ml ddH ₂ O
Sodium-carbonate formaldehyde solution	10g Na ₂ CO ₃ (Merck 6392) with 25 ml of 37% formaldehyde solution to 100 ml ddH ₂ O
Van Gieson's mixture	Chroma 2E050
Sodium thiosulfate	5 g Na ₂ S ₂ O ₃ (Merck, 6516) in 100 ml ddH ₂ O
Methyl green	1g in 100ml of 25% alcohol.

Protocol

1. Deplastify sections via MEA (2-methoxyethylacetat) [Merck 806061] 3 x 5 minutes and dehydrate using a descending percentage of ethanol 100%, 96%, 80%, 70% for 2 minutes each
2. Rehydrate in distilled water for 2 x 5 minutes
3. Stain in 3% aqueous solution of silver nitrate (AgNO_3) for 10 minutes
4. Rinse 3 x in distilled water
5. Incubate in sodium carbonate solution for 2 minutes
6. Rinse in running tap water for 10 minutes
7. Allow it to stay in 5% sodium thiosulfate solution ($\text{Na}_2\text{S}_2\text{O}_3$) for 5 minutes
8. Submerge in distilled water to stop the reaction.
9. Counter-stain by soaking in methyl green for 15 minutes
10. Rinse in running tap water for 10 minutes
11. Rinse 5 x in distilled water
12. Place in the Weigert's iron hematoxylin stain for 6 minutes
13. Rinse in running tap water for 10 minutes
14. Place in Van Gieson's mixture for 3 minutes
15. Dehydrate by rinsing in 96% ethanol
16. Place in absolute ethanol, two changes for 1 minute each
17. Clear in xylene, two changes for 5 minutes each
18. Cover-slip after mounting with DEPEX (VWR 361254 D)

3.9.2 Immunohistochemical staining

Immunohistochemistry detects antigens (e.g., proteins) on cell surfaces or tissue sections by exploiting the principle of antibodies binding specifically to antigens in biological tissues. This provides a scope for qualitative evaluation of both specific cell types and matrix proteins. A colored reaction occurs depicting the antigen-antibody complex. Generally this technique employs unlabeled primary antibody, in which sections are incubated for 1 hour (may vary). Sections are then incubated with a normal serum originated from the same animal species. This is to avoid unspecific binding of the secondary antibody. The incubation with the secondary antibody is then carried out for 30 minutes following which the incubation with avidin and biotinylated horseradish peroxidase macromolecular complex is performed (Vectastain Elite ABC KIT, VECTOR,

PK-6100). NovaRED substrate kit for peroxidase (Vector, SK-4800) was then used as a substrate solution which catalyzes the hydrolysis of a variety of phosphate containing substances producing a colored insoluble precipitate thus visualizing the antigen presence (Fig.15). For a better representation, tissue was counter-stained with hematoxylin (Shandon Instant Hematoxylin, 6765015).

In some cases in this study, the Envision+System (Dako, K4006), HRP IHC staining technique was employed. This system is a two step process where the secondary antibody is conjugated with the HRP labeled polymer. The labeled polymer is devoid of avidin or biotin and thus avoids nonspecific staining resulting from the endogenous avidin-biotin activity (Vectastain Elite ABC KIT, VECTOR, PK-6100). In principle, endogenous peroxidase activity is quenched by incubating the specimen for 45 minutes with Peroxidase Block (6% H₂O₂). The specimen is then incubated with an appropriately characterized and diluted primary antibody, followed by incubation with the labeled polymer. Staining was completed by 5-10 minute incubation with 3, 3'-diaminobenzidine (DAB+) substrate-chromogen which results in a brown colored precipitate at the antigen site.

3.9.2.1 Bone-morphogenetic protein 2- BMP2

Bone morphogenetic protein 2, belongs to the transforming growth factor-beta (TGFB) super family, plays an important role in the development of bone and cartilage. BMP2 is known to stimulate the production of bone. It is involved in the hedgehog pathway, TGF beta signaling pathway and in cytokine-cytokine receptor interaction. BMP2 is osteo-inductive in nature. It has potential to induce osteoblast differentiation in a variety of cell types. Sections were treated with BMP2 primary antibody (Acris AP20597PU-N) at a concentration of 1:200 in Dako Antibody Diluent with background reducing components (S3022); with protocol for IHC using the ABC system (Vectastain Elite ABC KIT, VECTOR, PK-6100).

3.9.2.2 Osteocalcin

Osteoblasts form woven bone during the reparative phase and compact bone in the remodeling phase of bone healing. Discrepancies in the count and location of osteoblasts affect bone healing. Osteocalcin is a protein secreted by osteoblasts and belongs to the non-mineralized bone extracellular matrix. It is often used as a marker for the bone

formation process. Also known as bone gamma-carboxyglutamic acid-containing protein (BGLAP), osteocalcin is a non-collagenous protein found in bone. It plays an important role in the body's metabolic regulation and is pro-osteoblastic, or bone-building. It is also implicated in bone mineralization and calcium ion homeostasis. Sections were treated with osteocalcin (Monoclonal Anti-human Osteocalcin, R&D, MAB1419) primary antibody using a dilution of 1:500 in Dako Antibody Diluent with background reducing components with protocol for IHC using the ENVISON system.

3.9.2.3 Osteoprotegerin

Osteoprotegerin (OPG), also known as osteoclastogenesis inhibitory factor (OCIF), or tumor necrosis factor receptor super family member 11B (TNFRSF11B), is a protein that in humans is encoded by the *TNFRSF11B* gene. It is a decoy receptor for the receptor activator of nuclear factor kappa B ligand (RANKL). By binding RANKL, OPG inhibits nuclear kappa B (NF- κ B) which is a central and rapid acting transcription factor for immune-related genes, and a key regulator of inflammation, innate immunity, and cell survival and differentiation. OPG can reduce the production of osteoclasts by inhibiting the differentiation of osteoclast precursors into mature osteoclasts and also regulates the resorption of osteoclasts. OPG binding to RANKL on osteoblasts, blocks the RANKL-RANK ligand interaction between osteoblast cells and osteoclast precursors. This has the effect of inhibiting the differentiation of the osteoclast precursor into a mature osteoclast. Sections were treated with OPG (Rabbit Anti-Osteoprotegerin Polyclonal Antibody; Abbiotec; 250800) primary antibody using a dilution of 1:300 in Dako Antibody Diluent with background reducing components with protocol for IHC using the ABC system.

3.9.2.4 Receptor activator of nuclear factor kappa-B ligand, RANKL

Receptor activator of nuclear factor kappa-B ligand (RANKL), also known as tumor necrosis factor ligand super family member 11 (TNFSF11), TNF-related activation-induced cytokine (TRANCE), osteoprotegerin ligand (OPGL), and osteoclast differentiation factor (ODF), is a protein that in humans is encoded by the *TNFSF11* gene. It is needed for adequate bone metabolism. It is a surface-bound molecule (also known as CD254) found on osteoblasts which serves to activate osteoclasts. Osteoclastic activity is triggered via the osteoblasts surface-bound RANKL activating the osteoclasts surface-bound receptor activator of nuclear factor kappa-B (RANK). Sections were treated with 0.6 μ g/ml of RANKL primary antibody (Polyclonal Antibody to CD254/

RANKL-Aff-Purified, Acris, AP30826PU-N) with protocol for IHC using the ABC system.

3.9.2.5 Platelet endothelial cell adhesion molecule, PECAM-1

Platelet endothelial cell adhesion molecule (PECAM-1) also known as cluster of differentiation 31(CD31) is a protein encoded by the *PECAM1* gene. It is found on the surface of endothelial cells and intercellular junctions. The encoded protein is a member of the immunoglobulin super family and is likely to be involved in new blood vessel formation. CD31 immunohistochemistry can thus be used to demonstrate angiogenesis. Sections were treated with PECAM-1 primary antibody (CD31 Antibody, Abbiotec, 250590) using a dilution of 1:350 in Dako Antibody Diluent with background reducing components with protocol for IHC using the ABC system.

3.9.2.6 Alpha smooth muscle actin, α -SMA

Alpha-actin-2 also known as actin, aortic smooth muscle or alpha smooth muscle actin (α -SMA, SM actin, alpha-SM-actin, ASMA) is a protein that in humans is encoded by the *ACTA2* gene. Alpha-smooth muscle actin (α -SMA) is commonly used as a marker of myofibroblast formation. It is used as a marker to detect the smooth muscle actin and myofibrils surrounding the blood vessels. Sections were treated with α -SMA primary antibody (Monoclonal mouse Anti-Human Smooth Muscle Actin, Dako, M0851) using a dilution of 1:1000 in Dako Antibody Diluent with background reducing components with protocol for IHC using the ENVISON system.

3.9.2.7 ED1

ED1 is a monoclonal antibody that recognizes a single chain heavily glycosylated protein of 90-110 kDa that is expressed on the lysosomal membrane of phagocytes as well as on the cell surface (weak expression). This antigen is the rat homologue of human CD68. The expression of this antigen in cells increases during phagocytic activity. The antigen is expressed by the majority of tissue macrophages and hence makes the monoclonal antibody a useful marker for rat macrophages. Sections were treated with ED-1 primary antibody (Mouse Anti-Rat Monocytes/Macrophages Monoclonal Antibody) using a dilution of 1:3000 in Dako Antibody Diluent with background reducing components with protocol for IHC using the ENVISON system.

Table 7: Preparation of the ingredients for immunohistochemistry

MATERIAL	
Tris-NaCl-Buffer (TBS)	(0.15 mol/l NaCl, 0.05 mol/l Tris/HCl) for 10 x: 60.57 g (0.5 mol/l) Tris Base 87.66 g (1.5 mol/l) NaCl in 1000 ml dH ₂ O Dissolve Tris Base and NaCl in 800 ml dH ₂ O, adjust pH with 25 % hydrochloric acid till it reaches 7.4 and make up to 1000 ml.
TBS-Buffer 1 x	Dilute the above in the ratio of 1:10 with distilled water
Tris-Washbuffer	TBS 1 x, 0.025 % Triton-X-100 To 100 ml TBS 10 x add 0.25 g of Triton X-100 and make the volume up to 1000 ml with dH ₂ O

Protocol for IHC using the ABC system

1. Deplastify sections via MEA (2-methoxyethylacetat) [Merck 806061] 3 x 5 minutes and dehydrate using a descending percentage of ethanol 100%, 96%, 80%, 70% for 5 minutes each
2. Rinse 3 x 5 min in wash-buffer
3. Dry the slide on the back and around the section, mark around the section with PAP Pen.
4. Add tested dilution of antibody in background reducing dilution buffer (DAKO).
5. Incubate over night at 4°C in humid chamber.
6. Discard the antibody. Wash every slide separately with washing buffer with disposable pipette, avoid contamination of different antibodies.
7. Rinse 3 x 5 min in wash-buffer
8. Incubate in secondary goat anti rabbit antibody 1:500 (DAKO, biotinylated) at RT for 30 minutes. Dilution of antibody is made in 1 % BSA in TBS with 1:8 serum of species of interest
9. Rinse 2 x 5 min in wash-buffer
10. Incubate with Vectastain ELITE ABC (Fa. Vector, PK 6100) in humid chamber for 30 minutes at RT
11. Rinse 2 x in wash-buffer

12. Rinse 5 min in dH₂O
13. Stain with Nova Red: (Substrate kit for peroxidase, Vector) for 5 min at RT
14. Rinse 5 min in ddH₂O followed by rinsing in dH₂O for 2 x 5 min
15. Counter stain with hematoxylin (Shandon, Diluted 1 + 3 with double distilled water) for 5 sec at RT
16. Rinse 10 minutes in running tap water
17. Rehydrate using an ascending percentage of ethanol 70%, 80%, 96%, 100% for 5 minutes each
18. Clear in xylene, two changes for 5 minutes each
19. Cover-slip after mounting with DEPEX (VWR 361254 D)

Protocol for IHC using the ENVISON system

1. Deplastify sections via MEA (2-methoxyethylacetat) [Merck 806061] 3 x 5 minutes
2. Dehydrate in 100% Acetone 2 x 5 minutes
3. Rehydrate in Acetone + Wash-buffer (1:1) 2 x 5 minutes
4. Rinse 3 x 5 min in wash-buffer
5. Block the endogenous peroxidase using 6 % H₂O₂ in wash-buffer for 5 minutes at RT
6. Rinse 3 x 5 min in wash-buffer
7. Dry the slide on the back and around the section, mark around the section with PAP pen
8. Add tested dilution of antibody in background reducing dilution buffer (DAKO). Incubate for 1 hour at RT in humid chamber
9. Discard the antibody. Wash every slide separately with washing buffer with disposable pipette, avoid contamination of different antibodies
10. Rinse 3 x 5 min in wash-buffer
11. Treat the sections with serum from the animal of the same species (12.5 % rat serum [Sigma, R9759] in 1 % BSA in TBS 1 x) in order to avoid non-specific staining. This is done at RT for 15 min. Tapp off the solution
12. Incubate in the labeled polymer for 30 mins at RT in a humid chamber

13. Rinse 3 x 5 min in wash-buffer and incubate in DAB + substrate at RT for 5-15 minutes
14. Rinse in ddH₂O for 10 seconds using a disposable pipette and then rinse 4 x 5 minutes in dH₂O
15. Counter stain with hematoxylin (Shandon, Diluted 1 + 3 with double distilled water) for 30 seconds at RT
16. Rinse 10 minutes in running tap water
17. Rehydrate using an ascending percentage of ethanol 70%, 80%, 96%, 100% for 5 minutes
18. Clear in xylene, 2 x 5 minutes and cover-slip with DEPEX (SERVA, 18243.02)

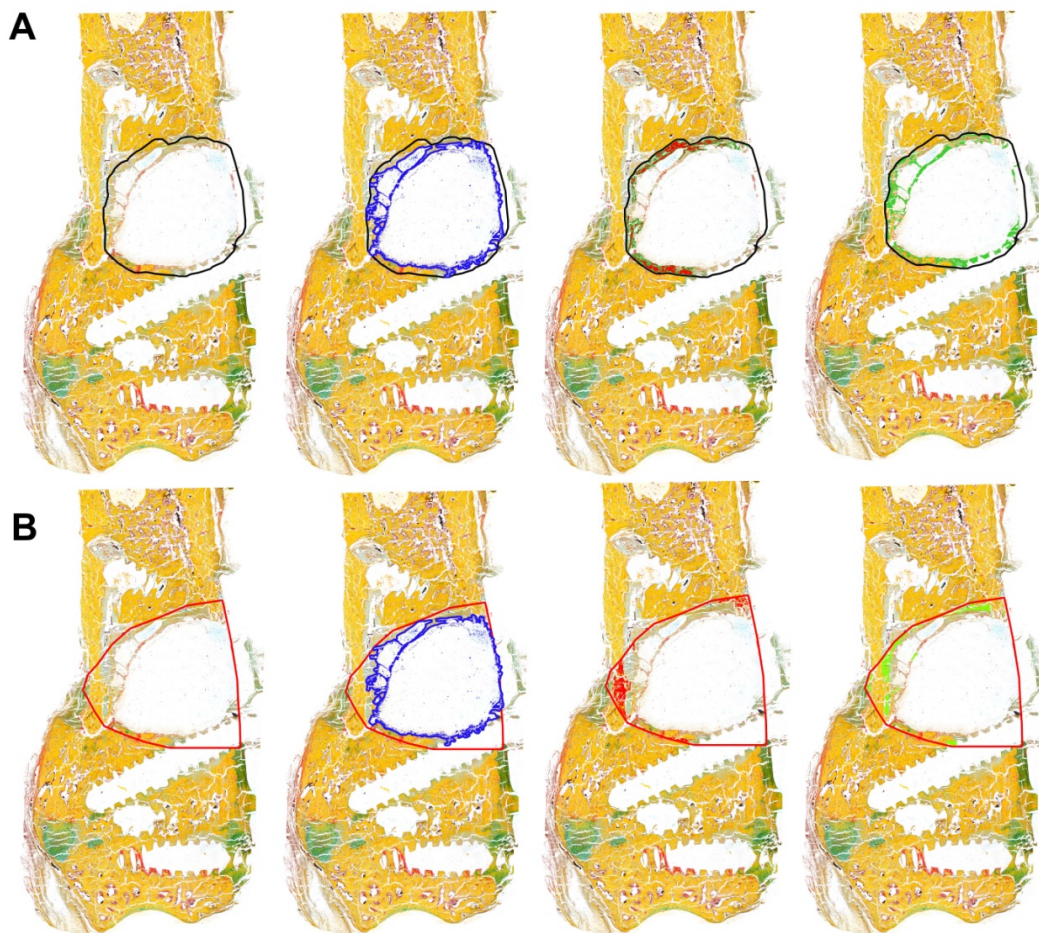


Fig. 13: Histomorphometric analysis using Adobe Photoshop CS6 A) Measurement of region of interest 1 (ROI1), implant, bone and unmineralized tissue area in 1st ROI. B) Measurement of region of interest 2 (ROI2), implant, bone and unmineralized tissue area in 2nd ROI.

3.10 HISTOMORPHOMETRY

Standardized histomorphometrical analyses are essential to determine the therapeutic efficacy and address cellular and tissue responses during the bone repair process. These results in turn can be integrated with molecular, immunohistochemical and TOF-SIMS analysis. In this study the movat-pentachrome staining was thus used for semi-automated measurements represented as BV/TV (unit mm²). The VKVG staining was used for the measurement of the unmineralized tissue (UT/TV in mm²). Images were taken using a light microscope (Axioplan 2 imaging with photomodule Axiophot 2, Carl Zeiss, Jena, Germany) using a Leica DC500 camera (Leica, Bensheim, Germany), acquired with Leica IM1000 software and processed using Adobe Photoshop version CS6 (Adobe, Karlsruhe, Germany). The histomorphometry used in this study includes a semi-automated quantification, sorts different tissues according to the color. In this measurement, yellow represents the ossified issue (bone) and green implies unmineralized tissue (cartilage in green and osteoid in red). The yellow colored tissue was not specific for ossified tissue, mineralized patches were also seen in the unmineralized tissue (mostly in the regions of high chondrocyte activity) and vice versa. Therefore, the calcified regions and the cartilage tissue were hand contoured and assessed (Fig. 13).

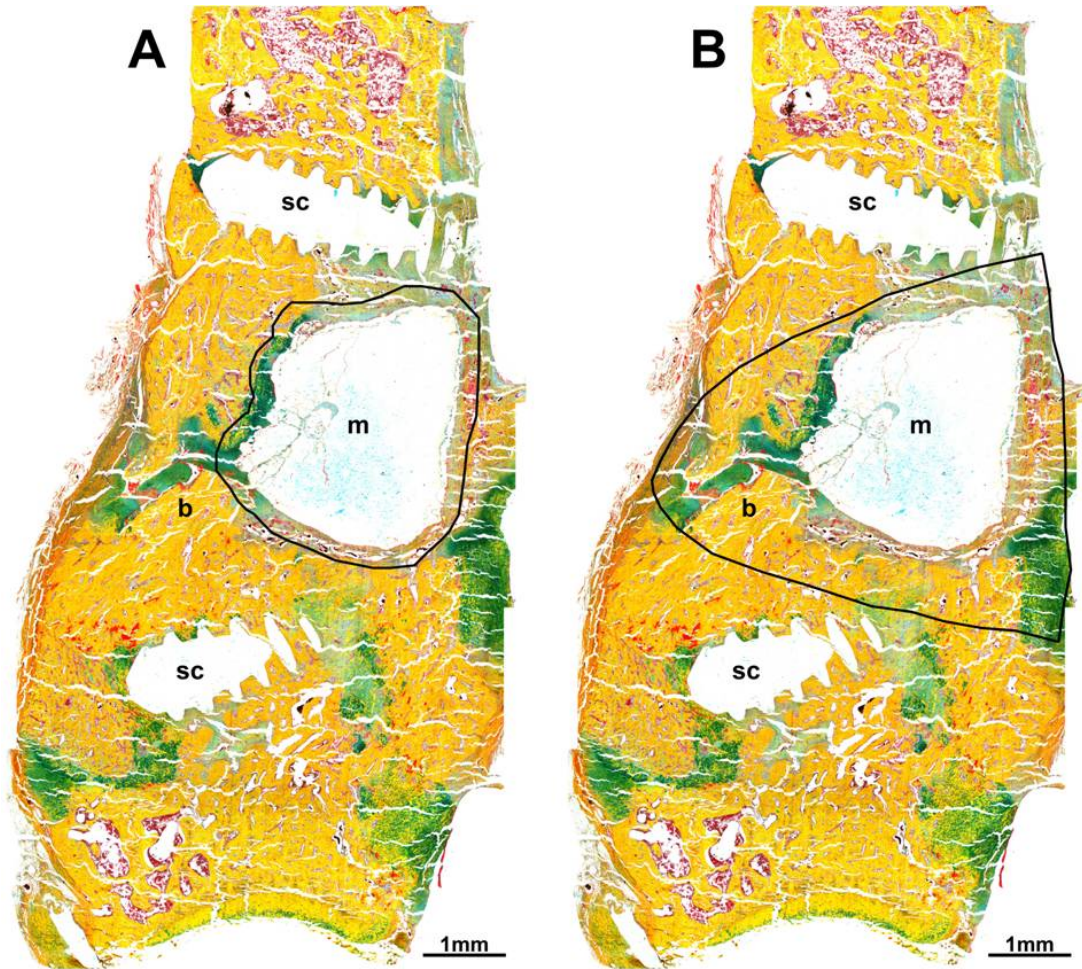


Fig. 14: Schematic diagram of a movat-pentachrome staining of undecalcified technovit sections with the two regions of interest (ROI's) for quantitative histomorphometric evaluation: First ROI (within black outline) was used to evaluate the new bone formation at the tissue-implant interface (A). The second ROI (enclosed within black outline) comprises the entire defect region to examine the new bone formation in the initial fracture defect (B). Specific regions are labeled as follows: b, bone; m, material; sc, screw.

Two regions of interest (ROI's) were used for histomorphometric evaluations. The first ROI was made by directly tracing over the material followed by a 100 pixels increase to include the biomaterial tissue interface (Fig. 14A). The second ROI comprised the entire initial wedge-shaped osteotomized defect area (4 mm in the lateral side and 0.35 mm in the medial side of the left femur) to assess the new bone formation within the former fracture defect area (Fig. 14B). With the help of Adobe Photoshop CS6, the measurements for area of bone, ROI's, implant, and the void were made respectively to determine bone versus tissue ratio (BV/TV). In principle, the analysis depends on the measuring of pixels of the same color, which were then scaled as area (unit mm^2). A

count for macrophages (ED1 i.e. Macrophages/TV) positive cells was also performed. The consecutive sections were then used for all described methods. The measurements were done blind folded with regards to the test groups. The shifts in the cortices were also taken into consideration. The animals thus measured by histomorphometry had no plate breakages.

3.11 mRNA PREPARATION AND EXPRESSION ANALYSIS

3.11.1 Samples

Left femurs obtained 6 weeks post-osteotomy were snap frozen in *RNAlater*® RNA stabilization solution (Ambion, CA, USA) and stored at - 80°C until RNA isolation for expression analysis of the target genes. For RNA isolation the area of interest chosen comprised the original defect area (containing CPC and SrCPC implants respectively) along with connecting bone or tissue.

3.11.2 Quantitative RT-PCR

The expression analysis was carried out for the following target genes.

1. Alkaline phosphatase (ALP) as an osteoblast marker which helps in mineralization of the bone.
2. Osteocalcin (OCN), a non-collagenous protein secreted by osteoblasts which plays a vital role in the mineralization and calcium homeostasis in the bone.
3. Collagen type 10 alpha 1 (Col 10a1), a marker for hypertrophic chondrocytes.
4. Runt-related transcription factor 2 (Runx 2), an essential protein for osteoblastic differentiation.
5. Collagen type I alpha1 (Col1a1) which encodes the major component of type I collagen, the fibrillar collagen found in most connective tissues, including cartilage.
6. Beta-2 microglobulin (B2M) was used as reference gene.

Table 8: Primer sequences

Target gene	Sense, antisense primers (5'-3') sequence	Amplicon length (bp)
B2M	TGT CTC AGT TCC ACC CAC CT GGG CTC CTT CAG AGT GAC G	191
OCN	GAG GGC AGT AAG GTG GTG AA GTC CGC TAG CTC GTC ACA AT	135
ALPL	ATC GGA CCC TGC CTT ACC CTC TTG GGC TTG CTG TCG	78
Runx2	CCA TAA CGG TCT TCA CAA ATC C GCG GTC AGA GAA CAA ACT AGG	137
Col1a1	TCC TGA CGC ATG GCC AAG AA CAT AGC ACG CCA TCG CAC AC	145
Col10a1	CAT GTG AAG GGG ACT CAC G GAA GCC TGA TCC AAG TAG CC	101

Total RNA of the area of interest in control group (empty defect, 4 mm), CPC and SrCPC was isolated using the Lipid Tissue Mini Kit (Qiagen, Hilden, Germany) according to the manufacturer's protocol. The quantity and quality of the RNA was measured using the Nanodrop 2000[®] (Thermo scientific, Schwerte, Germany) using an optical density of 260/280 nm. The samples had an average RNA concentration between 113 ng/μl and 800 ng/μl and the average of the 260/280 nm ratio varied from 2.01 to 2.13.

In 0.5 μg of RNA contaminations of genomic DNA were removed and RNA was reverse-transcribed with the Quantitect[®] Kit (Qiagen) as described in the manufacturer's protocol.

3.11.3 Real-time RT-PCR

Quantitative RT-PCR was performed using the LightCycler detection system (Roche, Mannheim, Germany) in combination with the Quantifast SYBR Green PCR mastermix[®] (Qiagen, Hilden, Germany) for Runx-2, ALPL, OCN, Col1a1, Col10a1 primers as well as B2M reference gene-primers (Table. 8). For RT-PCR, 1 μl cDNA, 5 μl Quantifast SYBR Green PCR Mastermix x PCR mastermix and 0.1 μl of each primer (20 μM) supplemented with RNase free H₂O to a final volume of 10 μl was used. The thermal

cycling program with Quantifast Master mix[®] comprised one initial denaturation step of 5 min at 95°C followed by 40 cycles of 10 s at 95°C and 30 s at 60°C. Finally a melting curve was performed to verify the PCR product's specificity and identity by increasing the temperature from 60°C to 95°C in steps of 0.1°C every 1 s.

All analyses were done in duplicates and the means were used for further calculations. The following were used as controls: (a) every sample processed without reverse transcription (–RT) to control for contamination with genomic DNA, (b) RT-PCR runs without template (H₂O). Specificity of amplification was confirmed by melting curve analyses and 2 % agarose gel electrophoresis (Fig. 15).

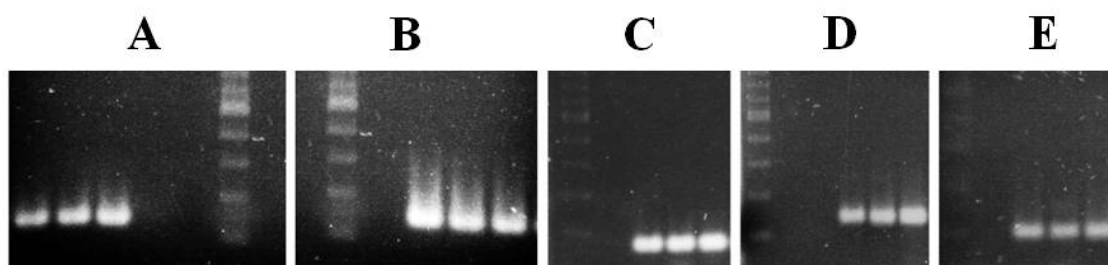


Fig. 15: Qualitative PCR for a) OCN (135bp) b) Col1a1 (145bp) c) ALP (78bp) d) Runx2 (137bp) and e) Col10a1 (101bp) run with a 100bp ladder.

3.11.4 Data processing

The amplification efficiency for the tested primer pairs varied from 1.93 to 2.00, which are the expected values for compared genes. The relative gene expression ratio for each gene was calculated using the REST[®] method, based on the PCR efficiency (E) and Ct of a sample compared with the control, and expressed in comparison to the reference gene, according to Pfaffl's mathematical model: $\text{Ratio} = (E_{\text{target}})^{\Delta\text{Ct}_{\text{target}} (\text{control-sample})} / (E_{\text{ref}})^{\Delta\text{Ct}_{\text{ref}} (\text{control-sample})}$.

3.12 TOF-SIMS MEASUREMENTS

All of the SIMS measurements were done with a TOF-SIMS 5-100 machine (IONTOF Company, Münster, Germany). The machine is equipped with a 25 kV Bi-cluster Primary Ion gun, 2 KV Cs⁺ and O₂⁺ sputter guns and a 10 kV C₆₀-gun. For data evaluation the Surface Lab 6.3 software (IONTOF Company, Germany) was used. The PCA analysis was done with the NESAC/BIO MVA Toolbox, University of Washington. For the depth profiles of the cements Bi⁺-ions were used as primary ions and 1 or 2 keV oxygen ions

for sputtering. The primary ion gun was operated in the high current bunched mode (hc-bu). The analysis area was $150 \times 150 \mu\text{m}^2$, and the sputter area being $250 \times 250 \mu\text{m}^2$.

The measurements used for the Principle Component Analysis (PCA) were obtained in the hc-bu mode using Bi_3^+ as primary ions for an area of $500 \times 500 \mu\text{m}^2$ with 128×128 pixels and 100 scans applying a primary ion dose of $<10^{12}$ ions cm^{-2} to maintain static conditions. From each sample 7 spots were collected in the positive as well as in the negative ion mode before and after having been immersed to obtain reproducibility within and between the samples. Positive and negative ion mass spectra were calibrated using H^+ , H_2^+ , CH_3^+ , C_2H_5^+ , C_3H_7^+ and H^- , H_2^- , C^- , C_2^- , C_3^- . The mass resolution ($m/\Delta m$) at the C_2H_5^+ ($m/z = 29$) or C_2H^- ($m/z = 25$) peak was above 4000 for all measurements in the positive ion mode and above 3000 for all measurements in the negative ion mode. The data were normalised to the sum of selected peaks and scaled by SQRT-mean centring. Peak selection was done manually considering especially inorganic and organic mass signals derived typically from calcium phosphates and amino acids.

Sample imaging of cells cultured on the cements was performed within an area of $200 \times 200 \mu\text{m}^2$ to $250 \times 250 \mu\text{m}^2$ using Bi^{3+} cluster ions. 100 scans were taken and each scan provided an image with 128×128 pixels. Images were recorded using the hc-bu mode ($m/\Delta m$ FWHM > 4000). To compare the TOF-SIMS images, optical images were taken using the 2D mode of a PLu neox 3D optical profiler (Sensofar, Terrassa, Spain) equipped with a blue LED (460 nm). The mass images of the bone cross sections were obtained by so called stage scans. The scans were done in hc-bu mode with Bi_3^+ as primary ions. The pixel density was 120/mm with a patch size of $300 \times 300 \mu\text{m}^2$. More detailed images of smaller areas were also done with Bi_3^+ in low current bunched (lc-bu) mode with lateral resolutions of $2 \mu\text{m}$. In this case the pixel density was 1000/mm.

3.13 STATISTICAL ANALYSES

The test for significance was analysed using both Statistical Package PASW 21.0 (SPSS Inc., USA) and GraphPad Prism (GraphPad Software, Inc., USA). Histomorphometric results are presented as mean \pm standard error of the mean (SEM). The Student's t test and Mann-Whitney U test were used to check for the significance level. Data were not found normally distributed and Mann-Whitney U unpaired nonparametric data with Bonferroni correction was used. Gene expression analysis is presented as box plots and

was analyzed using REST-method. P-values of less than 0.05 were chosen to indicate significance. The Student's *t* test can be used to determine if two sets of data are significantly different from each other. The Mann–Whitney *U* test (also called the Mann–Whitney–Wilcoxon (MWW), Wilcoxon rank-sum test, or Wilcoxon–Mann–Whitney test) is a non-parametric test of the null hypothesis that takes the difference between the mean ranks as statistics. The Bonferroni correction is a method used to counteract the problem of multiple comparisons. All the results are shown as Mean \pm SD. Statistical analysis were performed by Student's *t* test, with $p < 0.05$ (*) considered significant (** $p < 0.01$, *** $p < 0.001$).

4. RESULTS

4.1 INDUCTION OF OSTEOPOROSIS

4.1.1 Decreased BMD in the OVX group in comparison to the SHAM

BMD results are expressed as [Mean \pm SD] and were measured at the baseline (day of bilateral ovariectomy) and after three months of osteoporosis induction (day of femur osteotomy). Two anatomical sites: spine and femur were taken into account, being the prominent sites affected during osteoporosis. At baseline no significant difference in BMD was found in either site between the OVX and SHAM groups (Fig. 16). BMD values at the spine in the SHAM group were [0.13 \pm 0.01] compared to [0.13 \pm 0.01] in the OVX group. Whereas at the femur, the values were [0.19 \pm 0.04] for the SHAM group and [0.17 \pm 0.01] for the OVX group. On the other hand, BMD measured 3 months after ovariectomy at the spine was [0.17 \pm 0.01] in the SHAM group and [0.12 \pm 0.01] in the OVX group, where a statistically significant decrease in the OVX group was seen when compared to the SHAM group ($p < 0.05$). Similarly, BMD at the femur was found to be significantly lower in the OVX group [0.28 \pm 0.02] when compared to the SHAM group [0.34 \pm 0.027] ($p < 0.05$).

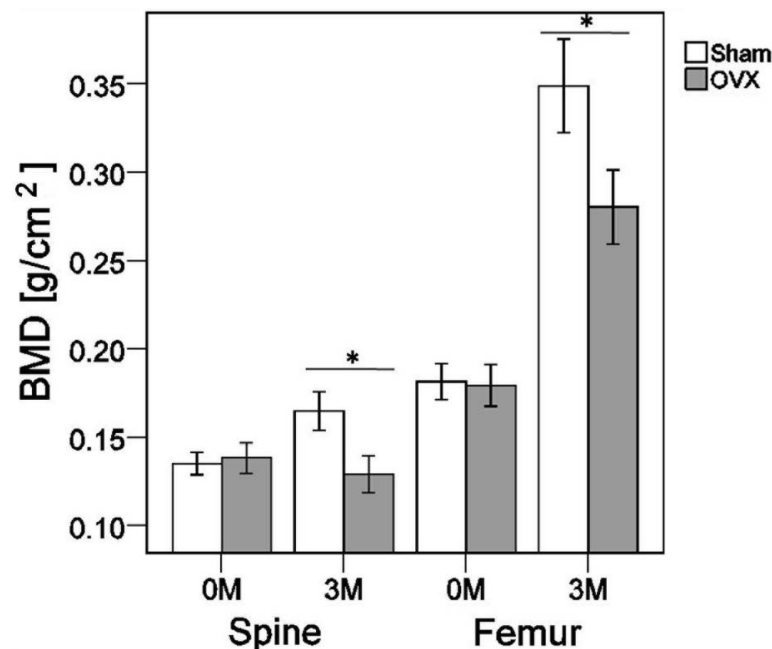


Fig. 16: BMD in spine and femur in SHAM and OVX animals. ($p \leq 0.05$ calculated with Mann – Whitney U test, whiskers exhibit standard error of mean).

4.2 CLINICAL OBSERVATIONS

The survival number in the entire observation period was 11 animals for the control, 15 animals for the SrCPC and 13 animals for the CPC group. Three animals were lost during anesthesia, one animal died directly after ovariectomy and two other rats later after femur surgery. Thus, 39 out of the 45 animals survived which were then used for further assessment. In these animals the clinical healing of the surgical wounds and recovery of mobility was monitored and normal progress was seen with no uneventful visible adverse effects in all the groups until the end of the observation period at 6 weeks post femur surgery. At the time of femur harvesting, plate breakage was noted in 2 out of the 11 animals in the control group, 4 out of 15 animals in the SrCPC group and 7 out of 13 animals in the CPC group without any statistically significant differences between the groups (empty defect vs. CPC: $p=0.58$; empty defect vs. SrCPC: $p=0.61$; SrCPC vs. CPC: $p=0.06$). In total there were 74.4 % of intact plates in all the groups. The empty defect group had 18.2 % plate breakage ($p=0.58$ compared to CPC group, and $p=0.61$ compared to SrCPC group). In the CPC group there was 53.8% plate breakage ($p=0.057$ compared to the SrCPC group which had 26.7% plate breakage).

4.3 DESCRIPTIVE HISTOLOGY

4.3.1 New bone formation

The implanted biomaterial was found in the correct position in all the animals where the wedge shaped defect was created initially, at the distal metaphyseal femur region in case of the SrCPC and CPC group. (Fig. 17B, C). With respect to fragmentation of the material, it was seen in 5 of 7 animals in the SrCPC group. In all these animals, the fragmented biomaterial was surrounded by new bone, osteoid, cartilage and fibrous tissue at the interface region (Fig. 17D, E). However in the CPC group only 2 out of 7 animals showed fragmentation of the material of which only one had very little fragmentation and was surrounded mostly by fibrous tissue. The empty defect showed mainly connective and granulation tissue (Fig. 17A).

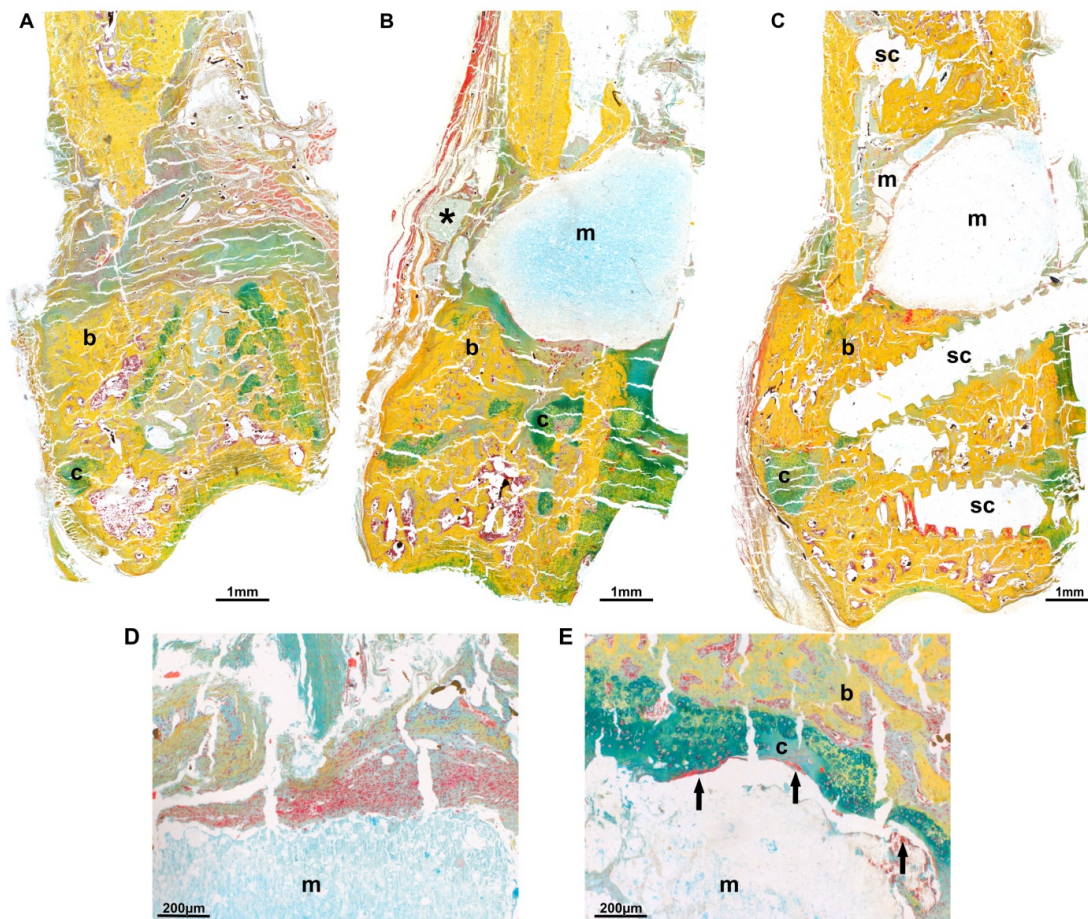


Fig. 17: Movat-pentachrome photomicrographs showing overview of histological sections of empty defect (A), CPC (B) and SrCPC (C). Enlarged images at the biomaterial interface depicting large amounts of fibrous connective tissue and proliferating chondrocytes in the CPC group (D) in contrast to new bone formation with large amounts of cartilage and osteoid in the SrCPC group (E). Specific regions are labeled as follows: b, bone; c, cartilage; m, material; sc, screw; * indicates material in the soft-tissue; arrow indicates osteoid formation.

4.3.2 Osteoid formation

Von-Kossa/Van-Gieson staining was used to evaluate mineralization. It specifically differentiates mineralized tissue black and osteoid tissue dark pink, whereas connective tissue and bone marrow appeared light pink (Fig. 18A-C). Capability of mineralizing the extracellular matrix was indicated by the osteoid surface in the defect gap. Unmineralized osteoid was the most common tissue type (next to new bone formation) found in the defect region in the SrCPC group, mainly in vicinity of the biomaterial and on the medial aspect of the distal femur. (Fig. 18F). The CPC group showed comparatively less osteoid formation (Fig. 18E) and the empty group (Fig. 18D) almost lacked any osteoid in the initial defect area.

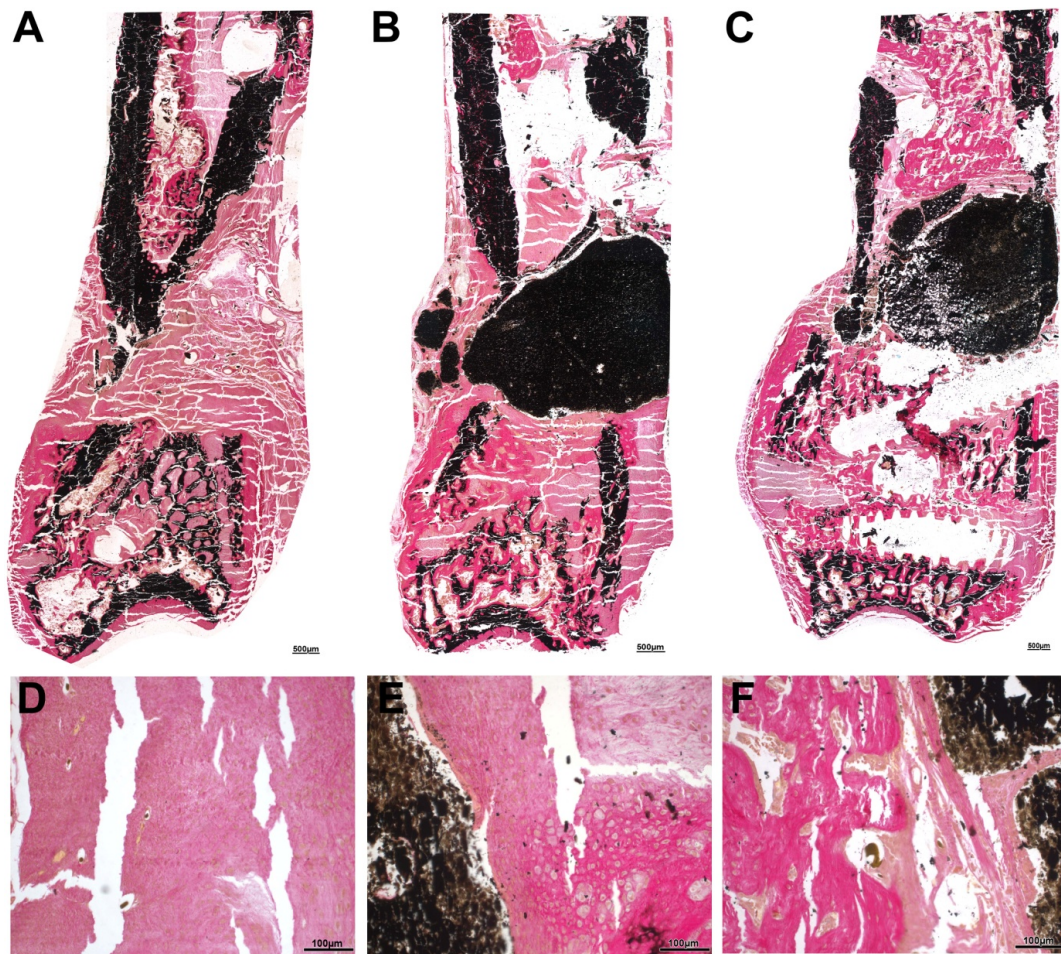


Fig. 18: *Von-Kossa/Van-Gieson photomicrographs showing overview of histological sections of empty defect (A), CPC (B) and SrCPC (C). Enlarged images at the biomaterial interface depicting increased osteoid formation (dark pink region) in the SrCPC group (F) in comparison to the CPC (E) and Empty group (D).*

4.3.3 Cartilage formation

In addition to the increased osteoid formation, mainly bone and cartilage tissue with hypertrophic chondrocytes were found in the SrCPC group in the defect region surrounding the biomaterial (Fig. 19). On the contrary, in the animals of the CPC group mainly cell dense fibrous tissue and proliferating chondrocytes were the predominant types (Fig. 19E) and in the empty defect it was the fibrous tissue (Fig. 19D). This was further confirmed by the movat-pentachrome staining which revealed a noticeably less cartilage formation in the empty defect control group compared to the other two groups (Fig. 20A, B, C). The empty defect was mostly filled with fibrous tissue (Fig. 20A).

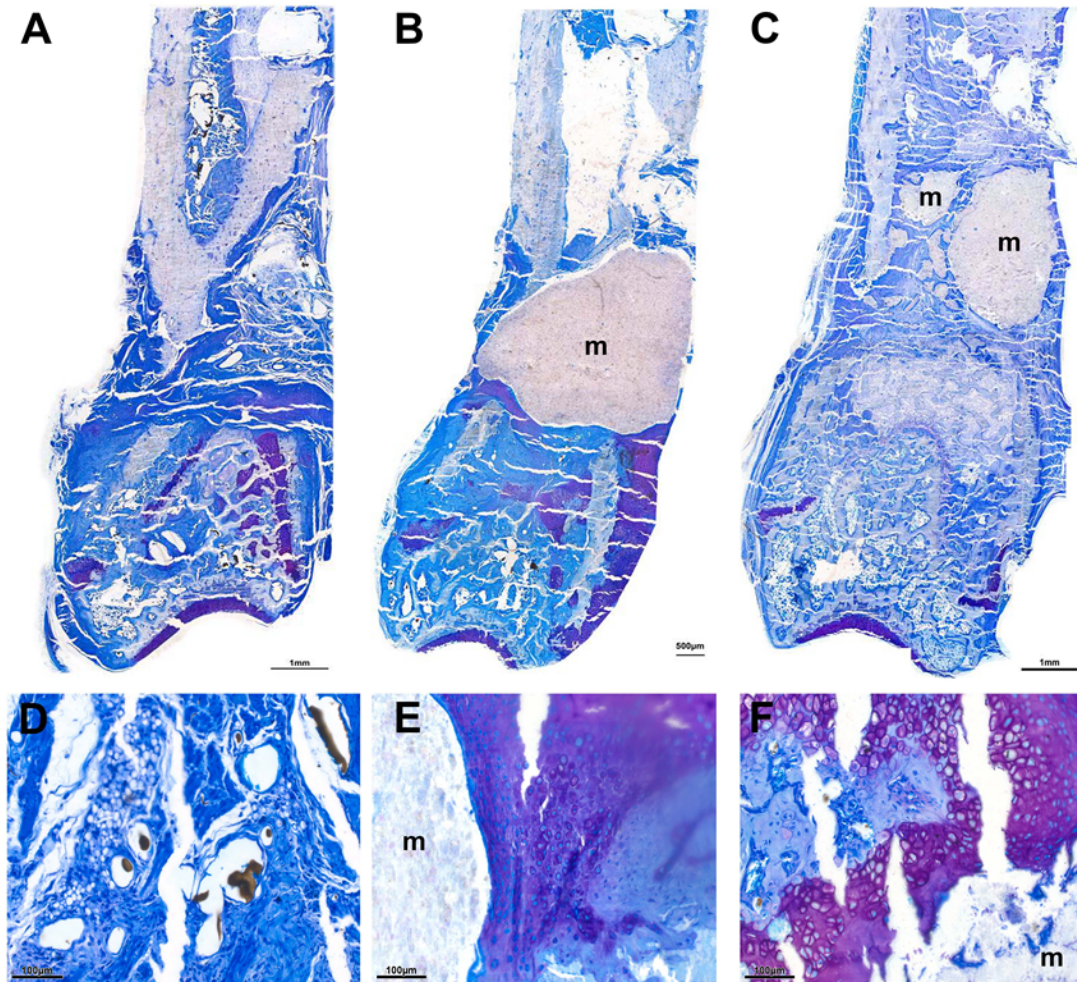


Fig. 19: Toluidine-blue photomicrographs showing overview of histological sections of empty defect (A), CPC (B), and SrCPC (C). Enlarged images at the biomaterial interface depicting increased chondrocyte activity (mostly hypertrophic chondrocyte stained dark purple) in the SrCPC group (F), in comparison to the CPC (E), where proliferating chondrocyte is the most dominant type. In the empty group there is almost no chondrocyte activity seen (D).

Moreover, in context to the medial side of the osteotomy (apex of the wedge-shaped defect), the gap was filled with cartilage and connective tissue in the SrCPC group whereas in the CPC group, and to a greater extent in the control group, large shifting of the cortical bones were seen (Fig. 21A, B, C). This space was predominantly occupied with fibrous tissue in case of the empty defect group (Fig. 21A, 22A). However, in case of the CPC (Fig. 22B) group small traces of connective tissue and cartilage were also seen besides fibrous tissue formation. The best gap closure was seen in case of the SrCPC group with the highest amount of cartilage, osteoid and bony tissue (Fig. 22C).

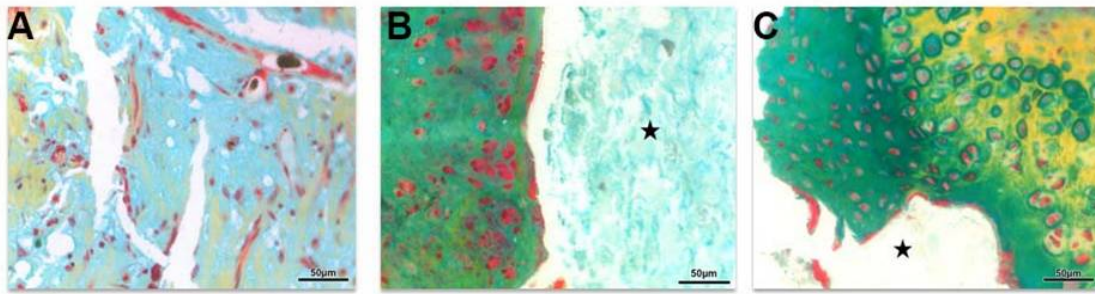


Fig. 20: *Movat-pentachrome photomicrographs showing magnified images at the biomaterial interface of empty defect (A), CPC (B) and SrCPC (C) depicting large amounts of cartilage (green) and hypertrophic chondrocytes in the SrCPC group thereby validating the toluidine-blue findings. * indicates material.*

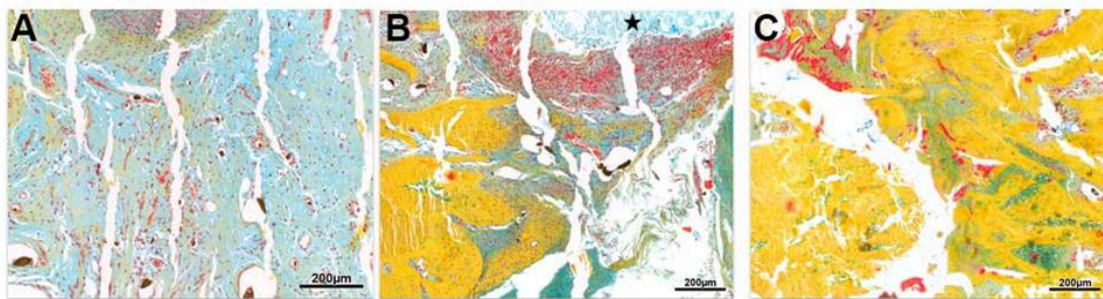


Fig. 21: *Movat-pentachrome photomicrographs showing larger shifts of cortical bone (yellow) in the CPC group (B), in comparison to the SrCPC group (C). These shifts were also seen in case of the empty defect (A), being highest in the same due to instability. Due to large shifts in the cortical bone in CPC, only left cortical bone is visible. However, no visibility of the cortical bones in case of the empty defect, the shifts being the highest.*

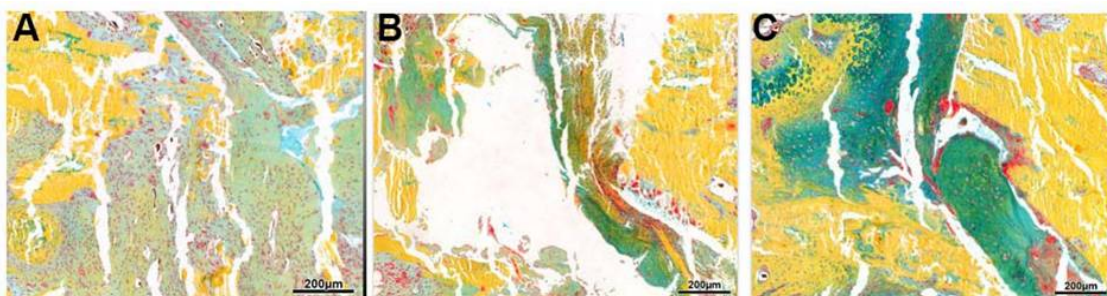


Fig. 22: *Movat-pentachrome photomicrographs at higher magnifications (medial side of the defect) showing tissue type in the defect gap in empty defect (A), CPC (B) and SrCPC (C) group. An increased amount of cartilage (green) and connective tissue (blue-green) was seen in the defect gap of SrCPC group. This space was filled with fibrous tissue in case of the empty defect and CPC group. Small traces of cartilage and connective tissue seen in CPC group.*

4.4. IMMUNOHISTOCHEMICAL ANALYSIS

4.4.1 Macrophage activity

In order to investigate the resorption capacity and the rate of bone remodeling, bone sections were stained with ED1. The macrophages were stained brown due to the antigen-antibody reaction. ED1-positive cells were found to be higher in the SrCPC group when compared to the CPC and empty defect group (Fig. 23A, B, C). The highest ED1 activity was seen at the biomaterial interface. A statistical evaluation was made to confirm the histological findings (4.5.3).

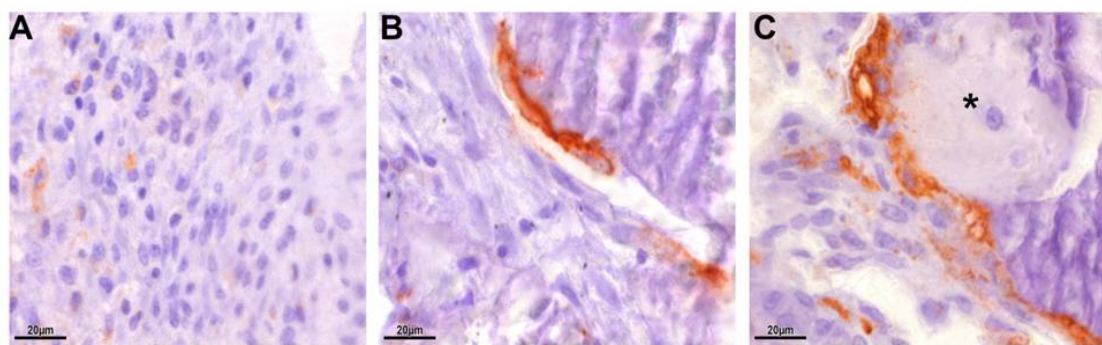


Fig. 23: Macrophage count based on ED1 staining. Photomicrographs of histologically stained sections with ED1 at higher magnification showing an elevated distribution of red stained cells in SrCPC group (C) when compared to CPC (B) and (A) empty control group. * indicates material remnants.

4.4.2 BMP2 expression

Bone morphogenetic protein 2 is known to potently induce osteoblast differentiation and thereby stimulate new bone formation. Immunohistological staining with BMP2 revealed a strong positive expression in the SrCPC group, mainly in the direct vicinity of the biomaterial i.e. at the biomaterial interphase and mid cortical regions. BMP-2 expression was almost negligible in CPC and in the control group (Fig. 24A-F). This increased BMP2 activity could be co-related to the increase in the bone formation as revealed by the histomorphometric analysis.

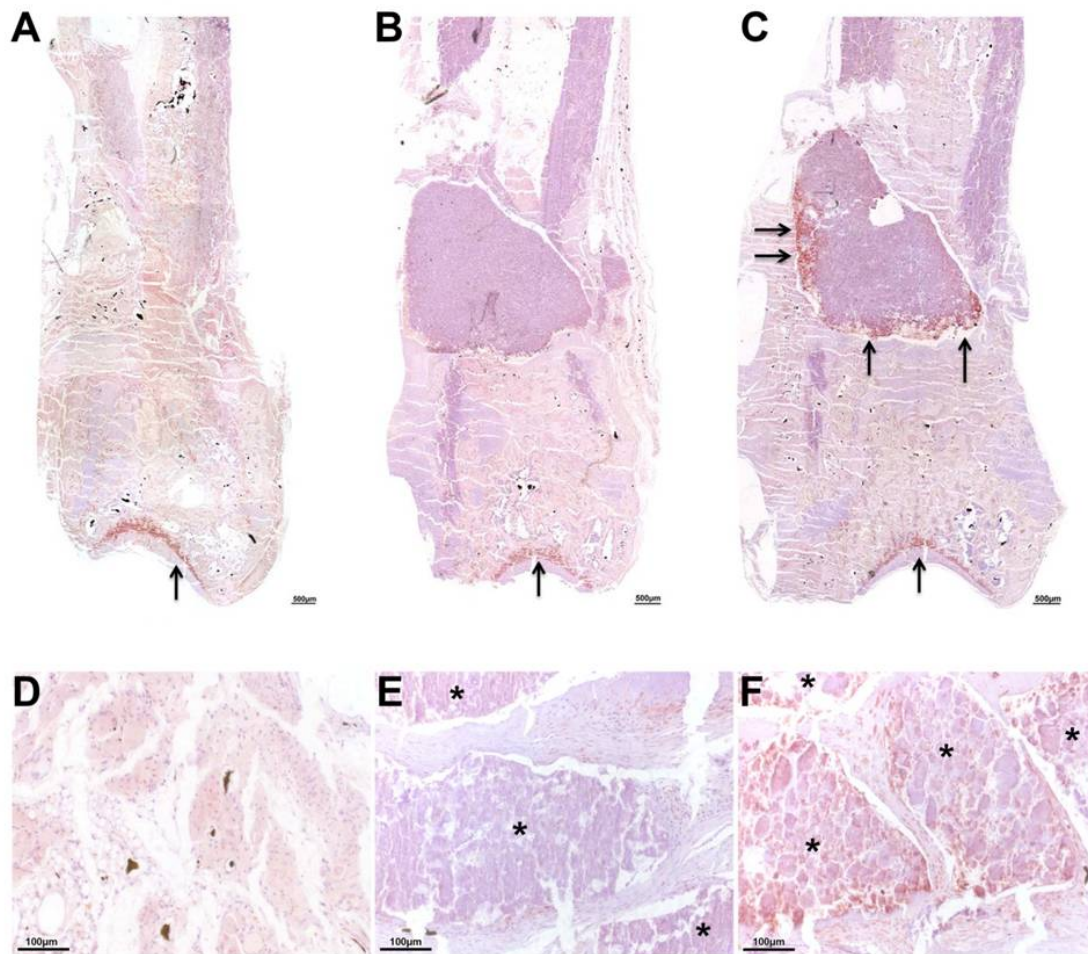


Fig. 24: *BMP2 immunohistochemistry on undecalcified technovit sections showing an increased expression of the same in SrCPC group (A-C). Increased expression was seen at the tissue implant interface in the SrCPC group (C) when compared to the CPC group alone (B) and empty defect (A)). Arrows indicate areas of highest activity.* indicates material remnant in the defect region of CPC and SrCPC group.*

4.4.3 OPG/RANKL expression

OPG/RANKL ratio is an important index for osteoclastogenesis. OPG a specific marker for active osteoblasts was used as a key factor to analyze the osteoclast regulation. An increased expression of OPG was seen at the proximal and mid level of the fracture gap in the SrCPC group when compared to CPC and empty defect group (Fig. 25A-F). At the same time, a simultaneous reduction in the RANKL expression in SrCPC was also detected (Fig. 26A-F). OPG expression was increased at the onset of mineralization and remained high throughout, thereby resulting in a lower RANKL/OPG ratio in mature osteoblasts. These changes indicate that mature osteoblasts may have different roles in the maintenance of the bone remodeling balance.

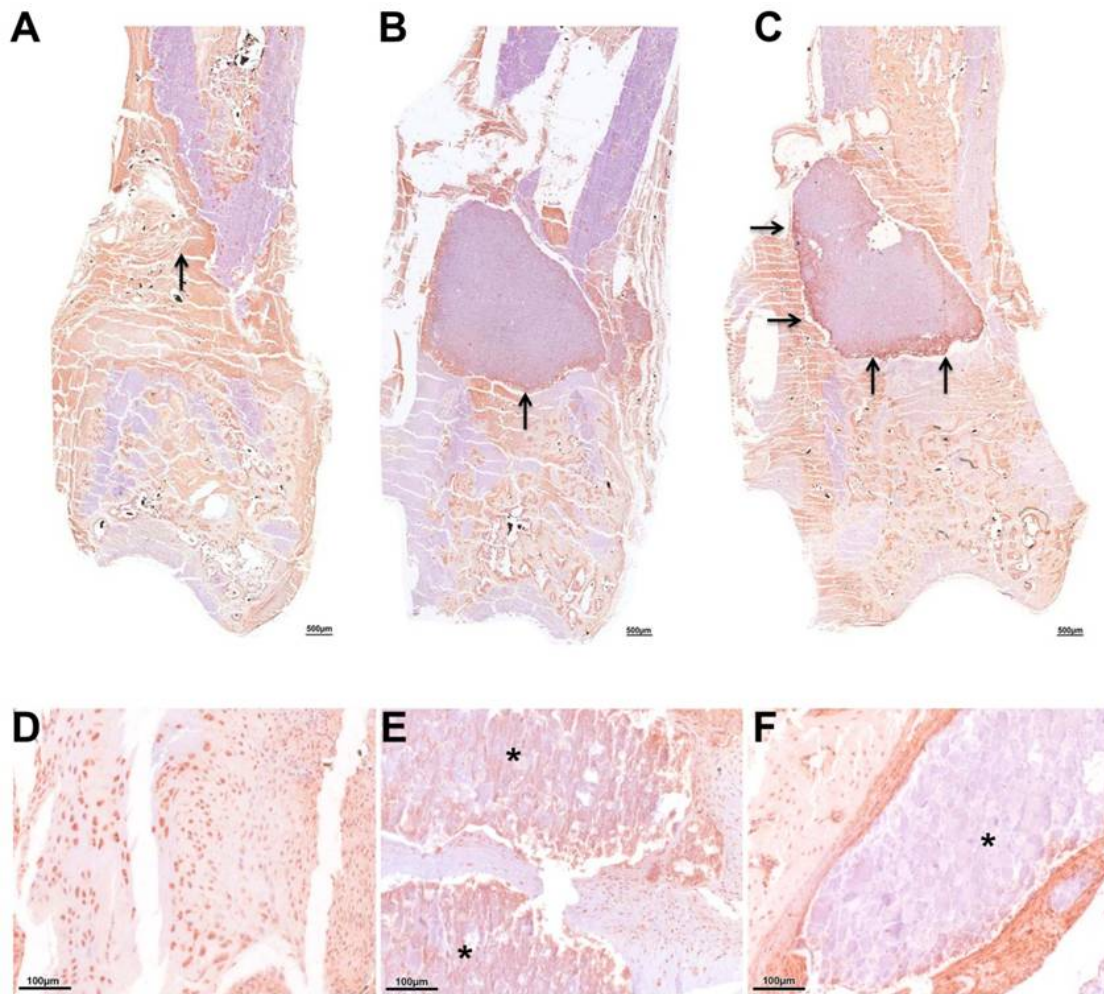


Fig. 25: Immunohistochemistry on undecalcified technovit sections showing an increased expression of OPG in the SrCPC group (C), compared to CPC (B) and empty defects (A). A high expression was seen at the tissue implant interface in the SrCPC group (F) when compared to the CPC group alone (E) and empty defect (D). Arrows indicate areas of highest activity. * indicates material remnant in the defect region of CPC and SrCPC group.

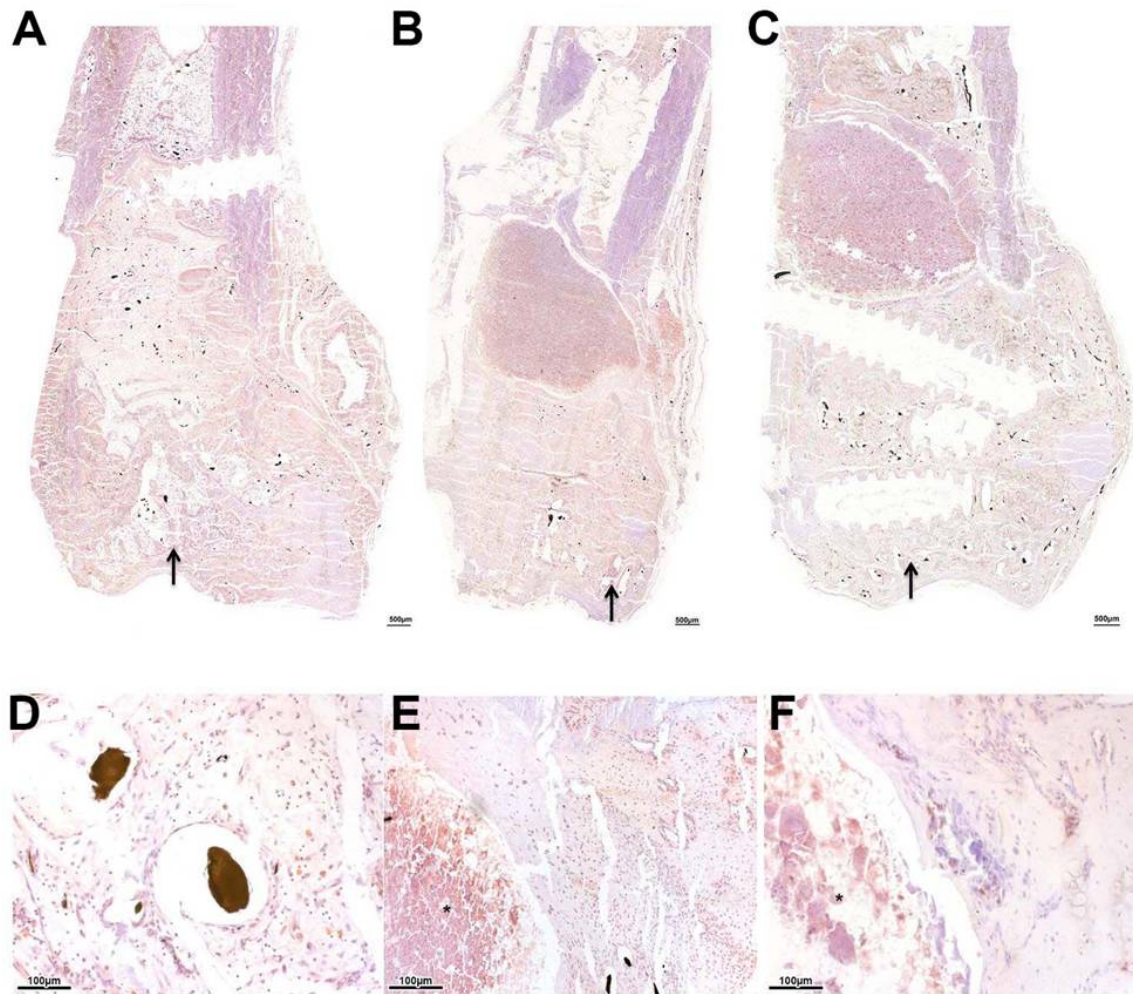


Fig. 26: Immunohistochemistry on undecalcified technovit sections showing a complete absence of RANKL activity in all the three subgroups (A, empty, B, CPC, C, SrCPC). Arrows indicate the areas of highest enzyme activity outside the defect gap i.e. the growth plate cartilage. With respect to the biomaterial interface, almost no activity was detected (D, empty, E, CPC, F, SrCPC). * indicates material remnant in the defect region of CPC and SrCPC group.

4.4.4 OCN expression

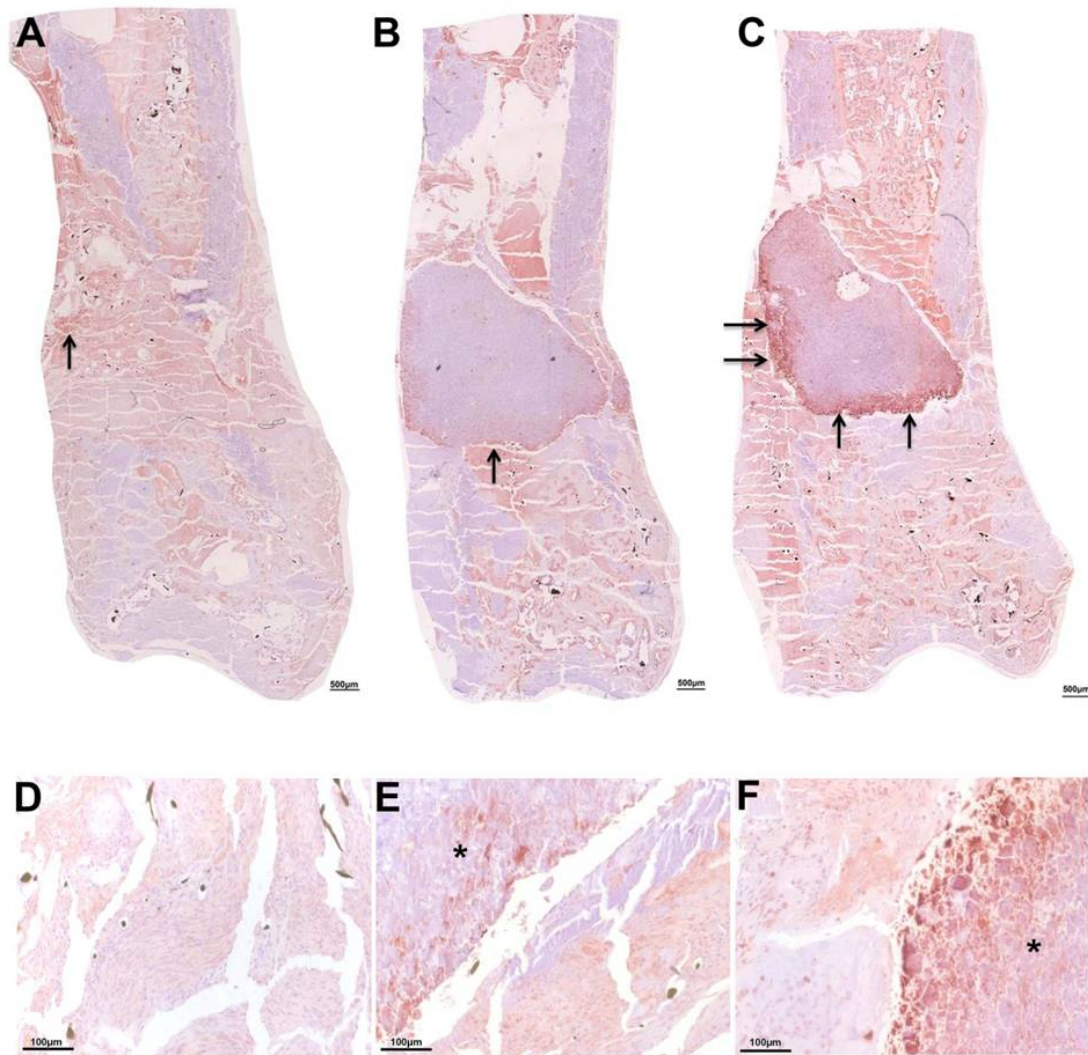


Fig. 27: Immunohistochemistry on undecalcified technovit sections showing an increased expression of OCN in the SrCPC group (C, SrCPC). At the tissue implant interface in the SrCPC group an increased expression of OCN was seen when compared to the CPC group alone (E, CPC, F, SrCPC). Arrows indicate areas of highest activity. * indicates material remnant in the defect region of CPC and SrCPC group

Osteocalcin is a specific marker for active osteoblasts and was used as a marker for the bone formation process. An increased OCN expression was seen in the distal and mid cortical region of the fracture gap in the SrCPC group when compared to CPC filled and empty defect group (Fig. 27A-F). Further, increased vascularization is known to induce osteogenesis. The results of osteoblast labeling are complemented with the examination of the endothelial derived cells that represent blood vessel formation.

4.4.5 Vascularization

The analysis of new blood vessel formation using CD31 antibody revealed a comparatively higher number of positively stained vessels in the SrCPC group in comparison to the CPC group (Fig 28B, C). An increased positive reaction was seen with an increase in the biomaterial fragmentation (SrCPC) thereby leading to an increase in the granulation tissue and thus leading to an increased vessel formation. Based on this principle, the empty defect which was filled predominantly with the granulation tissue, showed a comparatively higher CD31 expression (Fig. 28A).

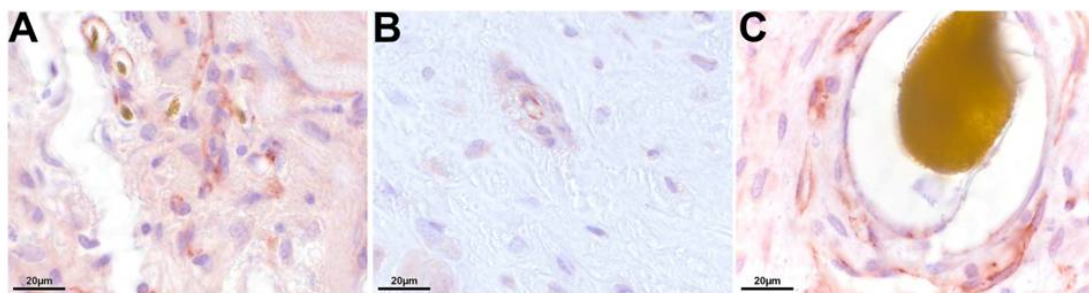


Fig. 28: Immunohistochemistry on undecalcified technovit sections showing an increased expression of CD31 in the SrCPC group (C) when compared to the CPC group alone (B). The highest CD31 expression was seen in the empty defect group (A).

4.4.6 Alpha (α) SMA expression

The analysis of new blood vessel formation using α -smooth muscle actin antibody revealed a comparatively larger and higher number of positively stained vessels in the

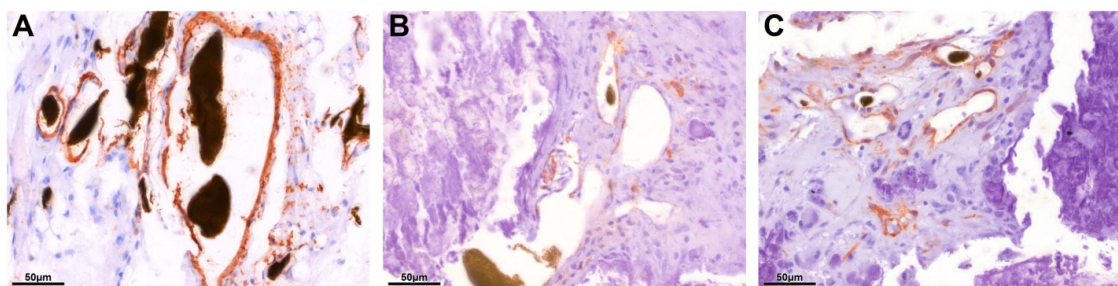


Fig. 29: Immunohistochemistry on undecalcified technovit sections showing an increased activity of alpha smooth muscle actin in the SrCPC group (C) when compared to the CPC group alone (B). The highest expression was however seen in the empty defect group (A).

empty and SrCPC group respectively (Fig. 29A, C). Interestingly, the CPC group demonstrated very scarcely stained blood vessels in the vicinity of the biomaterial

remnant (Fig. 29B). These vessels were comparatively fewer and smaller when compared to the other two groups.

4.5 HISTOMORPHOMETRY

4.5.1 Bone formation

Histomorphometric analysis at the defined ROI's showed a statistically significant increase in the bone formation for the CPC [0.042 ± 0.03] ($p=0.0002$) and the SrCPC [0.11 ± 0.01] ($p=0.0001$) treatment group compared to the empty defect [0.004 ± 0.002] in the former fracture defect zone (Fig. 30A). SrCPC treated animals showed a statistically higher new bone formation in relation to the defect areas filled with CPC ($p=0.005$).

Furthermore, there was increased bone formation at the bone-biomaterial interface region for the SrCPC [47.5 ± 13.8] compared to CPC [6.4 ± 1.5] which was also statistically significant ($p<0.01$) (Fig. 30B).

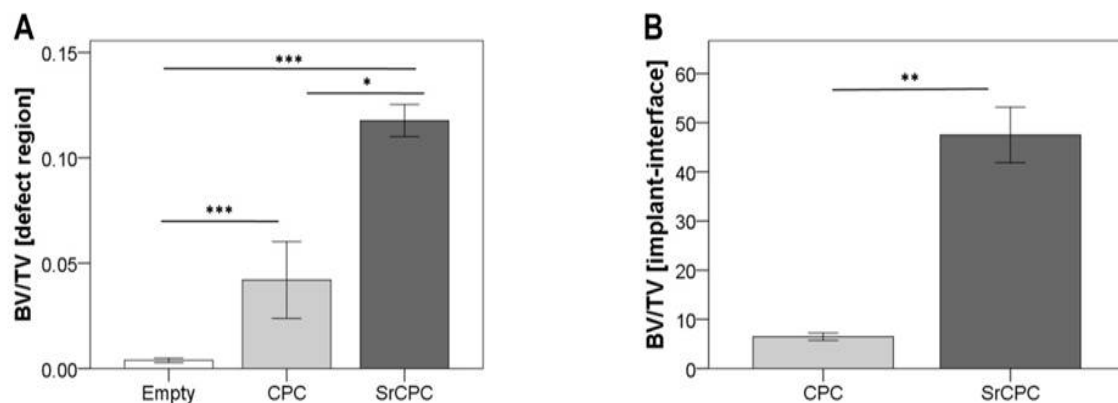


Fig. 30: Histomorphometrical analysis of new bone formation of SrCPC, CPC and empty control group in the initial fracture defect zone (A) and at the tissue-biomaterial interface (B) Asterisks indicate (*) $p < 0.05$, () $p < 0.01$ and (***) $p < 0.001$, respectively.**

4.5.2 Unmineralized tissue

The total unmineralized tissue area in the control group was the highest followed by the CPC and SrCPC (Fig. 33, $p<0.05$), indicating a better mineralization progress in the presence of CPC and SrCPC. Furthermore, SrCPC also showed a statistically significant decrease in the unmineralized tissue in comparison to the CPC alone (Fig. 31, $p<0.05$).

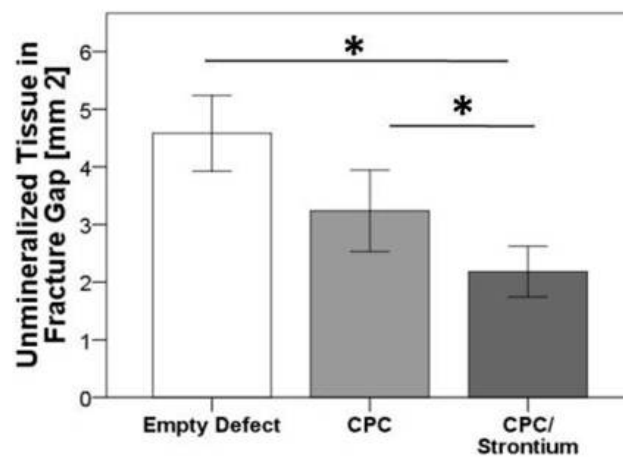


Fig. 31: Histomorphometrical analysis of unmineralized tissue of SrCPC, CPC and empty control group in the initial fracture defect zone. Asterisks indicate (*) $p < 0.05$, (**) $p < 0.01$ and (***) $p < 0.001$, respectively.

4.5.3 Macrophage count

The previously stained ED1-sections were used to perform the macrophage count. For statistical evaluation the macrophage counts were normalized to the trabecular area. ED1-positive cells were found to be significantly higher in the SrCPC group [87.5 ± 21.9] in comparison to the CPC group [CPC: 43.7 ± 2.6] ($p=0.033$) and the empty defect control group [30.6 ± 2.5] ($p=0.005$) (Fig. 32). Most of the ED1 positive cells were found in at the biomaterial-tissue interface region.

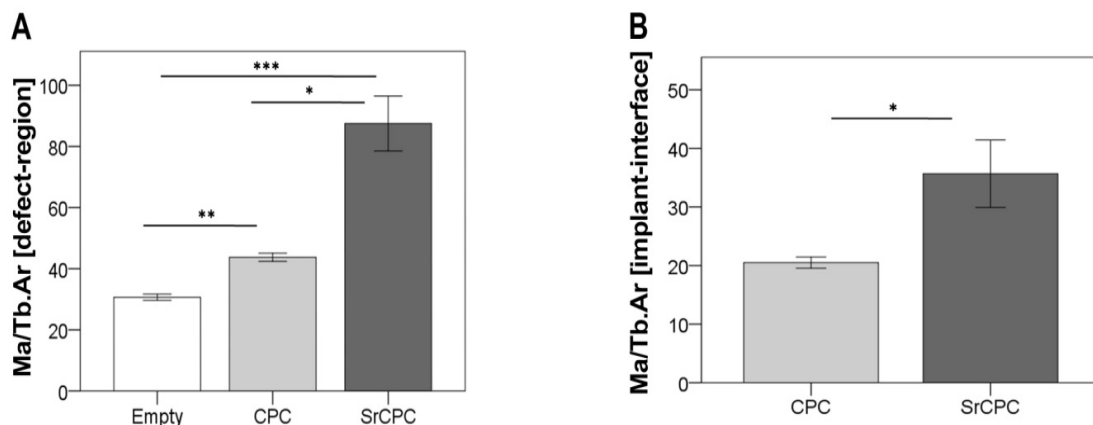


Fig. 32: Macrophage count based on ED1-immunohistochemistry over trabecular area (Ma/Tb.Ar) of SrCPC, CPC and empty control groups in the initial fracture defect zone (A) and at the tissue-biomaterial interfaces (B). The asterisks indicate (*) $p < 0.05$, (**) $p < 0.01$ and (***) $p < 0.001$ respectively.

4.6 MOLECULAR BIOLOGY

4.6.1 Genes involved in bone formation

Expression of ALP, an osteoblast marker showed a significant increase indicating mineralization of bone was higher in the SrCPC group when compared to the CPC group ($p=0.027$). Likewise, on analysis of osteocalcin, a prominent bone formation marker showed a higher expression in the SrCPC group when compared to the CPC group ($p\leq 0.001$). In addition Col X, marker specific for hypertrophic chondrocytes also showed a significantly higher expression in case of SrCPC group when compared to CPC group ($p=0.03$) (Fig.33). However, Runx2 and Col1a1 expression analysis showed no significant difference between the SrCPC and the CPC group.

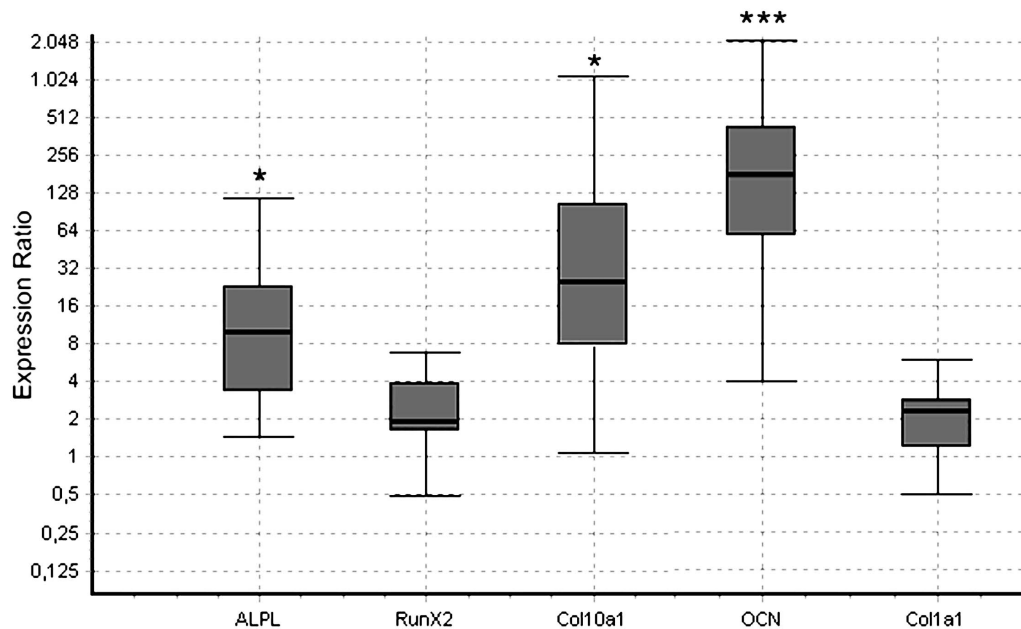


Fig. 33: Relative gene expression analysis between SrCPC and CPC. Alkaline phosphatase (ALP), Runt-related transcription factor 2 (Runx2), collagen type X alpha1 (Col10a1), osteocalcin (OCN) as bone formation markers (A). β_2 -microglobulin (B2M) was used as a reference gene. The asterisks indicate (*) $p < 0.05$, () $p < 0.01$ and (***) $p < 0.001$ respectively.**

4.7 TOF-SIMS analysis

4.7.1 Strontium release in SrCPC

TOF-SIMS was used to estimate the strontium distribution in all the three groups (Fig. 34). The evaluation of the strontium distribution in the empty defect showed a natural Sr background count rate of about 11 counts, which was taken as the standard count. In case of the CPC implants a mean Sr count rate of 24 counts was obtained. However, the

highest Sr count rate was obtained in the center region of the Sr²⁺ modified SrCPC implant which was about 3000 counts. Count rates ranging about 80 counts were also seen in the biomaterial-tissue interface up to a distance of 1 mm surrounding the biomaterial. Moreover, there was also a Sr concentration gradient seen in all the sides of the implant material which decreased with increasing distance from the implant. However, an increased Sr concentration could be detected up to a distance of 6 mm from the implant surface, which decreased with the increasing distance from the biomaterial.

Calcium, one of the major components of the bone was found not only in the cortical bone in all three groups but also in the CPC and SrCPC cements itself. The bone marrow areas in all the specimens were almost devoid of Ca signals. Interestingly, Sr and Ca signals were also found at the region of newly formed bone (tissue-implant interface). These signals overlapped with the areas of the collagen signal, indicating its role in bone formation.

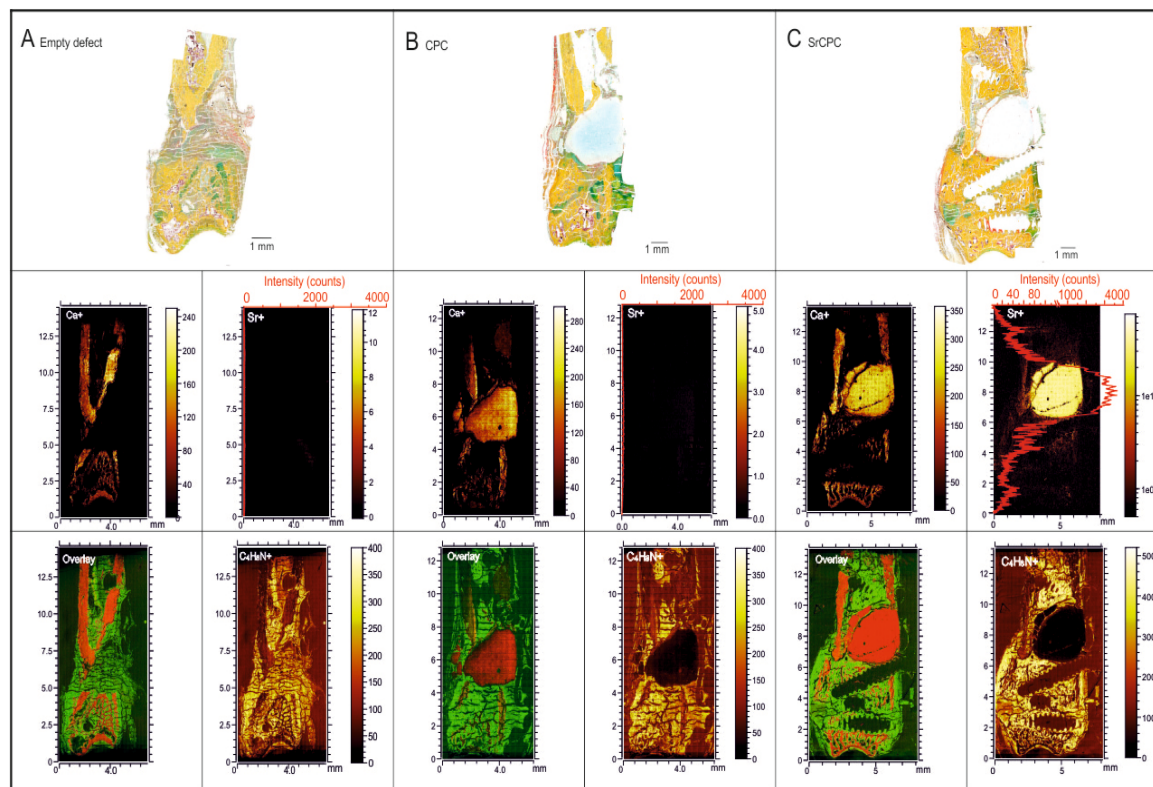


Fig. 34: Overview of movat-pentachrome stained sections of representative specimens of the empty defect (A), CPC (B) and SrCPC group (C) used for TOF-SIMS analysis. The small images under the overview images show mass distribution of Ca⁺ (upper left), Sr⁺ (upper right), C₄H₈N⁺ (lower right) and an overlay image of the Ca⁺ and of the C₄H₈N⁺ signal (lower left). For better distribution analysis of Sr⁺, the local count rates of Sr⁺ are plotted versus the y-axis and placed over the Sr-images.

4.7.2 Strontium concentration gradient from the implant material into the bone

The Ca distribution in Fig. 35 gives a measure of the bone quality. Nearly no calcium is found in the area of the empty defect. However, mass fragments of $C_4H_8N^+$ can be seen everywhere since it has multiple origins e.g. bone matrix, cartilage as well as from the connective tissue. With respect to the strontium signal, low background intensity can be measured in the empty defect sample and in the sample with the CPC. A Sr histogram of a line scan (line scan position is marked in red; Fig. 34) is added to each Sr mass image. The Sr-image and the line scan show clearly that there is a Sr-concentration gradient from the implant material into the bone. The Sr thus released is incorporated into the surrounding connective tissue, newly formed bone and in the matured pre-existing bone.

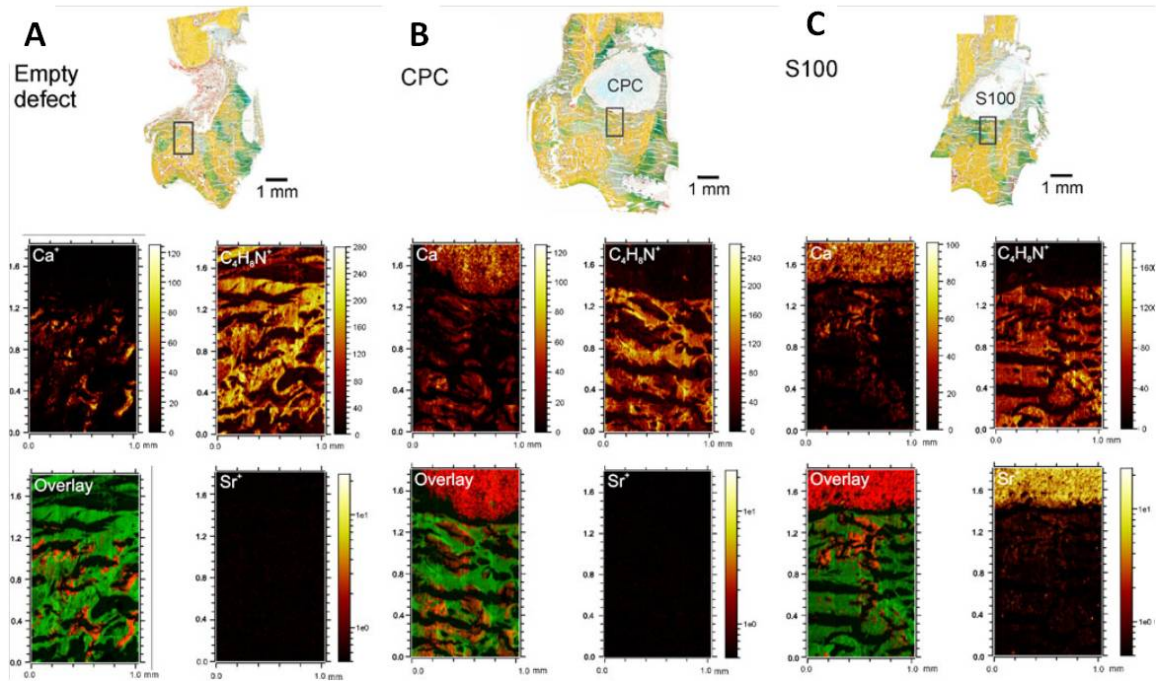


Fig. 35: Light microscopy images of movat-stained bone cross sections (top) and detailed mass images (bottom) of unstained bone cross sections: empty defect (A), bone with CPC (B), bone with S100 (C). The black rectangles in the light microscopy images mark the area scanned by mass spectrometry. They originate from the interface empty defect/bone and cement/bone respectively. Mass imaging was carried out with Bi^{3+} as primary ion species and a higher lateral resolution ($2\ \mu m$). The mass images show the distributions of Ca^+ , $C_4H_8N^+$, Sr^+ and an overlay of the Ca^+ in red and $C_4H_8N^+$ in green. The mass images for each sample starting in the upper left corner in clockwise direction. The black rectangles in the light microscopy images mark the area scanned by mass spectrometry.

Fig. 35 shows more detailed mass images of the interface between the newly formed bone and the biomaterials CPC and SrCPC. The overlay and the strontium mass images (Fig. 35C) show clearly that there is calcium- and strontium- mineralized tissue (new formed bone) close to the SrCPC implant.

5. DISCUSSION

Calcium phosphate cements (CPC) used in this study are known for their favorable biological response having excellent biocompatibility, bioactivity and osteoconduction properties. When inserted in the receiving site, it does not cause any adverse immune reaction, is able to connect directly to the bone tissue and allows bone growth on its surface [2, 113]. Similarly, the second functionalizing agent strontium has been shown effectively to stimulate both bone formation and inhibit resorption [3]. Apart from being used as an oral medication against osteoporosis [3, 5], local administration from functionalized titanium implant surfaces [5-10] or from strontium substituted hydroxyl-apatite coatings [11, 12] has accentuated the rate of new bone formation and eventually helps in better implant fixation.

The purpose of the study conducted in this thesis was to investigate the effect of strontium when substituted in CPC. The main questions addressed were:

1. Does Sr modified CPC play a better role in new bone formation than CPC?
2. Can the released strontium be detected using TOFSIMS?

To elucidate answers to these questions, this study was conducted where strontium was delivered to the surrounding bone tissue by strontium modified calcium phosphate cement (SrCPC). The effects were then compared to CPC and empty defect groups.

5.1 A clinically relevant model

Biomaterials should be investigated in a clinically relevant model targeting their intended clinical use. Although most calcium phosphate cements are applied in fracture defects in patients, *in vivo* testing of these materials is mainly done in simple drill hole defects that does not represent clinical reality [114, 115]. Rat long bones have been used as experimental models in order to assess bone healing [116]. As surgical site, the metaphyseal area was chosen, as osteoporosis mainly affects the metaphyseal trabecular bone e.g. distal radius, proximal humerus and femur or the vertebral bodies and not likely the diaphyseal part of the long bone [52-55]. The strength of the used animal model [13] is that it allows investigation of biomaterials in a clinical relevant situation. It exposes the materials to a fracture defect in the metaphyseal region of long bone in rats. Internal fixation with the T-shaped plate on the distal femur also corresponds to the human situation. Ovariectomy and special diet was shown to lead to a significant reduction of bone mineral density compared to sham animals [13, 117, 118]. The materials are

challenged with typical defect fracture healing processes for bone consolidation in this model under systemically impaired bone conditions. In this study we used a 4 mm fracture defect instead as it could fulfill all requirements for a critical size defect in the empty defect control group where it did not show any bony consolidation after 6 weeks in this study. Therefore, the 4 mm fracture defect is a good model to study potential bone enhancement effects of biomaterials.

Plate breakages in this model could be regarded as a drawback. However, even this fact links the model to clinical reality as plate breakages in the human situation are a typical sign for implant failure in case of impaired bone healing such as delayed or non-unions [119]. Although, there was no statistical significant difference in plate breakages, with a p-value of $p=0.06$, there was a strong trend with fewer implant failure in the SrCPC compared to the CPC suggesting better bone healing for this parameter.

5.2 Bone formation enhanced in SrCPC group

Strontium ranelate has been studied in various rat and animal models, including intact animals, immobilization-induced osteopenia and ovariectomy induced osteoporosis [87, 95, 120, 121]. The results from these *in vivo* experiments showed strontium ranelate to increase bone formation markers, decrease bone resorption markers, promote bone gain as revealed by increase in the external diameter of the long bones, enhanced bone mass evaluated by DXA and micro architecture improvement as assessed by histomorphometry. These observations are in accordance with the results of strontium ranelate in clinical trials that have shown uncoupling of bone markers, increase in DXA results [84] and histomorphometric bone improvement [94]. Furthermore, these positive effects on bone were obtained without affecting bone mineralization [122].

The bone gain induced by strontium ranelate treatment was predictive of increased bone strength that was indirectly confirmed by the reduction in fracture risk in clinical trials [84, 85]. This capacity of strontium ranelate to stimulate bone formation was subsequently shown in animal studies as they provide objective information on all the structural determinants of bone strength e.g. bone geometry, cortical thickness and porosity, trabecular bone morphology and intrinsic properties of bone tissue [95]. The first set of experiments were on normal adult mice where administration of 1800 mg/kg/day of strontium ranelate for a period of 2 years improved the bone mass [120]. This was further affirmed with improved bone mass in rats which were given a dose of

225-900 mg/kg [95]. There was not only an increase in the external diameter and cortical thickness of long bones but also an improvement in vertebral bone mass, trabecular bone volume, trabeculae number, trabecular thickness, connectivity and cortical thickness, reflecting improved bone geometry, cortical properties, porosity and trabecular bone morphology. Additionally, six month old ovariectomized rats treated over a period of 1 year with strontium ranelate also showed a dose-dependent prevention of bone strength alteration and partial prevention of microarchitecture bone changes [95].

Although there are a lot of studies addressing the effects of anti-osteoporotic drugs on fracture healing, our study is one of its kind to study the *in vivo* effect of strontium modified calcium phosphate cement in traumatically induced fractures (a critical size defect in the metaphyseal area of the distal femur in ovariectomized rats). A statistically significant increase in new bone formation was seen in CPC and SrCPC compared to the empty defect, the highest bone formation being in SrCPC. The histological findings in case of SrCPC are in agreement with the literature [3, 87, 123]. It could be shown that the SrCPC treated animals not only exhibited an increased new bone formation at the biomaterial-bone interface but also in the entire fracture defect area compared to CPC and empty defect group suggesting that the local release of Sr from SrCPC has a positive influence on osteogenesis. This increase in matrix mineralization also supports the lack of any deleterious effect *in vivo*. Furthermore, the immunohistochemical data from the BMP2 and OPG stains indicate how Sr can be an important factor for bone formation.

5.3 Bone formation markers up-regulated in SrCPC group

Osteoblast differentiation is crucial for bone formation. The immunohistological investigations could confirm the enhanced new bone formation activities in the SrCPC group with enhanced expression of BMP2. Previous studies on animals show a positive effect of strontium in proliferation, differentiation and mineralization of osteoblasts by activation of calcium sensing receptors on their surface, the effect being proportional to the therapy period and the drug dosage administered [124, 125].

Strontium is also known to have a positive effect on osteoblasts by controlling its influence on the PGE2 production. Thus strontium ranelate acts through Ras/Map kinase pathway thereby phosphorylating ERK (extracellular signal regulated kinase), consequently increasing the expression of BMP2 [126] .

Immunological staining revealed a strong positive BMP2 expression in the SrCPC group which was restricted predominantly to the boundaries and in the vicinity of the biomaterial, highest concentration being on the proximal cancellous region and mid cortical regions. This could be explained on the binding of the strontium with the cancellous bone at the proximal level and the cortical bone at the mid level [127]. Since, cancellous bone differs from the cortical bone in many aspects including vascularity and density; this may in turn result in different dissolution of strontium in CPC when bonding with them. However, this kind of an expression was almost negligible in CPC and empty defect group. This indicates the substitution of strontium in the calcium phosphate cements increases the BMP2 activity, which might in turn lead to better osteoblast differentiation and thus in bone remodeling.

In addition osteocalcin, a non collagenous protein secreted by osteoblasts which plays a major role in mineralization and calcium homeostasis [128], showed increased activity in the SrCPC group compared to CPC and the empty defect control group as revealed by the gene expression analysis. qPCR analysis also showed a significant up-regulation of osteoanabolic markers e.g. collagen type 10a1; a hypertrophic chondrocyte marker [129], ALP; an essential protein for osteoblastic differentiation [130] and Runx2; an essential protein for osteoblast differentiation [129]. These findings suggested that strontium increases the differentiation from early progenitor cells to mature osteoblasts.

5.4 Decreased bone resorption in SrCPC

There was an increased OPG/RANKL ratio as revealed by the immunohistochemical findings. These observations suggest that when strontium stimulates osteoblasts, two types of signals are produced simultaneously thereby activating the anabolic pathways in the pre-osteoblasts and osteoblasts, and an anti-catabolic pathway in the pre-osteoclasts and osteoclasts [3]. OPG (osteoprotegerin) is produced by the osteoblasts. In accordance with the previous studies about the positive effects of strontium with regards to the osteoblasts and differentiation of the osteocytes [3], an increased expression of OPG was seen at the proximal and mid level of the fracture gap in SrCPC group. This increase in the OPG concentration results in its competition with RANK. Thus OPG goes and binds to the RANKL present on the osteoblast surface, thereby blocking RANK/RANKL interaction, thereby inhibiting osteoclast precursors to become mature osteoclasts. This pronounced OPG activity in case of SrCPC group in turn led to a simultaneous reduction

in the RANKL expression. The supplementation of strontium in the calcium phosphate cement thus blocks osteoblast induced osteoclast osteogenesis.

However the increase in the macrophage count as revealed by the ED1 count could be explained on the basis of a better surface activity in SrCPC cement which attracts macrophages in turn leading to enhanced biomaterial degradation.

5.5 Enhanced vascularization in both SrCPC and empty group

Bone development and remodeling depend on complex interactions between bone-forming osteoblasts and other cells present within the bone microenvironment, particularly vascular endothelial cells (ECs) that may be pivotal members of a complex interactive communication network in bone. Therefore, adequate callus vascularization is required for normal fracture healing [131].

Lienau et al. (2009) established that a compromised healing situation would affect vessel formation molecularly as well as temporally. Due to the absence of a prominent vessel marker both CD31 and ASMA was used in order to confirm angiogenesis. High CD31 and ASMA expression suggests concomitant new blood vessel formation in the SrCPC group. These findings are in line with better new bone formation and implant-bone contact of other *in vivo* studies on strontium substituted hydroxyapatite coatings [11] or strontium-doped hydroxyapatite bone graft extender [132]. However, the highest expression was seen in case of the empty defect group, which could be explained on the basis of the empty spaces available for in-growing of granulation tissue that allows the formation of blood vessels.

5.6 Strontium release in the SrCPC group

The strontium modified calcium phosphate bone cement used in the present study has been developed recently by complete substitution of the CaCO_3 portion in the precursor mixture of a well established, α -TCP based cement by SrCO_3 . This simple approach which has been described in detail recently leads to a cement which releases strontium ions in relevant dosages *in vitro* [133]. A comparison of the *in vitro* strontium release and the findings of the current animal trial is difficult. However, this *in vivo* study can demonstrate that a considerable amount of strontium is released from the SrCPC into the interface region and into the surrounding tissue which is most likely related to enhanced

bone formation confirming the *in vitro* findings that biologically active doses of strontium can be released from SrCPC.

Recent studies show that the local delivery of strontium from surface functionalized titanium implants could enhance bone-to-implant contact for implants in the femoral shaft of healthy female Wistar rats [5]. The authors concluded that strontium can be released into the local milieu of osseointegrating implants to accelerate bone in-growth into the implant surface. However, all previous works did not analyze the *in vivo* release of Sr into the bone which could be done in our study with the help of TOF-SIMS. The high Sr concentration in the interface region of the SrCPC implant implicated that the released Sr in the SrCPC cement is most likely to be responsible for increased new bone formation compared to the CPC group. This can be regarded as the paradigm that the local delivery of strontium from Sr-modified/loaded implants or biomaterials is possible and that strontium's biological activity to stimulate new bone formation is preserved within the CPC.

Ni et al. also reported a similar case about the detection of Sr, Ca etc. of a Sr-doped hydroxyapatite cement that was implanted into the proximal femoral intramedullary canal for 6 months by EDX and TOF-SIMS [127]. However, there was only a maximum count rate for Sr of 3 in the 70 mm thick hydroxyapatite interface layer. In contrast to this study, we found a high release of Sr up to a distance of 6mm to the implant. It is also known that due the almost similar physical and chemical properties of both Ca and Sr, the later is a natural bone-seeking trace element that accumulates in the skeleton. Johnson et.al showed the similarity in the incorporation of both these elements into the bone [134]. In accordance with this we also found increased Sr, Ca and the collagen signals in the same areas of the newly formed bone suggesting that the released Sr from SrCPC was incorporated into the new bone. It would be also interesting to know if the Sr thus detected stays in the bone or is later replaced by Ca and if the bone building with strontium shows the same stability as that from Ca.

5.7 Biomaterial degradation highest in SrCPC group

Body tissues in contact with biomaterials lead to a biologic response [135]. Body fluids represent extremely corrosive mixtures of fluid, ions and proteins which in turn help in further degradation of the biomaterials. Furthermore, the movement of the body also results in mechanical stress which further promotes biomaterial degradation.

Additionally, passive degradation is also carried out as a result of the inflammatory cellular response to foreign bodies, which includes immune cells, neutrophils, lymphocytes, macrophages and osteoclasts which in turn help in the resorption process. The degree and nature of this foreign body response is also dependant on the properties of the implant e.g. composition, three dimensional morphology including porosity, surface structure and chemistry [136]. The main strategy for recruiting these tendency of the body to attack external materials is i) to have inert materials which do not evoke inflammatory response and ii) to integrate the body's innate repair mechanisms into such materials which can be slowly degraded and replaced by healthy tissue [136]. An ideal biomaterial should thus be biodegradable and resorb at the same rate as that of the tissue repair in bone. This allows sufficient space for cell adhesion, extracellular matrix regeneration, facilitates homogenous tissue formation, allows vascularization and proper nutrient delivery [137]. An increase in the biodegradability will also allow a faster recovery in patients as well [138-140]. In accordance with this the *in vivo* degradation behavior of SrCPC although minimal, was higher when compared to the CPC and should be improved through.

The better degradation of SrCPC was associated with a statistically significant higher number of multinuclear cells in the vicinity of the biomaterial. With the assumption that at least some multinuclear cells are macrophages and foreign body giant cells, it can be suggested that the SrCPC degradation process is not impaired by a potential anti-osteoclastic effect of the released Sr as shown by reduction of RANKL expression in immunohistochemistry. A better understanding of the foreign body reaction is important as it may impact the biocompatibility of the implanted material and may significantly affect short- and long-term tissue responses with tissue engineered constructs containing proteins, cells, and other biological components for use in tissue engineering and regenerative medicine.

6. CONCLUSION AND FUTURE PROSPECTS

6.1 Conclusion

Using a systemic histological sampling methodology and defined histomorphometric analysis it is shown that both CPC and SrCPC revealed a statistically significantly enhanced new bone formation compared to the empty defect in a critical size defect in the metaphyseal area of the distal femur in ovariectomized rats. It could also be shown that the SrCPC treated animals exhibited a statistical significant higher new bone formation both at the biomaterial-bone interface and in the entire fracture defect area compared to CPC. The immunohistochemistry and molecular biology analysis could also be related accurately to the histology and histomorphometry data as these bear direct relevance to functional outcome. In addition, TOF-SIMS analysis could detect high count rates Sr from the SrCPC in the interface region and up to a distance of 6mm from the implant. This suggests that the enhanced new bone formation is attributable to local release from the SrCPC.

6.2 Perspective and future research

The thesis along with the previous findings supports the positive influence of strontium on bone healing in osteoporotic conditions. Despite the interesting results from this study, there are still scopes to investigate the in depth molecular characterization involved, the pathways associated and the optimal method of strontium delivery in the entire defect region. Since the maximum bone remodeling was seen at the biomaterial-tissue interface, it is encouraging to pursuit the ideal of having a uniform strontium delivery throughout which would aid in new bone formation.

Analysis must be conducted for the mechanical strength of these biomaterials before implantation with additional *in vivo* investigations and at different strontium doses. Moreover, CPC cements may not be the most ideal carrier for strontium delivery mostly because of its delayed or insufficient degradation. Hence, different carrier cements should be tested for their ability for enhanced strontium delivery to the interface.

On the other hand, 6 weeks after biomaterial implantation in the defect region might be a too short time gap for the study of new bone formation. Hence, analysis should be carried out over a prolonged time period in order to study the time related effects of strontium on bone formation. Additionally, more attention should be given to increase the process of

biomaterial degradation process or have rather more porous cement with highly interconnected networks which would facilitate proper tissue in growth.

In spite of the enhanced performance seen in the SrCPC cement, the main conclusion seems to be that there is still need for sophisticated materials to be developed in order to match the biological complexity at the molecular level. The future biomaterial implants should be resorbable, developed with a porous tri-dimensional framework filled with osteoinductive and osteoanabolic agents. A gradual resorption of the framework would release the trapped bioactive factors thereby allowing the transplanted and host cells to grow in this intertwining pattern. This would provide the scope for bone growth not only at the surface of the implant but also within the framework. However, the task of tailoring the biomaterial's surfaces for different purposes of implant integration and tissue regeneration seems a feasible challenge in the future, and requires a synergistic interdisciplinary work of materials science, engineering, biology, chemistry, physics and medicine.

REFERENCES

- 1 Conference Cd. Diagnosis, prophylaxis, and treatment of osteoporosis. *Consensus development conference*: Am J Med, 1993, 646-50.
- 2 Low KL, Tan SH, Zein SHS, Roether JA, Mouriño V, Boccaccini AR. Calcium phosphate-based composites as injectable bone substitute materials. *Journal of Biomedical Materials Research Part B: Applied Biomaterials*. 2010; **94B**: 273-86. 10.1002/jbm.b.31619.
- 3 Marie PJ. Strontium ranelate: New insights into its dual mode of action. *Bone*. 2007; **40**: S5-S8.
- 4 Bonnelye E, Chabadel A, Saltel F, Jurdic P. Dual effect of strontium ranelate: Stimulation of osteoblast differentiation and inhibition of osteoclast formation and resorption in vitro. *Bone*. 2008; **42**: 129-38.
- 5 Andersen OZ, Offermanns V, Sillassen M, Almtoft KP, Andersen IH, Sorensen S, Jeppesen CS, Kraft DC, Bottiger J, Rasse M, Kloss F, Foss M. Accelerated bone ingrowth by local delivery of strontium from surface functionalized titanium implants. *Biomaterials*. 2013; **34**: 5883-90. 10.1016/j.biomaterials.2013.04.031.
- 6 Xin Y, Jiang J, Huo K, Hu T, Chu PK. Bioactive SrTiO₃ nanotube arrays: strontium delivery platform on Ti-based osteoporotic bone implants. *ACS nano*. 2009; **3**: 3228-34. 10.1021/nn9007675.
- 7 Zhao L, Wang H, Huo K, Zhang X, Wang W, Zhang Y, Wu Z, Chu PK. The osteogenic activity of strontium loaded titania nanotube arrays on titanium substrates. *Biomaterials*. 2013; **34**: 19-29. 10.1016/j.biomaterials.2012.09.041.
- 8 Park JW, Kim YJ, Jang JH, Song H. Positive modulation of osteogenesis- and osteoclastogenesis-related gene expression with strontium-containing microstructured Ti implants in rabbit cancellous bone. *Journal of biomedical materials research Part A*. 2013; **101**: 298-306. 10.1002/jbm.a.34433.
- 9 Park JW, Kim HK, Kim YJ, Jang JH, Song H, Hanawa T. Osteoblast response and osseointegration of a Ti-6Al-4V alloy implant incorporating strontium. *Acta biomaterialia*. 2010; **6**: 2843-51. 10.1016/j.actbio.2010.01.017.

-
- 10 Park JW, Kim YJ, Jang JH. Enhanced osteoblast response to hydrophilic strontium and/or phosphate ions-incorporated titanium oxide surfaces. *Clinical oral implants research*. 2010; **21**: 398-408. 10.1111/j.1600-0501.2009.01863.x.
 - 11 Li Y, Li Q, Zhu S, Luo E, Li J, Feng G, Liao Y, Hu J. The effect of strontium-substituted hydroxyapatite coating on implant fixation in ovariectomized rats. *Biomaterials*. 2010; **31**: 9006-14. 10.1016/j.biomaterials.2010.07.112.
 - 12 Fu DL, Jiang QH, He FM, Yang GL, Liu L. Fluorescence microscopic analysis of bone osseointegration of strontium-substituted hydroxyapatite implants. *Journal of Zhejiang University Science B*. 2012; **13**: 364-71. 10.1631/jzus.B1100381.
 - 13 Alt V, Thormann U, Ray S, Zahner D, Durselen L, Lips K, El Khassawna T, Heiss C, Riedrich A, Schlewitz G, Ignatius A, Kampschulte M, von Dewitz H, Heinemann S, Schnettler R, Langheinrich A. A new metaphyseal bone defect model in osteoporotic rats to study biomaterials for the enhancement of bone healing in osteoporotic fractures. *Acta biomaterialia*. 2013; **9**: 7035-42. 10.1016/j.actbio.2013.02.002.
 - 14 Raisz LG. Physiology and Pathophysiology of Bone Remodeling. *Clinical Chemistry*. 1999; **45**: 1353-8.
 - 15 Karsenty G, Wagner EF. Reaching a genetic and molecular understanding of skeletal development. *Developmental cell*. 2002; **2**: 389-406.
 - 16 Raggatt LJ, Partridge NC. Cellular and Molecular Mechanisms of Bone Remodeling. *Journal of Biological Chemistry*. 2010; **285**: 25103-8.
 - 17 Maes C, Kobayashi T, Kronenberg HM. A novel transgenic mouse model to study the osteoblast lineage in vivo. *Annals of the New York Academy of Sciences*. 2007; **1116**: 149-64. 10.1196/annals.1402.060.
 - 18 Cao Y, Zhou Z, de Crombrughe B, Nakashima K, Guan H, Duan X, Jia SF, Kleinerman ES. Osterix, a transcription factor for osteoblast differentiation, mediates antitumor activity in murine osteosarcoma. *Cancer research*. 2005; **65**: 1124-8. 10.1158/0008-5472.CAN-04-2128.
 - 19 Henriksen K, Sorensen MG, Nielsen RH, Gram J, Schaller S, Dziegiel MH, Everts V, Bollerslev J, Karsdal MA. Degradation of the organic phase of bone by osteoclasts: a secondary role for lysosomal acidification. *Journal of bone and*
-

- mineral research : the official journal of the American Society for Bone and Mineral Research*. 2006; **21**: 58-66. 10.1359/JBMR.050905.
- 20 Hong YH, Hishikawa D, Miyahara H, Tsuzuki H, Nishimura Y, Gotoh C, Choi KC, Hokari Y, Takagi Y, Lee HG, Cho KK, Roh SG, Sasaki S. Up-regulation of adipogenin, an adipocyte plasma transmembrane protein, during adipogenesis. *Molecular and cellular biochemistry*. 2005; **276**: 133-41. 10.1007/s11010-005-3673-0.
- 21 Suzuki R, Domon T, Wakita M. Some osteocytes released from their lacunae are embedded again in the bone and not engulfed by osteoclasts during bone remodeling. *Anatomy and embryology*. 2000; **202**: 119-28.
- 22 Hughes DE, Boyce BF. Apoptosis in bone physiology and disease. *Molecular pathology : MP*. 1997; **50**: 132-7.
- 23 Nakamura T, Imai Y, Matsumoto T, Sato S, Takeuchi K, Igarashi K, Harada Y, Azuma Y, Krust A, Yamamoto Y, Nishina H, Takeda S, Takayanagi H, Metzger D, Kanno J, Takaoka K, Martin TJ, Chambon P, Kato S. Estrogen prevents bone loss via estrogen receptor alpha and induction of Fas ligand in osteoclasts. *Cell*. 2007; **130**: 811-23. 10.1016/j.cell.2007.07.025.
- 24 Villanueva AR, Sypitkowski C, Parfitt AM. A new method for identification of cement lines in undecalcified, plastic embedded sections of bone. *Stain technology*. 1986; **61**: 83-8.
- 25 Boyce BF, Xing L. Biology of RANK, RANKL, and osteoprotegerin. *Arthritis research & therapy*. 2007; **9 Suppl 1**: S1. 10.1186/ar2165.
- 26 Kong YY, Yoshida H, Sarosi I, Tan HL, Timms E, Capparelli C, Morony S, Oliveira-dos-Santos AJ, Van G, Itie A, Khoo W, Wakeham A, Dunstan CR, Lacey DL, Mak TW, Boyle WJ, Penninger JM. OPGL is a key regulator of osteoclastogenesis, lymphocyte development and lymph-node organogenesis. *Nature*. 1999; **397**: 315-23. 10.1038/16852.
- 27 Lyritis GP. Fracture healing and antiosteoporotic treatments. *Medicographia*. 2010; **32**, No.1.

-
- 28 Lyritis GP, Georgoulas T, Zafeiris CP. Bone anabolic versus bone anticatabolic treatment of postmenopausal osteoporosis. *Annals of the New York Academy of Sciences*. 2010; **1205**: 277-83. 10.1111/j.1749-6632.2010.05666.x.
- 29 Einhorn TA. The cell and molecular biology of fracture healing. *Clinical orthopaedics and related research*. 1998: S7-21.
- 30 Schmidt-Bleek K, Schell H, Kolar P, Pfaff M, Perka C, Buttgereit F, Duda G, Lienau J. Cellular composition of the initial fracture hematoma compared to a muscle hematoma: a study in sheep. *Journal of orthopaedic research : official publication of the Orthopaedic Research Society*. 2009; **27**: 1147-51. 10.1002/jor.20901.
- 31 Bolander ME. Regulation of fracture repair by growth factors. *Proceedings of the Society for Experimental Biology and Medicine Society for Experimental Biology and Medicine*. 1992; **200**: 165-70.
- 32 Frost HM. The biology of fracture healing. An overview for clinicians. Part II. *Clinical orthopaedics and related research*. 1989: 294-309.
- 33 Pittenger MF, Mackay AM, Beck SC, Jaiswal RK, Douglas R, Mosca JD, Moorman MA, Simonetti DW, Craig S, Marshak DR. Multilineage potential of adult human mesenchymal stem cells. *Science*. 1999; **284**: 143-7.
- 34 Brighton CT, Hunt RM. Histochemical localization of calcium in the fracture callus with potassium pyroantimonate. Possible role of chondrocyte mitochondrial calcium in callus calcification. *The Journal of bone and joint surgery American volume*. 1986; **68**: 703-15.
- 35 Einhorn TA, Hirschman A, Kaplan C, Nashed R, Devlin VJ, Warman J. Neutral protein-degrading enzymes in experimental fracture callus: a preliminary report. *Journal of orthopaedic research : official publication of the Orthopaedic Research Society*. 1989; **7**: 792-805. 10.1002/jor.1100070604.
- 36 RB H. *Fracture Treatment and Healing*. Philadelphia: WB Saunders, 1980.
- 37 Griffin XL, Smith CM, Costa ML. The clinical use of platelet-rich plasma in the promotion of bone healing: a systematic review. *Injury*. 2009; **40**: 158-62. 10.1016/j.injury.2008.06.025.
-

-
- 38 Reginster JY, Burlet N. Osteoporosis: a still increasing prevalence. *Bone*. 2006; **38**: S4-9. 10.1016/j.bone.2005.11.024.
- 39 Compston JE, Papapoulos SE, Blanchard F. Report on osteoporosis in the European Community: current status and recommendations for the future. Working Party from European Union Member States. *Osteoporosis international : a journal established as result of cooperation between the European Foundation for Osteoporosis and the National Osteoporosis Foundation of the USA*. 1998; **8**: 531-4.
- 40 Lin JT, Lane JM. Osteoporosis: a review. *Clinical orthopaedics and related research*. 2004: 126-34.
- 41 (NOF) NOF. America's bone health: the state of osteoporosis and low bone mass in our nation. Washington DC. 2002, 1–55.
- 42 Cooper C, Campion G, Melton LJ, 3rd. Hip fractures in the elderly: a world-wide projection. *Osteoporosis international : a journal established as result of cooperation between the European Foundation for Osteoporosis and the National Osteoporosis Foundation of the USA*. 1992; **2**: 285-9.
- 43 Cornell CN CN. Current. Opinion in Orthopaedics. Oct;16(5):376–381 edn, 2005.
- 44 Currey JD, Brear K, Zioupos P. The effects of ageing and changes in mineral content in degrading the toughness of human femora. *Journal of biomechanics*. 1996; **29**: 257-60.
- 45 Burr DB, Forwood MR, Fyhrie DP, Martin RB, Schaffler MB, Turner CH. Bone Microdamage and Skeletal Fragility in Osteoporotic and Stress Fractures. *Journal of Bone and Mineral Research*. 1997; **12**: 6-15. 10.1359/jbmr.1997.12.1.6.
- 46 Boskey AL, DiCarlo E, Paschalis E, West P, Mendelsohn R. Comparison of mineral quality and quantity in iliac crest biopsies from high- and low-turnover osteoporosis: an FT-IR microspectroscopic investigation. *Osteoporosis International*. 2005; **16**: 2031-8. 10.1007/s00198-005-1992-3.
- 47 Lim TH, An HS, Evanich C, Hasanoglu KY, McGrady L, Wilson CR. Strength of anterior vertebral screw fixation in relationship to bone mineral density. *Journal of spinal disorders*. 1995; **8**: 121-5.
-

-
- 48 Mosekilde L. Age-related changes in bone mass, structure, and strength--effects of loading. *Zeitschrift fur Rheumatologie*. 2000; **59 Suppl 1**: 1-9.
- 49 Pearce AI, Richards RG, Milz S, Schneider E, Pearce SG. Animal models for implant biomaterial research in bone: a review. *European cells & materials*. 2007; **13**: 1-10.
- 50 Bonnarens F, Einhorn TA. Production of a standard closed fracture in laboratory animal bone. *Journal of orthopaedic research : official publication of the Orthopaedic Research Society*. 1984; **2**: 97-101. 10.1002/jor.1100020115.
- 51 Stuermer EK, Sehmisch S, Rack T, Wenda E, Seidlova-Wuttke D, Tezval M, Wuttke W, Frosch KH, Stuermer KM. Estrogen and raloxifene improve metaphyseal fracture healing in the early phase of osteoporosis. A new fracture-healing model at the tibia in rat. *Langenbecks Arch Surg*. 2010; **395**: 163-72. 10.1007/s00423-008-0436-x.
- 52 Claes L, Blakytyn R, Gockelmann M, Schoen M, Ignatius A, Willie B. Early dynamization by reduced fixation stiffness does not improve fracture healing in a rat femoral osteotomy model. *Journal of orthopaedic research : official publication of the Orthopaedic Research Society*. 2009; **27**: 22-7. 10.1002/jor.20712.
- 53 Danielsen CC, Mosekilde L, Svenstrup B. Cortical bone mass, composition, and mechanical properties in female rats in relation to age, long-term ovariectomy, and estrogen substitution. *Calcified tissue international*. 1993; **52**: 26-33.
- 54 Thompson DD, Simmons HA, Pirie CM, Ke HZ. FDA Guidelines and animal models for osteoporosis. *Bone*. 1995; **17**: 125s-33s.
- 55 Stuermer EK, Sehmisch S, Rack T, Wenda E, Seidlova-Wuttke D, Tezval M, Wuttke W, Frosch KH, Stuermer KM. Estrogen and raloxifene improve metaphyseal fracture healing in the early phase of osteoporosis. A new fracture-healing model at the tibia in rat. *Langenbecks Arch Surg*. 2010; **395**: 163-72. 10.1007/s00423-008-0436-x.
- 56 Kolios L, Hoerster A, Sehmisch S, Malcherek M, Rack T, Tezval M, Seidlova-Wuttke D, Wuttke W, Stuermer K, Stuermer E. Do Estrogen and Alendronate Improve Metaphyseal Fracture Healing When Applied as Osteoporosis
-

- Prophylaxis? *Calcified tissue international*. 2010; **86**: 23-32. 10.1007/s00223-009-9318-7.
- 57 Kubo T, Shiga T, Hashimoto J, Yoshioka M, Honjo H, Urabe M, Kitajima I, Semba I, Hirasawa Y. Osteoporosis influences the late period of fracture healing in a rat model prepared by ovariectomy and low calcium diet. *The Journal of steroid biochemistry and molecular biology*. 1999; **68**: 197-202.
- 58 Meyer RA, Jr., Tsahakis PJ, Martin DF, Banks DM, Harrow ME, Kiebzak GM. Age and ovariectomy impair both the normalization of mechanical properties and the accretion of mineral by the fracture callus in rats. *Journal of orthopaedic research : official publication of the Orthopaedic Research Society*. 2001; **19**: 428-35. 10.1016/s0736-0266(00)90034-2.
- 59 Namkung-Matthai H, Appleyard R, Jansen J, Hao Lin J, Maastricht S, Swain M, Mason RS, Murrell GA, Diwan AD, Diamond T. Osteoporosis influences the early period of fracture healing in a rat osteoporotic model. *Bone*. 2001; **28**: 80-6.
- 60 Lill CA, Hessel J, Schlegel U, Eckhardt C, Goldhahn J, Schneider E. Biomechanical evaluation of healing in a non-critical defect in a large animal model of osteoporosis. *Journal of orthopaedic research : official publication of the Orthopaedic Research Society*. 2003; **21**: 836-42. 10.1016/s0736-0266(02)00266-8.
- 61 Xu SW, Wang JW, Li W, Wang Y, Zhao GF. [Osteoporosis impairs fracture healing of tibia in a rat osteoporotic model]. *Zhonghua yi xue za zhi*. 2004; **84**: 1205-9.
- 62 Islam AA, Rasubala L, Yoshikawa H, Shiratsuchi Y, Ohishi M. Healing of fractures in osteoporotic rat mandible shown by the expression of bone morphogenetic protein-2 and tumour necrosis factor-alpha. *The British journal of oral & maxillofacial surgery*. 2005; **43**: 383-91. 10.1016/j.bjoms.2004.10.018.
- 63 Wang JW, Li W, Xu SW, Yang DS, Wang Y, Lin M, Zhao GF. Osteoporosis influences the middle and late periods of fracture healing in a rat osteoporotic model. *Chinese journal of traumatology = Zhonghua chuang shang za zhi / Chinese Medical Association*. 2005; **8**: 111-6.

-
- 64 Qiao L, Xu KH, Liu HW, Liu HQ. [Effects of ovariectomy on fracture healing in female rats]. *Sichuan da xue xue bao Yi xue ban = Journal of Sichuan University Medical science edition*. 2005; **36**: 108-11.
- 65 Carano A, Teitelbaum SL, Konsek JD, Schlesinger PH, Blair HC. Bisphosphonates directly inhibit the bone resorption activity of isolated avian osteoclasts in vitro. *The Journal of clinical investigation*. 1990; **85**: 456-61. 10.1172/jci114459.
- 66 Auer JA, Goodship A, Arnoczky S, Pearce S, Price J, Claes L, von Rechenberg B, Hofmann-Amttenbrinck M, Schneider E, Muller-Terpitz R, Thiele F, Rippe KP, Grainger DW. Refining animal models in fracture research: seeking consensus in optimising both animal welfare and scientific validity for appropriate biomedical use. *BMC musculoskeletal disorders*. 2007; **8**: 72. 10.1186/1471-2474-8-72.
- 67 Gerstenfeld LC, Sacks DJ, Pelis M, Mason ZD, Graves DT, Barrero M, Ominsky MS, Kostenuik PJ, Morgan EF, Einhorn TA. Comparison of effects of the bisphosphonate alendronate versus the RANKL inhibitor denosumab on murine fracture healing. *Journal of bone and mineral research : the official journal of the American Society for Bone and Mineral Research*. 2009; **24**: 196-208. 10.1359/jbmr.081113.
- 68 Larsson S, Fazzalari NL. Anti-osteoporosis therapy and fracture healing. *Archives of orthopaedic and trauma surgery*. 2014; **134**: 291-7. 10.1007/s00402-012-1558-8.
- 69 Hock JM, Gera I. Effects of continuous and intermittent administration and inhibition of resorption on the anabolic response of bone to parathyroid hormone. *Journal of bone and mineral research : the official journal of the American Society for Bone and Mineral Research*. 1992; **7**: 65-72. 10.1002/jbmr.5650070110.
- 70 Kakar S, Einhorn TA, Vora S, Miara LJ, Hon G, Wigner NA, Toben D, Jacobsen KA, Al-Sebaei MO, Song M, Trackman PC, Morgan EF, Gerstenfeld LC, Barnes GL. Enhanced chondrogenesis and Wnt signaling in PTH-treated fractures. *Journal of bone and mineral research : the official journal of the American Society for Bone and Mineral Research*. 2007; **22**: 1903-12. 10.1359/jbmr.070724.
- 71 Atkins GJ, Welldon KJ, Halbout P, Findlay DM. Strontium ranelate treatment of human primary osteoblasts promotes an osteocyte-like phenotype while eliciting an osteoprotegerin response. *Osteoporosis international : a journal established as result of cooperation between the European Foundation for Osteoporosis and the*
-

- National Osteoporosis Foundation of the USA*. 2009; **20**: 653-64. 10.1007/s00198-008-0728-6.
- 72 Yamaguchi T. The calcium-sensing receptor in bone. *Journal of bone and mineral metabolism*. 2008; **26**: 301-11. 10.1007/s00774-008-0843-7.
- 73 Goodship AE, Walker PC, McNally D, Chambers T, Green JR. Use of a bisphosphonate (pamidronate) to modulate fracture repair in ovine bone. *Annals of oncology : official journal of the European Society for Medical Oncology / ESMO*. 1994; **5 Suppl 7**: S53-5.
- 74 Li C, Mori S, Li J, Kaji Y, Akiyama T, Kawanishi J, Norimatsu H. Long-term effect of incadronate disodium (YM-175) on fracture healing of femoral shaft in growing rats. *Journal of bone and mineral research : the official journal of the American Society for Bone and Mineral Research*. 2001; **16**: 429-36. 10.1359/jbmr.2001.16.3.429.
- 75 Habermann B, Kafchitsas K, Olender G, Augat P, Kurth A. Strontium ranelate enhances callus strength more than PTH 1-34 in an osteoporotic rat model of fracture healing. *Calcified tissue international*. 2010; **86**: 82-9. 10.1007/s00223-009-9317-8.
- 76 Nozaka K, Miyakoshi N, Kasukawa Y, Maekawa S, Noguchi H, Shimada Y. Intermittent administration of human parathyroid hormone enhances bone formation and union at the site of cancellous bone osteotomy in normal and ovariectomized rats. *Bone*. 2008; **42**: 90-7. 10.1016/j.bone.2007.08.041.
- 77 Cipriano CA, Issack PS, Shindle L, Werner CM, Helfet DL, Lane JM. Recent advances toward the clinical application of PTH (1-34) in fracture healing. *HSS journal : the musculoskeletal journal of Hospital for Special Surgery*. 2009; **5**: 149-53. 10.1007/s11420-009-9109-8.
- 78 Alkhiary YM, Gerstenfeld LC, Krall E, Westmore M, Sato M, Mitlak BH, Einhorn TA. Enhancement of experimental fracture-healing by systemic administration of recombinant human parathyroid hormone (PTH 1-34). *The Journal of bone and joint surgery American volume*. 2005; **87**: 731-41. 10.2106/jbjs.d.02115.
- 79 Doetsch AM, Faber J, Lynnerup N, Watjen I, Bliddal H, Danneskiold-Samsøe B. The effect of calcium and vitamin D3 supplementation on the healing of the

- proximal humerus fracture: a randomized placebo-controlled study. *Calcified tissue international*. 2004; **75**: 183-8. 10.1007/s00223-004-0167-0.
- 80 Lyritis G, Boscainos PJ. Calcitonin effects on cartilage and fracture healing. *Journal of musculoskeletal & neuronal interactions*. 2001; **2**: 137-42.
 - 81 Wong KL, Wong CT, Liu WC, Pan HB, Fong MK, Lam WM, Cheung WL, Tang WM, Chiu KY, Luk KD, Lu WW. Mechanical properties and in vitro response of strontium-containing hydroxyapatite/polyetheretherketone composites. *Biomaterials*. 2009; **30**: 3810-7. 10.1016/j.biomaterials.2009.04.016.
 - 82 Cabrera WE, Schrooten I, De Broe ME, D'Haese PC. Strontium and bone. *Journal of bone and mineral research : the official journal of the American Society for Bone and Mineral Research*. 1999; **14**: 661-8. 10.1359/jbmr.1999.14.5.661.
 - 83 Ma YF, Ferretti JL, Capozza RF, Cointry G, Alippi R, Zanchetta J, Jee WS. Effects of on/off anabolic hPTH and remodeling inhibitors on metaphyseal bone of immobilized rat femurs. Tomographical (pQCT) description and correlation with histomorphometric changes in tibial cancellous bone. *Bone*. 1995; **17**: 321s-7s.
 - 84 Meunier PJ, Roux C, Seeman E, Ortolani S, Badurski JE, Spector TD, Cannata J, Balogh A, Lemmel EM, Pors-Nielsen S, Rizzoli R, Genant HK, Reginster JY. The effects of strontium ranelate on the risk of vertebral fracture in women with postmenopausal osteoporosis. *The New England journal of medicine*. 2004; **350**: 459-68. 10.1056/NEJMoa022436.
 - 85 Reginster JY, Seeman E, De Vernejoul MC, Adami S, Compston J, Phenekos C, Devogelaer JP, Curiel MD, Sawicki A, Goemaere S, Sorensen OH, Felsenberg D, Meunier PJ. Strontium ranelate reduces the risk of nonvertebral fractures in postmenopausal women with osteoporosis: Treatment of Peripheral Osteoporosis (TROPOS) study. *The Journal of clinical endocrinology and metabolism*. 2005; **90**: 2816-22. 10.1210/jc.2004-1774.
 - 86 Boivin G, Deloffre P, Perrat B, Panczer G, Boudeulle M, Mauras Y, Allain P, Tsouderos Y, Meunier PJ. Strontium distribution and interactions with bone mineral in monkey iliac bone after strontium salt (S 12911) administration. *Journal of bone and mineral research : the official journal of the American Society for Bone and Mineral Research*. 1996; **11**: 1302-11. 10.1002/jbmr.5650110915.

-
- 87 Marie PJ, Hott M, Modrowski D, De Pollak C, Guillemain J, Deloffre P, Tsouderos Y. An uncoupling agent containing strontium prevents bone loss by depressing bone resorption and maintaining bone formation in estrogen-deficient rats. *Journal of bone and mineral research : the official journal of the American Society for Bone and Mineral Research*. 1993; **8**: 607-15. 10.1002/jbmr.5650080512.
- 88 Morohashi T, Sano T, Harai K, Yamada S. Effects of strontium on calcium metabolism in rats. II. Strontium prevents the increased rate of bone turnover in ovariectomized rats. *Japanese journal of pharmacology*. 1995; **68**: 153-9.
- 89 Leeuwenkamp OR, van der Vijgh WJ, Husken BC, Lips P, Netelenbos JC. Human pharmacokinetics of orally administered strontium. *Calcified tissue international*. 1990; **47**: 136-41.
- 90 Aerssens J, Boonen S, Lowet G, Dequeker J. Interspecies differences in bone composition, density, and quality: potential implications for in vivo bone research. *Endocrinology*. 1998; **139**: 663-70.
- 91 Raffalt AC, Andersen JE, Christgau S. Application of inductively coupled plasma-mass spectrometry (ICP-MS) and quality assurance to study the incorporation of strontium into bone, bone marrow, and teeth of dogs after one month of treatment with strontium malonate. *Analytical and bioanalytical chemistry*. 2008; **391**: 2199-207. 10.1007/s00216-008-2171-0.
- 92 Dahl SG, Allain P, Marie PJ, Mauras Y, Boivin G, Ammann P, Tsouderos Y, Delmas PD, Christiansen C. Incorporation and distribution of strontium in bone. *Bone*. 2001; **28**: 446-53.
- 93 Gryn timer MD, Hamilton E, Cheung R, Tsouderos Y, Deloffre P, Hott M, Marie PJ. Strontium increases vertebral bone volume in rats at a low dose that does not induce detectable mineralization defect. *Bone*. 1996; **18**: 253-9.
- 94 Arlot ME, Jiang Y, Genant HK, Zhao J, Burt-Pichat B, Roux JP, Delmas PD, Meunier PJ. Histomorphometric and microCT analysis of bone biopsies from postmenopausal osteoporotic women treated with strontium ranelate. *Journal of bone and mineral research : the official journal of the American Society for Bone and Mineral Research*. 2008; **23**: 215-22. 10.1359/jbmr.071012.
-

-
- 95 Ammann P, Shen V, Robin B, Mauras Y, Bonjour JP, Rizzoli R. Strontium ranelate improves bone resistance by increasing bone mass and improving architecture in intact female rats. *Journal of bone and mineral research : the official journal of the American Society for Bone and Mineral Research*. 2004; **19**: 2012-20. 10.1359/jbmr.040906.
- 96 Meunier PJ, Roux C, Ortolani S, Diaz-Curiel M, Compston J, Marquis P, Cormier C, Isaia G, Badurski J, Wark JD, Collette J, Reginster JY. Effects of long-term strontium ranelate treatment on vertebral fracture risk in postmenopausal women with osteoporosis. *Osteoporosis international : a journal established as result of cooperation between the European Foundation for Osteoporosis and the National Osteoporosis Foundation of the USA*. 2009; **20**: 1663-73. 10.1007/s00198-008-0825-6.
- 97 Boyd D, Carroll G, Towler MR, Freeman C, Farthing P, Brook IM. Preliminary investigation of novel bone graft substitutes based on strontium-calcium-zinc-silicate glasses. *Journal of materials science Materials in medicine*. 2009; **20**: 413-20. 10.1007/s10856-008-3569-0.
- 98 Towler MR, Boyd D, Freeman C, Brook IM, Farthing P. Comparison of in vitro and in vivo bioactivity of SrO-CaO-ZnO-SiO₂ glass grafts. *Journal of biomaterials applications*. 2009; **23**: 561-72. 10.1177/0885328208094306.
- 99 Tian M, Chen F, Song W, Song Y, Chen Y, Wan C, Yu X, Zhang X. In vivo study of porous strontium-doped calcium polyphosphate scaffolds for bone substitute applications. *Journal of materials science Materials in medicine*. 2009; **20**: 1505-12. 10.1007/s10856-009-3713-5.
- 100 Brennan TC, Rybchyn MS, Green W, Atwa S, Conigrave AD, Mason RS. Osteoblasts play key roles in the mechanisms of action of strontium ranelate. *British journal of pharmacology*. 2009; **157**: 1291-300. 10.1111/j.1476-5381.2009.00305.x.
- 101 Fromigue O, Hay E, Barbara A, Petrel C, Traiffort E, Ruat M, Marie PJ. Calcium sensing receptor-dependent and receptor-independent activation of osteoblast replication and survival by strontium ranelate. *Journal of cellular and molecular medicine*. 2009; **13**: 2189-99. 10.1111/j.1582-4934.2009.00673.x.
-

-
- 102 Caverzasio J. Strontium ranelate promotes osteoblastic cell replication through at least two different mechanisms. *Bone*. 2008; **42**: 1131-6. 10.1016/j.bone.2008.02.010.
- 103 Teitelbaum SL. Bone resorption by osteoclasts. *Science*. 2000; **289**: 1504-8.
- 104 Fletcher JS, Vickerman JC. Secondary ion mass spectrometry: characterizing complex samples in two and three dimensions. *Analytical chemistry*. 2013; **85**: 610-39. 10.1021/ac303088m.
- 105 Vickerman JC, Briggs D, SurfaceSpectra Ltd. *ToF-SIMS : surface analysis by mass spectrometry*. Chichester: IM, 2001.
- 106 Fletcher JS, Vickerman JC. A new SIMS paradigm for 2D and 3D molecular imaging of bio-systems. *Analytical and bioanalytical chemistry*. 2010; **396**: 85-104. 10.1007/s00216-009-2986-3.
- 107 Rabbani S, Barber AM, Fletcher JS, Lockyer NP, Vickerman JC. TOF-SIMS with argon gas cluster ion beams: a comparison with C60+. *Analytical chemistry*. 2011; **83**: 3793-800. 10.1021/ac200288v.
- 108 Oshima S, Kashiwara I, Moritani K, Inui N, Mochiji K. Soft-sputtering of insulin films in argon-cluster secondary ion mass spectrometry. *Rapid communications in mass spectrometry : RCM*. 2011; **25**: 1070-4. 10.1002/rcm.4959.
- 109 Borner K, Nygren H, Hagenhoff B, Malmberg P, Tallarek E, Mansson JE. Distribution of cholesterol and galactosylceramide in rat cerebellar white matter. *Biochimica et biophysica acta*. 2006; **1761**: 335-44. 10.1016/j.bbalip.2006.02.021.
- 110 Hagenhoff BB DT, E.; Möllers, R.; Niehuis, E.; Sperber, M.; Goricnik, B.; Wegener, J. . Detection of micro- and nano-particles in animal cells by ToF-SIMS 3D analysis. *Surf Interface Anal*. 2013; **45 (1)**:315-319.
- 111 Palmquist A EL, Sjoval P Chemical and structural analysis of the bone-implant interface by TOF-SIMS, SEM, FIB and TEM: Experimental study in animal. *Appl Surf Sci* 2012; **258 (17)**:6485-6494.
- 112 Henss A, Rohnke M, El Khassawna T, Govindarajan P, Schlewitz G, Heiss C, Janek J. Applicability of ToF-SIMS for monitoring compositional changes in bone in a long-term animal model. *Journal of the Royal Society, Interface / the Royal Society*. 2013; **10**: 20130332. 10.1098/rsif.2013.0332.
-

-
- 113 Sato I, Akizuki T, Oda S, Tsuchioka H, Hayashi C, Takasaki AA, Mizutani K, Kawakatsu N, Kinoshita A, Ishikawa I, Izumi Y. Histological evaluation of alveolar ridge augmentation using injectable calcium phosphate bone cement in dogs. *Journal of oral rehabilitation*. 2009; **36**: 762-9. 10.1111/j.1365-2842.2009.01991.x.
- 114 Theiss F, Apelt D, Brand B, Kutter A, Zlinszky K, Böhner M, Matter S, Frei C, Auer JA, von Rechenberg B. Biocompatibility and resorption of a brushite calcium phosphate cement. *Biomaterials*. 2005; **26**: 4383-94. 10.1016/j.biomaterials.2004.11.056.
- 115 Apelt D, Theiss F, El-Warrak AO, Zlinszky K, Bettschart-Wolfisberger R, Böhner M, Matter S, Auer JA, von Rechenberg B. In vivo behavior of three different injectable hydraulic calcium phosphate cements. *Biomaterials*. 2004; **25**: 1439-51.
- 116 Poser L, Matthys R, Schawalder P, Pearce S, Alini M, Zeiter S. A Standardized Critical Size Defect Model in Normal and Osteoporotic Rats to Evaluate Bone Tissue Engineered Constructs. 2014; **2014**: 348635.
- 117 Heiss C, Govindarajan P, Schlewitz G, Hemdan NY, Schliecke N, Alt V, Thormann U, Lips KS, Wenisch S, Langheinrich AC, Zahner D, Schnettler R. Induction of osteoporosis with its influence on osteoporotic determinants and their interrelationships in rats by DEXA. *Medical science monitor : international medical journal of experimental and clinical research*. 2012; **18**: Br199-207.
- 118 Schlewitz G, Govindarajan P, Schliecke N, Alt V, Bocker W, Elkhassawna T, Thormann U, Lips KS, Hemdan NY, Zahner D, Schnettler R, Heiss C. [Ovariectomy and calcium/vitamin D2/D3 deficient diet as a model of osteoporosis in the spine of Sprague-Dawley rats]. *Zeitschrift für Orthopädie und Unfallchirurgie*. 2013; **151**: 14-9. 10.1055/s-0032-1327976.
- 119 Giannoudis PV, Schneider E. Principles of fixation of osteoporotic fractures. *Journal of Bone & Joint Surgery, British Volume*. 2006; **88-B**: 1272-8.
- 120 Delannoy P, Bazot D, Marie PJ. Long-term treatment with strontium ranelate increases vertebral bone mass without deleterious effect in mice. *Metabolism: clinical and experimental*. 2002; **51**: 906-11.
- 121 Hott M, Deloffre P, Tsouderos Y, Marie PJ. S12911-2 reduces bone loss induced by short-term immobilization in rats. *Bone*. 2003; **33**: 115-23.
-

-
- 122 Boivin G, Farlay D, Khebbab MT, Jaurand X, Delmas PD, Meunier PJ. In osteoporotic women treated with strontium ranelate, strontium is located in bone formed during treatment with a maintained degree of mineralization. *Osteoporosis international : a journal established as result of cooperation between the European Foundation for Osteoporosis and the National Osteoporosis Foundation of the USA*. 2010; **21**: 667-77. 10.1007/s00198-009-1005-z.
- 123 Guimaraes KB, Vasconcelos BC, Limeira Junior Fde A, Sousa FB, Andrade ES, Vasconcellos RJ. Histomorphometric evaluation of calcium phosphate bone grafts on bone repair. *Brazilian journal of otorhinolaryngology*. 2011; **77**: 447-54.
- 124 Chattopadhyay N, Quinn SJ, Kifor O, Ye C, Brown EM. The calcium-sensing receptor (CaR) is involved in strontium ranelate-induced osteoblast proliferation. *Biochemical pharmacology*. 2007; **74**: 438-47. 10.1016/j.bcp.2007.04.020.
- 125 Takaoka S, Yamaguchi T, Yano S, Yamauchi M, Sugimoto T. The Calcium-sensing Receptor (CaR) is involved in strontium ranelate-induced osteoblast differentiation and mineralization. *Hormone and metabolic research = Hormon- und Stoffwechselforschung = Hormones et metabolisme*. 2010; **42**: 627-31. 10.1055/s-0030-1255091.
- 126 Magno AL, Ward BK, Ratajczak T. The calcium-sensing receptor: a molecular perspective. *Endocrine reviews*. 2011; **32**: 3-30. 10.1210/er.2009-0043.
- 127 Ni GX, Lin JH, Chiu PK, Li ZY, Lu WW. Effect of strontium-containing hydroxyapatite bone cement on bone remodeling following hip replacement. *Journal of materials science Materials in medicine*. 2010; **21**: 377-84. 10.1007/s10856-009-3866-2.
- 128 Kim YS, Paik IY, Rhie YJ, Suh SH. Integrative physiology: defined novel metabolic roles of osteocalcin. *Journal of Korean medical science*. 2010; **25**: 985-91. 10.3346/jkms.2010.25.7.985.
- 129 Zheng Q, Zhou G, Morello R, Chen Y, Garcia-Rojas X, Lee B. Type X collagen gene regulation by Runx2 contributes directly to its hypertrophic chondrocyte-specific expression in vivo. *The Journal of cell biology*. 2003; **162**: 833-42. 10.1083/jcb.200211089.
-

-
- 130 Qi H, Aguiar DJ, Williams SM, La Pean A, Pan W, Verfaillie CM. Identification of genes responsible for osteoblast differentiation from human mesodermal progenitor cells. *Proceedings of the National Academy of Sciences of the United States of America*. 2003; **100**: 3305-10. 10.1073/pnas.0532693100.
- 131 Lienau J, Schmidt-Bleek K, Peters A, Haschke F, Duda GN, Perka C, Bail HJ, Schutze N, Jakob F, Schell H. Differential regulation of blood vessel formation between standard and delayed bone healing. *Journal of orthopaedic research : official publication of the Orthopaedic Research Society*. 2009; **27**: 1133-40. 10.1002/jor.20870.
- 132 Vestermarck MT, Hauge EM, Soballe K, Bechtold JE, Jakobsen T, Baas J. Strontium doping of bone graft extender. *Acta orthopaedica*. 2011; **82**: 614-21. 10.3109/17453674.2011.618909.
- 133 Schumacher M, Henss A, Rohnke M, Gelinsky M. A novel and easy-to-prepare strontium(II) modified calcium phosphate bone cement with enhanced mechanical properties. *Acta biomaterialia*. 2013; **9**: 7536-44. 10.1016/j.actbio.2013.03.014.
- 134 Johnson AR, Armstrong WD, Singer L. The incorporation and removal of large amounts of strontium by physiologic mechanisms in mineralized tissues. *Calcified tissue research*. 1968; **2**: 242-52.
- 135 Anderson JM, Rodriguez A, Chang DT. Foreign body reaction to biomaterials. *Seminars in immunology*. 2008; **20**: 86-100. 10.1016/j.smim.2007.11.004.
- 136 Das D, Zhang Z, Winkler T, Mour M, Gunter CI, Morlock MM, Machens HG, Schilling AF. Bioresorption and Degradation of Biomaterials. *Advances in biochemical engineering/biotechnology*. 2011. 10.1007/10_2011_119.
- 137 Navarro M, Michiardi A, Castano O, Planell JA. Biomaterials in orthopaedics. *Journal of the Royal Society, Interface / the Royal Society*. 2008; **5**: 1137-58. 10.1098/rsif.2008.0151.
- 138 Wang H, Zou Q, Boerman OC, Nijhuis AW, Jansen JA, Li Y, Leeuwenburgh SC. Combined delivery of BMP-2 and bFGF from nanostructured colloidal gelatin gels and its effect on bone regeneration in vivo. *Journal of controlled release : official journal of the Controlled Release Society*. 2013; **166**: 172-81. 10.1016/j.jconrel.2012.12.015.
-

- 139 Binulal NS, Natarajan A, Menon D, Bhaskaran VK, Mony U, Nair SV. Gelatin nanoparticles loaded poly(epsilon-caprolactone) nanofibrous semi-synthetic scaffolds for bone tissue engineering. *Biomedical materials (Bristol, England)*. 2012; 7: 065001. 10.1088/1748-6041/7/6/065001.
- 140 Kundu B, Rajkhowa R, Kundu SC, Wang X. Silk fibroin biomaterials for tissue regenerations. *Advanced drug delivery reviews*. 2013; 65: 457-70. 10.1016/j.addr.2012.09.043.

SUMMARY

In this thesis, CPC and SrCPC were used to evaluate bone healing in a critical size metaphyseal defect model in osteoporotic rats after 6 weeks and compared to an empty defect. Control empty defect showed a significantly lower bone formation. The highest bone remodeling was seen in the SrCPC group six weeks after biomaterial implantation. Trabecular bone formation in the SrCPC group was highest at the bone-implant interface when compared to CPC group ($p < 0.01$). With respect to the entire defect region a similar scenario was seen in favor of SrCPC, where there was more bone formation when compared to both CPC ($p = 0.005$) and empty control groups ($p = 0.0001$). Moreover, an enhanced cortical bridging was seen in the SrCPC group in comparison to the others where large shifts in cortices were seen. In addition, these gaps were filled predominantly with cartilage and osteoid in case of the SrCPC group. Whereas fibrous tissue was the most common type in the CPC and empty control group. On examination of potential biomarkers for bone formation, a favorable condition was seen in the SrCPC group which exhibited an up regulation of bone formation markers such as bone morphogenic protein-2, osteocalcin and osteoprotegerin. At this time point differential gene expression also exhibited a remarkable up-regulation of bone formation genes like alkaline phosphatase, collagen 10a1 and osteocalcin in SrCPC group as well. Finally, a significantly higher Sr count was found in the SrCPC group by TOF-SIMS mostly in the areas of the new bone formation thereby suggesting the release of strontium ions from SrCPC. In summation, SrCPC enhanced bone formation in comparison to CPC and empty defects.

ZUSAMMENFASUNG

In dieser Doktorarbeit werden Biomaterialien aus CPC und SrCPC und Leerdefekte als Kontrolle genutzt, um die Frakturheilung in einem metaphysären Defekt-Modell kritischer Größe in Ratten 6 Wochen *post operationem* zu evaluieren. Die Leerdefekt-Kontrolle zeigte eine signifikant niedrigere Knochenheilung. Der höchste Knochenumbau war in der SrCPC-Gruppe zu sehen. Die trabekuläre Knochenbildung war verglichen mit der CPC-Gruppe an der Knochen-Implantat-Grenzfläche am höchsten ($p < 0.01$). Im Bezug auf die gesamte Defekt-Region kam es zu einem ähnlichen Ergebnis zugunsten SrCPC, wo mehr Knochenbildung, sowohl im Vergleich zu CPC ($p = 0.005$) als auch im Vergleich zur Leerdefekt-Kontroll-Gruppe ($p = 0.0001$) festgestellt wurde. Darüber hinaus wurde eine verbesserte Überbauung des Defekt-Spalt der Kortikalis in der SrCPC-Gruppe im Vergleich zu den anderen Gruppen festgestellt, in denen große Verschiebungen am Defekt-Spalt der Kortikalis zu sehen waren. Außerdem waren die Defekt-Regionen der SrCPC-Gruppe überwiegend mit Knorpel und Osteoid gefüllt, im Gegensatz zur CPC- und Leerdefekt-Kontroll-Gruppe, in denen im Defekt-Spalt überwiegend Bindegewebe festgestellt wurde. Immunhistochemisch zeigte sich eine Hochregulation von BMP-2 (bone morphogenic protein-2), Osteocalcin (OCN) und Osteoprotegerin (OPG) in der SrCPC-Gruppe im Vergleich zur Kontrolle. Zu diesem Zeitpunkt zeigte sich außerdem in der Genexpressions-Analyse eine bemerkenswerte Hochregulation der Expression von den Knochenbildungs-Markern Alkalische Phosphatase (ALPL), Kollagen Typ X alpha 1 (COL10A1) und Osteocalcin (OCN) in der SrCPC-Gruppe im Vergleich zur CPC-Gruppe. Schließlich wurde in den Bereichen, in denen sich der Knochen neu gebildet hat, in der SrCPC-Gruppe eine signifikant höhere Menge an Strontium im TOF-SIMS gefunden, was die positive Wirkung von Strontium auf den Knochenaufbau bestätigt. Zusammenfassend ist zu sagen, dass Strontium einen positiven Einfluss auf die knochenbauenden Parameter ausübt, was in einer verbesserten Knochenbildung resultiert.

DECLARATION

I declare that I have completed this dissertation single-handedly without the unauthorized help of a second party and only with the assistance acknowledged therein. I have appropriately acknowledged and referenced all text passages that are derived literally from or are based on the content of published or unpublished work of others, and all information that relates to verbal communication. I have abided by the principles of good scientific conduct laid down in the charter of the Justus Liebig University of Giessen in carrying out the investigations described in the dissertation.

Date:.....

RAY, SEEMUN
(Surname, First name)

ACKNOWLEDGEMENT

Behind every achievement lies an unfathomable sea of gratitude to those who accentuated it, without whom it would have never come into existence. Here I want to express and record my heartfelt feeling of gratefulness to all those who directly or indirectly helped me in this work.

I am highly obliged to my esteemed guide **Prof. Dr. Dr. Volker Alt**, Dept. of Trauma Surgery, Justus Liebig University, Giessen, Germany for letting me carry out my long term dream under his esteemed guidance. His indispensable views and dedicated involvement made my work easier. I am feeling so proud to work under Prof. Dr. Dr. Volker Alt who gave me complete freedom in applying my views and ideas to the work with his limitless patience.

I want to express my sincere gratitude to **Dr. Ursula Sommer**, Labor for Experimentalle Unfallchirurgie, JLU; Giessen who has been a source of continuous encouragement and inspiration to me and whose constructive critic helped me to pursue my dreams. I would also like to extend my deepest appreciation for her thorough revision of my thesis.

I am also grateful to **Univ. Prof. Prof. h.c. Dr. Dr. Dr. h.c. Reinhard Schnettler** for providing me a unique opportunity to be a part of the SFB/Transregio 79 and to carry out my project in his lab.

I would like to express my very great appreciation for **Dr. Ulrich Thormann**, Dept. of Trauma Surgery, JLU; Giessen for providing his invaluable expertise and help in the animal surgeries.

I would also like to thank **Dr. Thaqif El Khassawna** and **Dr. Saravanan Subramaniam** for providing me thorough insight of the statistical analysis.

I also want to express my sincere thanks to **Prof. Katrin Lips**, Labor for Experimentalle Unfallchirurgie, JLU; Giessen who permitted me to carry out my project in her lab and all my lab members for extending their support for completion of my project.

I am particularly grateful for the assistance given by **Mrs. Tanja Rehling**, Technical Assistant, Labor for Experimentalle Unfallchirurgie, JLU; Giessen not only for her expertise at work but also making it fun. On a personal level, I would like to thanks **Mrs. Ida Oberst, Annette Stengel, Martina Fink** and **Iris Schuetz** for their touching support.

I would also like to thank all the Lab assistants; technical and non-technical staff members those who have helped me whenever in need.

I am externally obliged to my funding agency Deutsche Forschungsgemeinschaft (**DFG**) **SFB/TRR 79** and Giessen graduate school of life sciences, **GGL**.

I would extend countless thanks to my friends, who are now scattered all over the world. Their chats and dinner dates helped me to keep sane.

I am ever grateful and thankful to my parents for their unwavering support, blessing and encouragement.

I would like to heartily thank my loving husband **Siddharth Sharma** for being with me through all times, good and bad and never failing to lift my spirits.

Last, but not least I would like to thank Almighty God. **Om Sai Ram**.

- Seemun Ray

**Der Lebenslauf wurde aus der elektronischen
Version der Arbeit entfernt.**

**The curriculum vitae was removed from the
electronic version of the paper.**